## Electronic Supplementary Information

# Oxatub[4]arene: A Smart Macrocyclic Receptor with Multiple Interconvertible Cavities

Fei Jia, Zhenfeng He, Liu-Pan Yang, Zhi-Sheng Pan, Min Yi, Ren-Wang Jiang, and Wei Jiang*

*Department of Chemistry, South University of Science and Technology of China (SUSTC), Xueyuan Blvd 1088, Nanshan District, Shenzhen, 518055, P. R. China*

**E-mail: jiangw@sustc.edu.cn*

## Table of Contents

## 1. Experimental Section

**1.1 General.** All the reagents involved in this research were commercially available and used without further purification unless otherwise noted. Solvents were either employed as purchased or dried prior to use by standard laboratory procedures. Thin-layer chromatography (TLC) was carried out on 0.25 mm Yantai silica gel plates (60F-254). Column chromatography was performed on silica gel 60 (Tsingdao 40 – 63 nm, 230 – 400 mesh). $^{1}$H, $^{13}$C, $^{1}$H-$^{1}$H COSY, and $^{1}$H-$^{1}$H ROESY NMR spectra were recorded on Bruker Avance-400, 500, or 600 spectrometers. All chemical shifts are reported in *ppm* with residual solvents or TMS (tetramethylsilane) as the internal standards. The following abbreviations were used for signal multiplicities: s, singlet; d, doublet; t triplet; m, multiplet. Electrospray-ionization time-of-flight high-resolution mass spectrometry (ESI-TOF-HRMS) experiments were conducted on an applied biosystems Elite ESI-QqTOF mass spectrometry system. X-ray diffraction data of single crystals were collected on an Oxford Gemini R Ultra diffractometer equipped with a CCD area detector. All the computations were performed at the AM1 level of theory by using Spartan '14 (Wavefunction, Inc.). Synthesis of Guests **D2D**$^{2+}$ - **D8D**$^{2+}$, **2D2**$^{2+}$ - **8D8**$^{2+}$, and **D5**$^{+}$ have been reported,[1] and guest **AVA**$^{2+}$ [2] were synthesized by following the literature procedures.

**1.2 Isothermal titration calorimetry, ITC.** Titration experiments were carried out in 1,2-dichloroethane/$CH_3CN$ 1 : 1 (v/v) at 25 °C on a NanoITC LV – 190 μL (Waters GmbH, TA Instruments, Eschborn, Germany). In a typical experiment, a 190 μL solution of **TA4** was placed in the sample cell at a concentration of 0.16 mM, and 50 μL of a solution of the hexafluorophosphate salt (1 mM in the same solvent) was in the injection syringe. The titrations were placed consisted of 25 consecutive injections of 1.96 μL each with a 5 min interval between injections. Heats of dilution, measured by titration of the salt into the sample cell with blank solvent, were subtracted from each data set. All solutions were degassed prior to titration. The data were analyzed using the instrumental internal software package and fitted with a 1:1 binding model. Errors are smaller than ±10%.

---

1. Z. He, G. Ye, W. Jiang, *Chem. – Eur. J.*, 2014, **21**, 3005.
2 . K. Ohga, Y. Takashima, H. Takahashi, Y. Kawaguchi, H. Yamaguchi, A. Harada, *Macromolecules*, 2005, **38**, 5897.

## 1.3 Synthetic Procedures

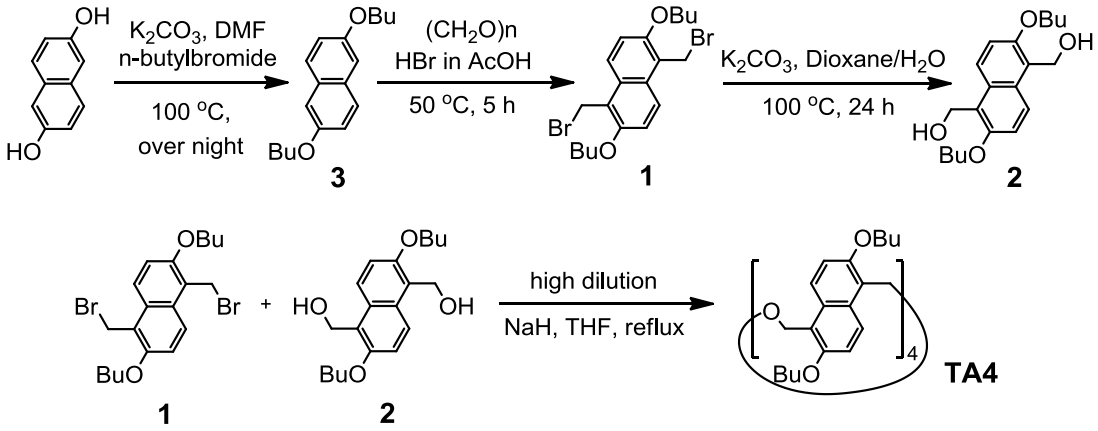


Synthetic procedure of compound **TA4**

### Compound 3

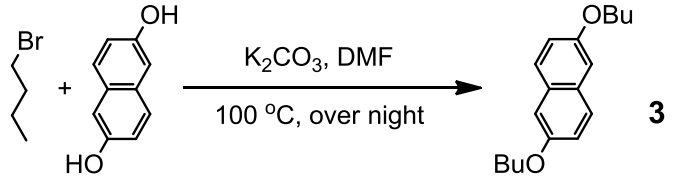


The mixture of 2,6-dihydroxynaphthalene (10 g, 62 mmol), 1-bromobutane (20 mL, 187 mmol), and $K_2CO_3$ (43 g, 312 mmol) in dry DMF (100 mL) were stirred overnight at 100°C under Argon protection. After cooling to to room temperature, the mixture was poured into water (500 mL). The precipitate was filtered and washed with copious $H_2O$ and MeOH. The filter cake was collected and dried in vacuum to give compound **3** (14 g, 82%) as a white solid, which was used for the next step without further purification. The characterization data is in line with the literature.[3] $^1$H NMR (400 MHz, $CDCl_3$, 298 K): δ [ppm] = 7.61 (d, *J* = 8.7 Hz, 2H), 7.17 – 7.05 (m, 4H), 4.05 (t, *J* = 6.5 Hz, 4H), 1.89 – 1.75 (m, 4H), 1.58 – 1.46 (m, 4H), 1.00 (t, *J* = 7.4 Hz, 6H) ; $^{13}$C NMR (100 MHz, $CDCl_3$, 298 K): δ [ppm] = 155.65, 129.81, 128.13, 119.30, 107.02, 67.85, 31. 50, 19.46, 14.04.

3. C. Cazorla, É. Pfordt, M.-C. Duclos, E. Métay, M. Lemaire, *Green Chem.,* 2011, **3**, 2482.

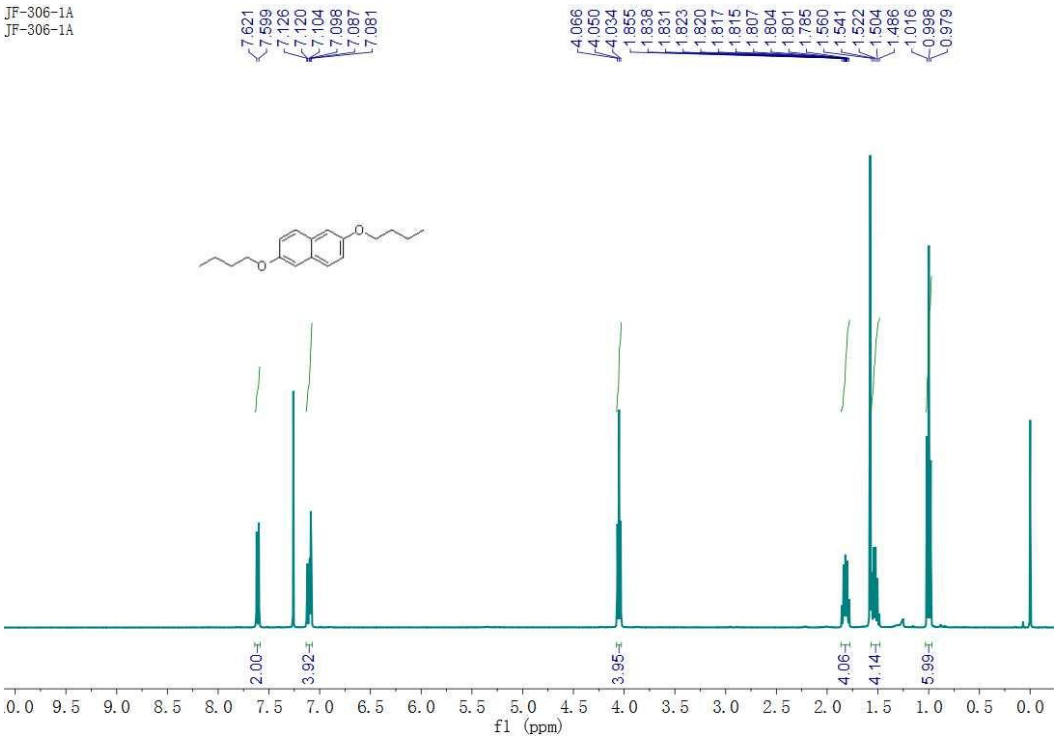


$^{1}$H NMR spectrum (400 MHz, $CDCl_3$, 298 K) of compound **3**

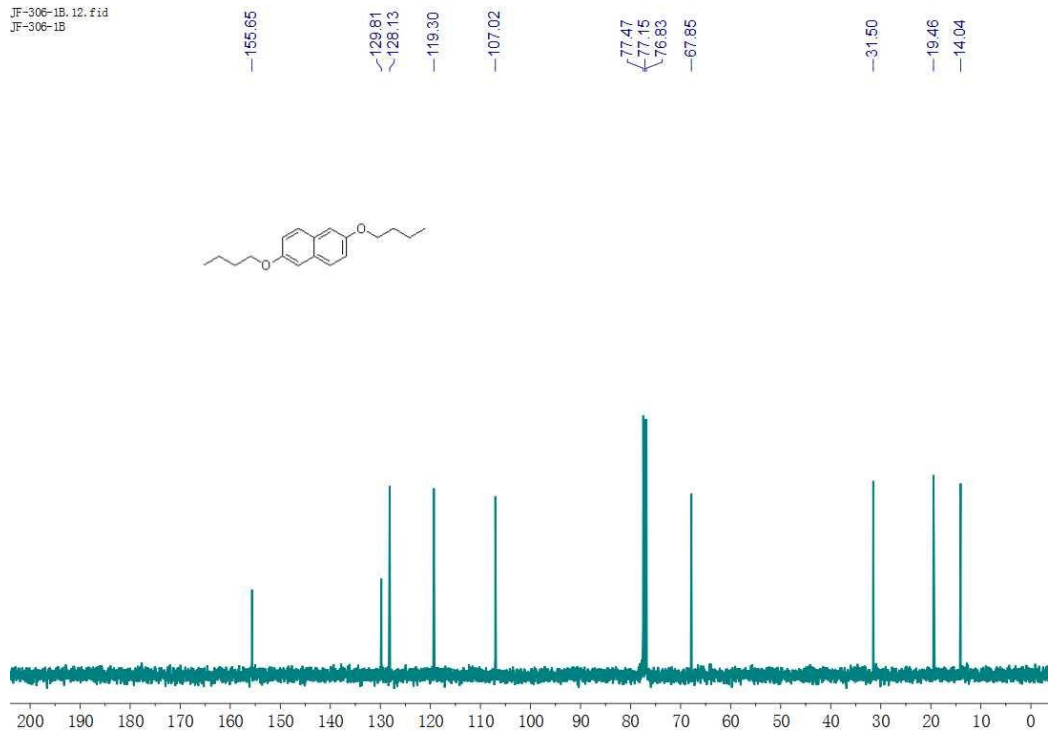


$^{13}$C NMR spectrum (100 MHz, $CDCl_3$, 298 K) of compound **3**

**Dibromide 1**

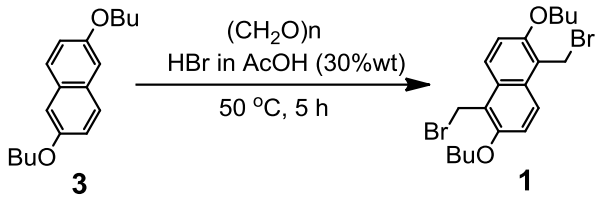


Compound **3** (5.0 g, 18.4 mmol) and paraformaldehyde (2.8 g, 91.8 mmol) were dissolved in HBr/AcOH(30% w/w, 50mL). The resulting mixture was heated to 50 $^{o}$C and stirred for 5h. The solution was cooled to room temperature. The light purple precipitate was filtered off and washed with copious $H_2O$ and MeOH. The crude product was dissolved in minimal amount of $CH_2Cl_2$ and then added dropwise into MeOH (150 mL) during stirring. The precipitate was collected through filtration and dried to afford dibromide **1** (5.4 g, 64%) as an off-white solid. m.p. 91-92 $^{o}$C; $^{1}$H NMR (400 MHz, $CDCl_3$, 298 K): δ [ppm] = 8.02 (d, *J* = 9.3 Hz, 2H), 7.34 (d, *J* = 9.4 Hz, 2H), 5.07 (s, 4H), 4.18 (t, *J* = 6.4 Hz, 4H), 1.94 – 1.80 (m, 4H), 1.66 – 1.53 (m, 4H), 1.02 (t, *J* = 7.4 Hz, 6H); $^{13}$C NMR (100 MHz, $CDCl_3$, 298 K): δ [ppm] = 153.30, 127.83, 125.50, 119.06, 115.55, 69.22, 31.62, 25.30, 19.35, 13.92; ESI-TOF-HRMS: *m/z* calcd for $[M\text{-}Br]^+$ $C_{20}H_{26}O_2Br$, 377.1111; found 377.1108 (100%).

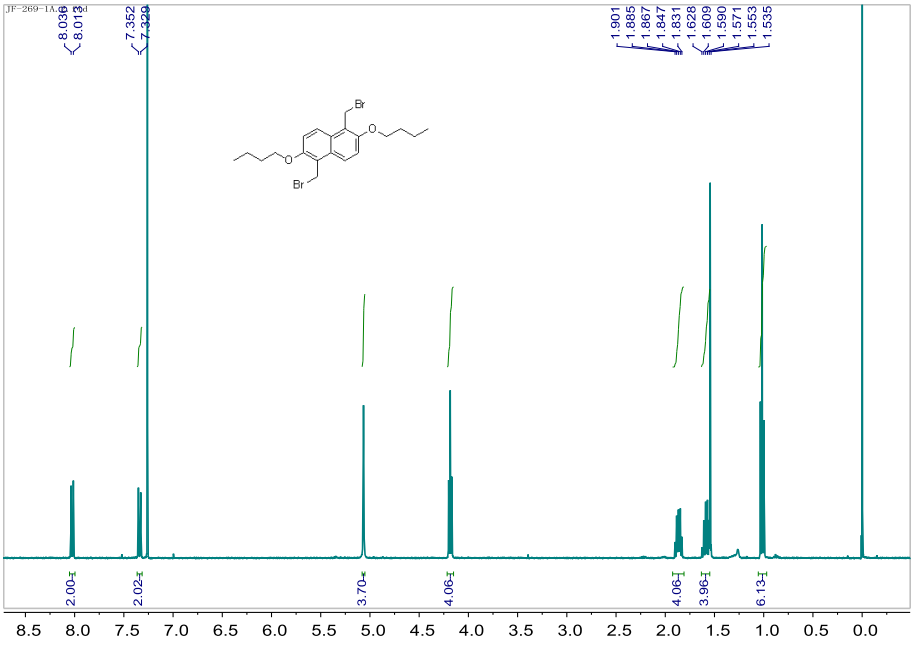


$^{1}$H NMR spectrum (400 MHz, $CDCl_3$, 298 K) of dibromide **1**

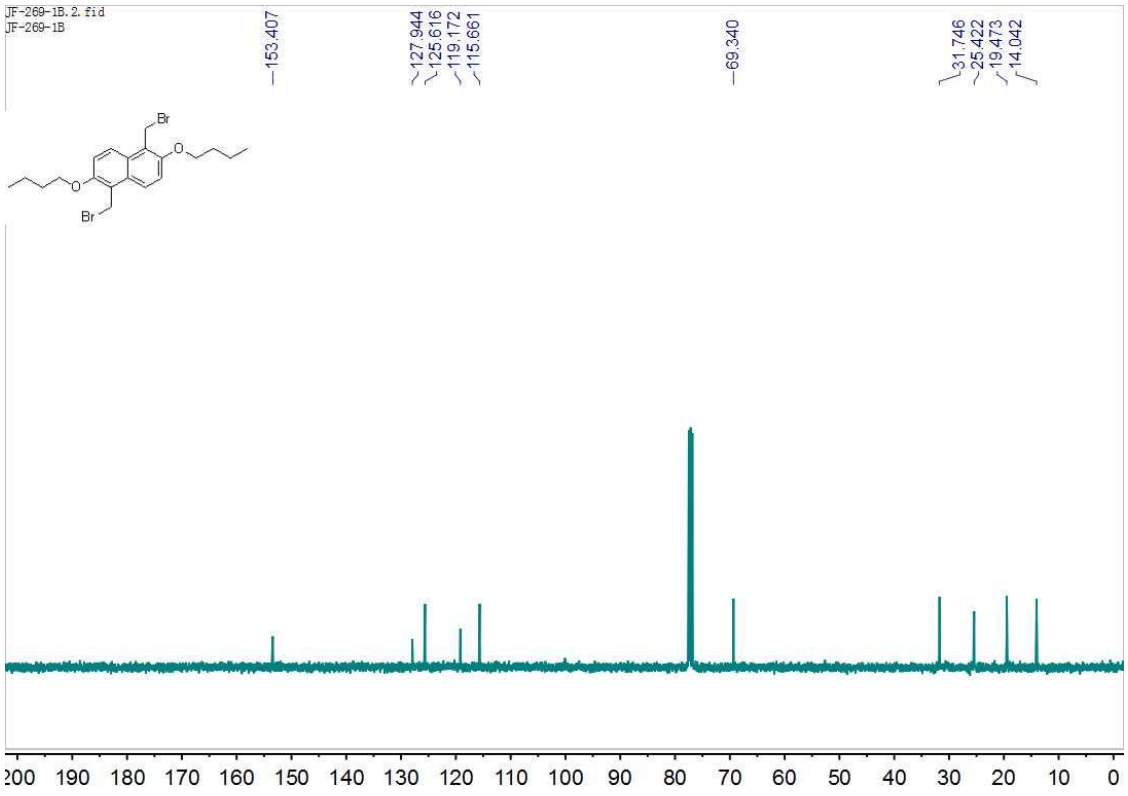


$^{13}$C NMR spectrum (100 MHz, $CDCl_3$, 298 K) of dibromide **1**

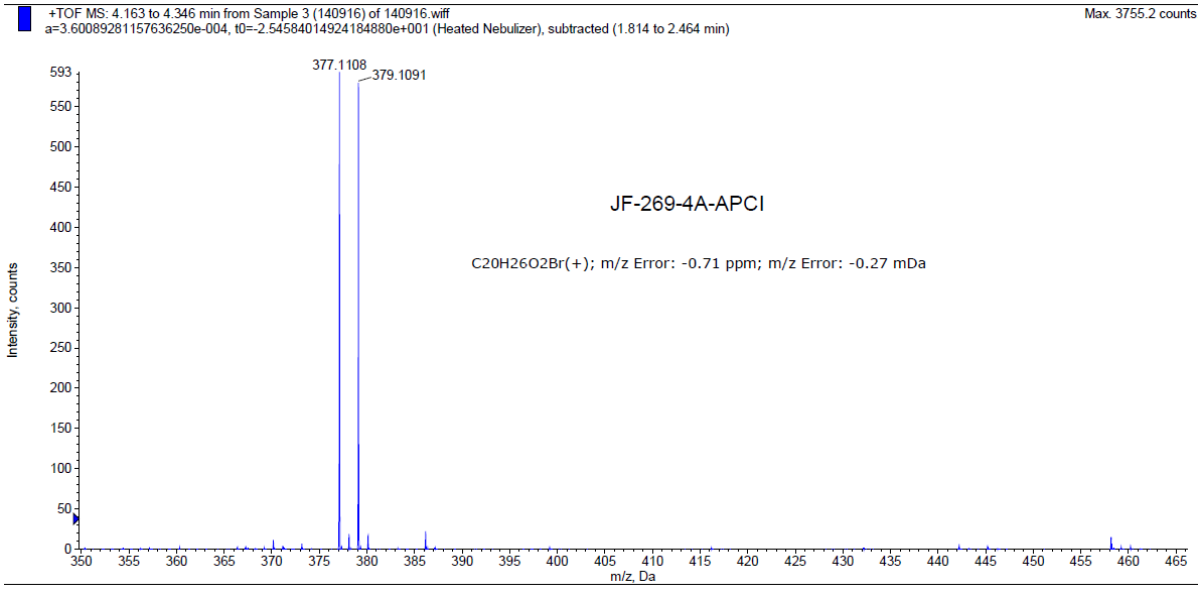


ESI-TOF mass spectrum of dibromide **1**

**Diol 2**

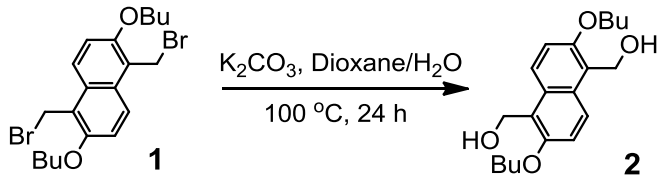


The mixture of dibromide **1** (3.0 g, 6.6 mmol) and $K_2CO_3$ (9.0 g, 58.9 mmol) in 1,4-Dioxane/$H_2O$ (1:1, 60 mL) were stirred at 100°C for 24 h. The mixture was concentrated with rotary evaporator and then extracted with ethylacetate (60 mL × 3). The organic phase was collected and then dried over anhydrous $Na_2SO_4$. The solvent was removed under reduced pressure. The remaining residue was subjected to column chromatography ($SiO_2$, petroleum ether: ethylacetate = 2:1) to give the diol **2** (1.2 g, 55%) as a white solid. m.p. 139-140 °C; $^1$H NMR (400 MHz, $CDCl_3$, 298 K): δ [ppm] = 8.10 (d, *J* = 9.2 Hz, 2H), 7.31 (d, *J* = 9.6 Hz, 2H), 5.17 (s, 4H), 4.14 (t, *J* = 6.4 Hz, 4H), 1.88 – 1.78 (m, 4H), 1.60 - 1.48 (m, 4H), 1.00 (t, *J* = 7.4 Hz, 6H); $^{13}$C NMR (100 MHz, $CDCl_3$, 298 K): δ [ppm] = 152.98, 128.58, 125.12, 122.00, 115.53, 69.35, 56.13, 31.67, 19.38, 13.91; ESI-TOF-HRMS: *m/z* calcd for $[M+Na]^+$ $C_{20}H_{28}NaO_4$, 355.1880; found 355.1879 (100%).

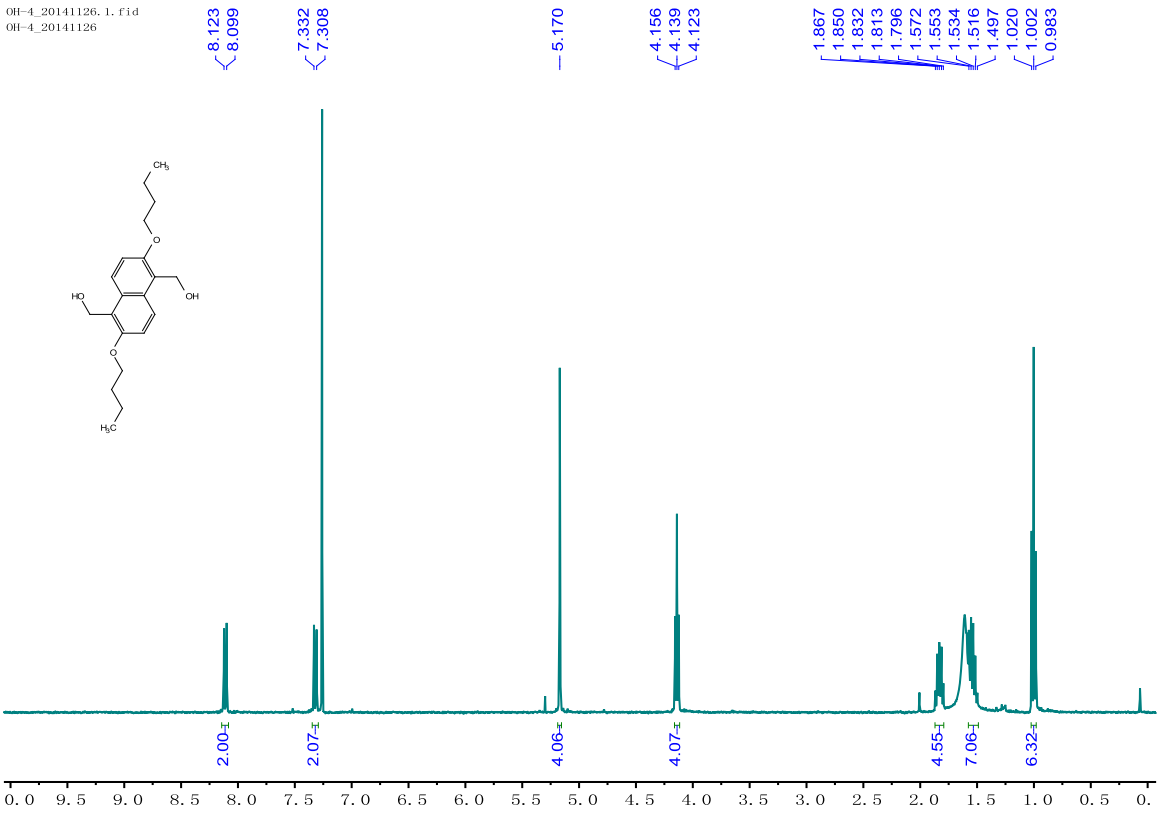


$^1$H NMR spectrum (400 MHz, $CDCl_3$, 298 K) of diol **2**

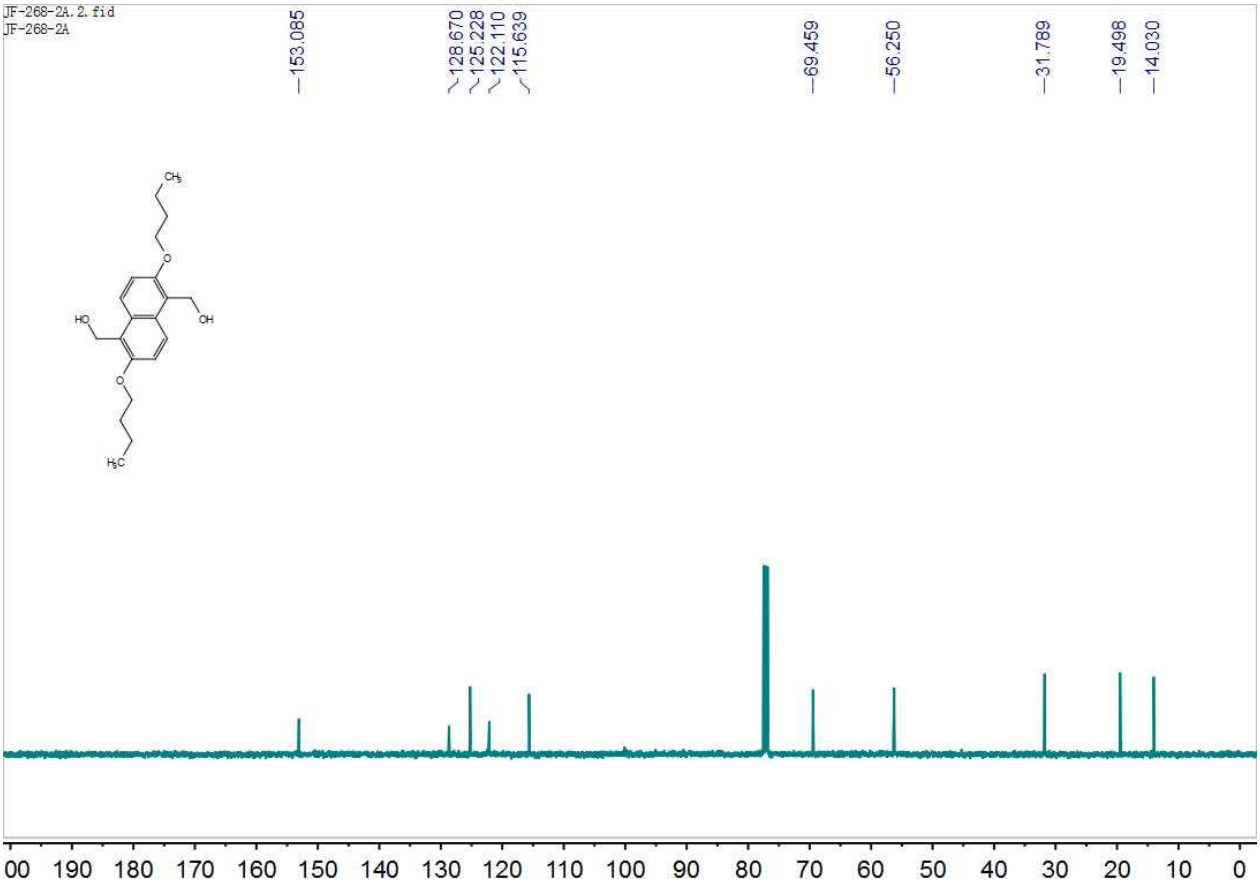


$^{13}C$ NMR spectrum (100 MHz, $CDCl_3$, 298 K) of diol **2**

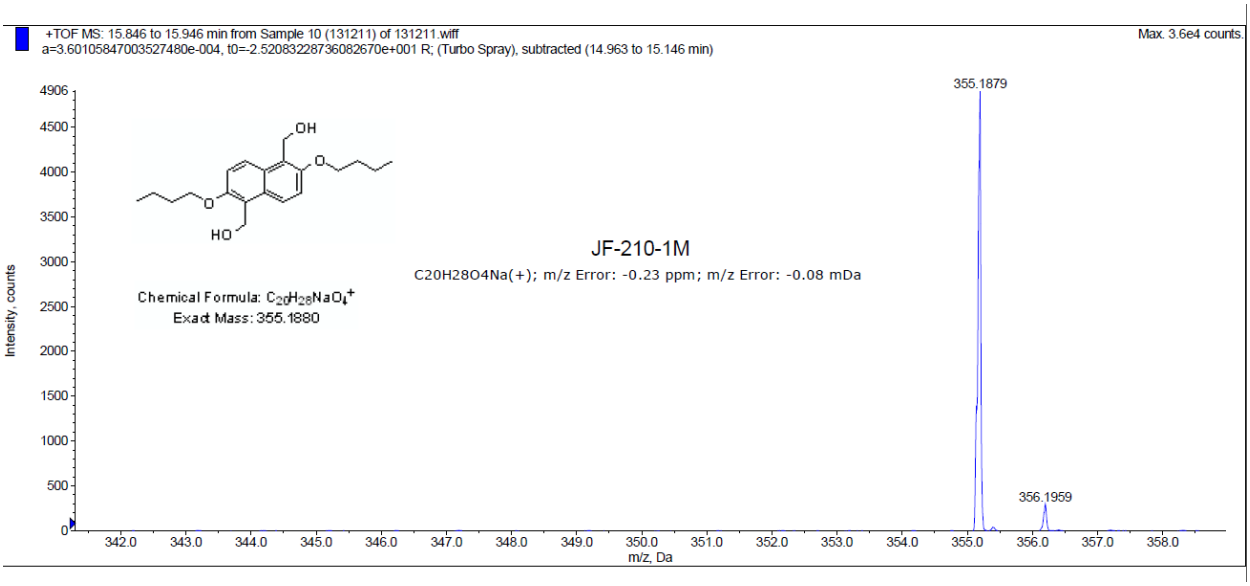


ESI-TOF mass spectrum of diol **2**

**TA4**

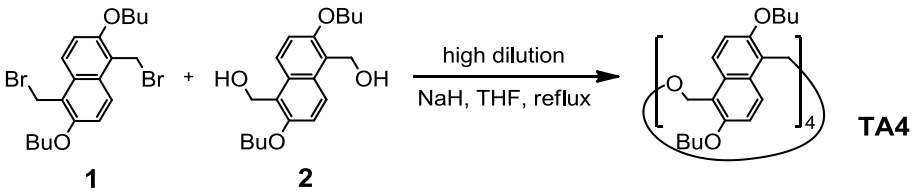


To the mixture of NaH (0.43 g, 18 mmol) and $Cs_2CO_3$ (5.9 g, 18 mmol )[4] in dry THF (400 mL) at reflux was added the solution of dibromide **1** (1.4 g, 3.0 mmol) and diol **2** (1.0 g, 3.0 mmol) in dry THF (60 mL) dropwise through a syringe pump during 6 h. The resulting mixture was stirred at reflux for another 60h. The solvent was removed under reduced pressure. The residue was suspended in $H_2O$ (30 mL), and then extracted with $CH_2Cl_2$ (30mL×3). The combined organic phase was washed with saturated NaCl and dried over anhydrous $Na_2SO_4$. Then, the solvent was removed with rotary evaporator to give the crude product which was purified by column chromatography ($SiO_2$, petroleum ether: ethylacetate = 30:1 ~ 8:1) to give pure per-butyl oxatub[4]arene (**TA4**) as a white solid (400 mg, 21%). m.p. 153-154 $^oC$; $^1H$ NMR (400 MHz, $CD_2Cl_2$, 298 K): δ [ppm] = 7.70 (d, *J* = 9.3 Hz, 8H), 6.89 (d, *J* = 9.3 Hz, 8H), 4.99 (s, 16H), 3.70 (t, *J* = 6.3 Hz, 16H), 1.58 – 1.48 (m, 16H), 1.44 – 1.32 (m, 16H), 0.92 (t, *J* = 7.3 Hz, 24H); $^{13}C$ NMR (100 MHz, $CD_2Cl_2$, 298 K): δ [ppm] = 153.52, 129.61, 126.14, 120.27, 115.63, 69.65, 62.14, 31.94, 19.73, 14.13; ESI-TOF-HRMS: *m/z* calcd for $[M+K]^+$ $C_{80}H_{104}O_{12}K^+$, 1295.7159; found 1295.7148 (100%).

4. Addition of $Cs_2CO_3$ can, to some extent, improve the yield of oxatub[4]arene. The detailed reason behind it is not clear, presumably due to a loose ion pair resulting from the "Cesium Effect": G. Dijkstra, W. H. Kruizinga, R. M. Kellogg, *J. Org. Chem.,* 1987, **52**, 4230.

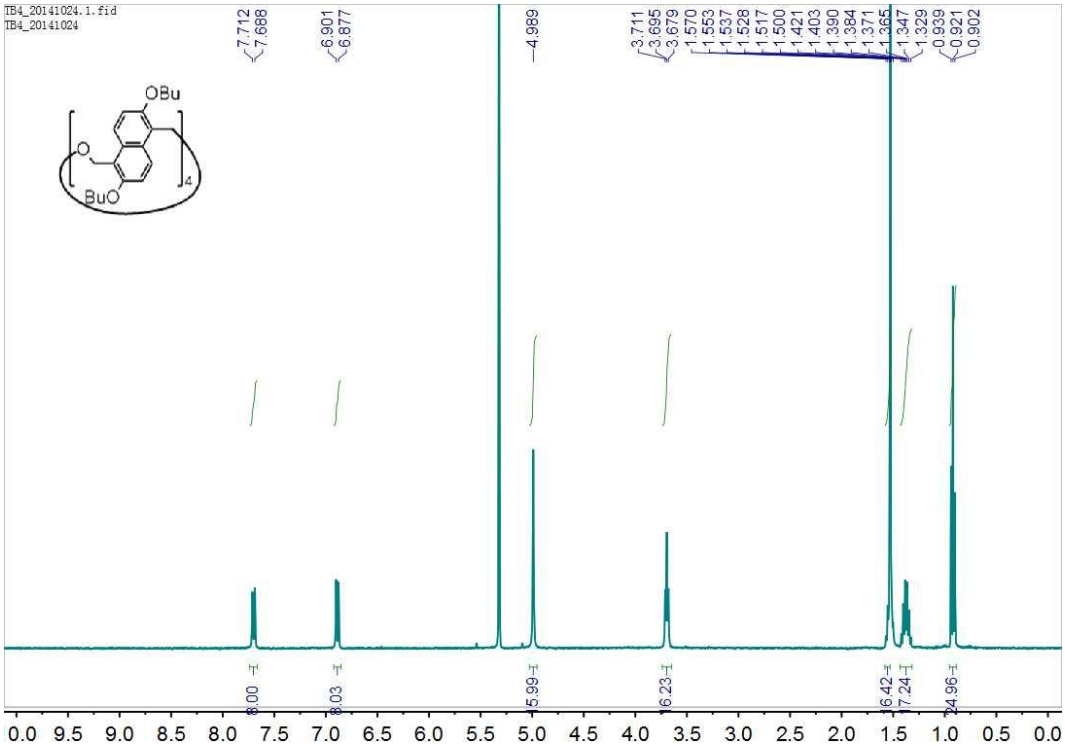


$^{1}$H NMR spectrum (400 MHz, $CD_2Cl_2$, 298 K) of **TA4**

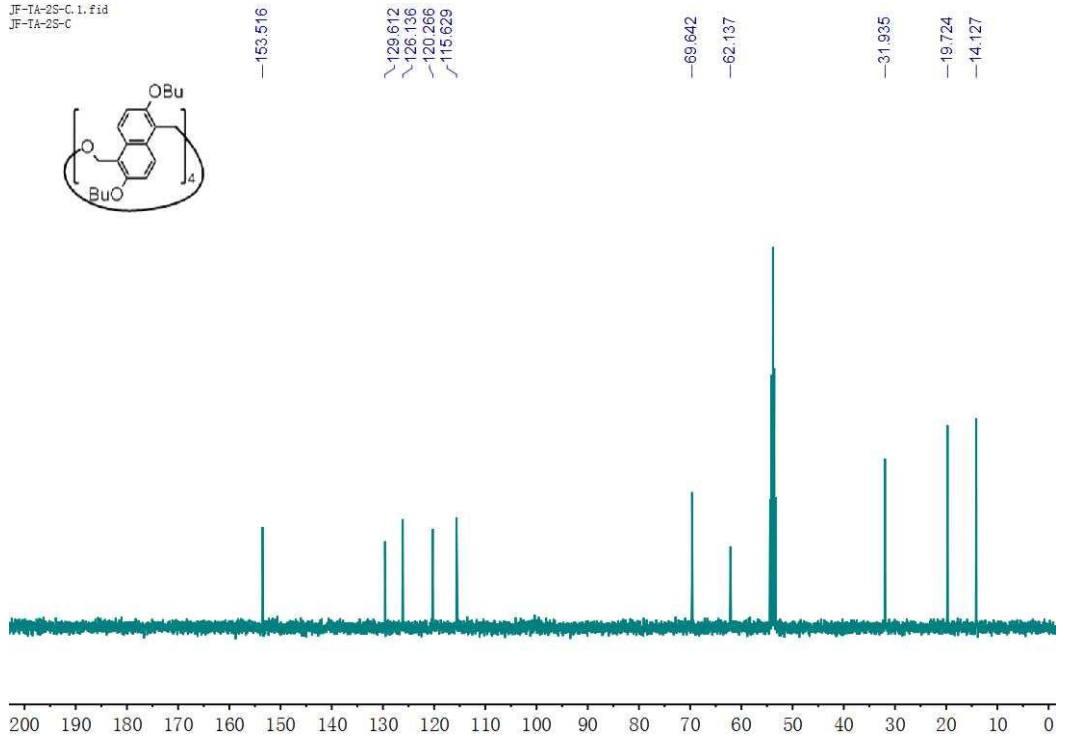


$^{13}$C NMR spectrum (100 MHz, $CD_2Cl_2$, 298 K) of **TA4**

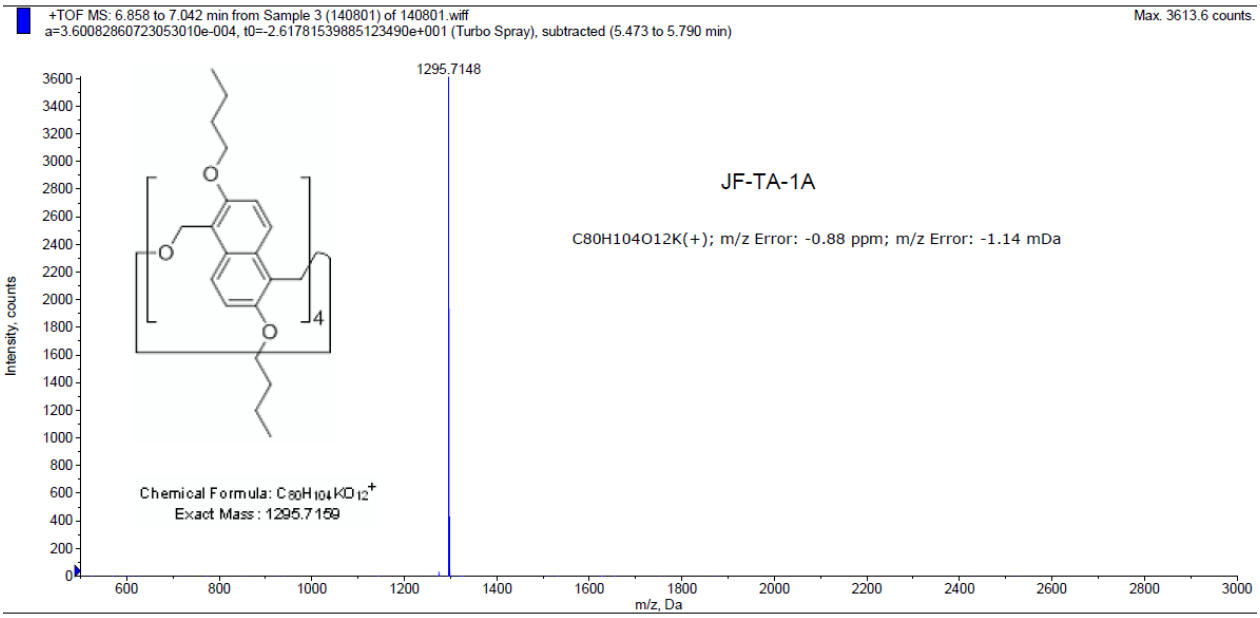


ESI-TOF mass spectrum of **TA4**

**General Synthetic Procedure for 10D10-2PF$_6$ and 12D12-2PF$_6$:**

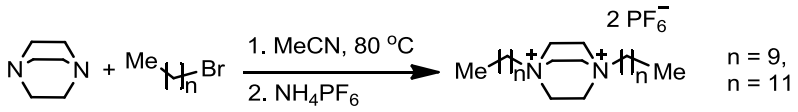


DABCO (2, 2'-Diazabicyclo[2.2.2] octane, 1.0 eq.) in MeCN was added dropwise into Alkyl bromide (8.0 eq.) in MeCN at 80$^o$C, and the resulting mixture was stirred overnight. After cooling to room temperature, the solution was concentrated under reduced pressure. The remaining solid was washed several times with ethyl ether to afford **nDn**-2Br, which was used directly in the next step. **nDn**-2Br was dissolved in deionized water and added dropwise into saturated aqueous $NH_4PF_6$. After stirring for 4 h, the white precipitate was collected via filtration and washed thoroughly with deionized water to give **nDn**-2$PF_6$ as a white solid after drying. The detailed characterization data of **nDn**-2$PF_6$ are listed below:

**10D10-2PF$_6$:** white solid, yield: 72%. $^1$H NMR (400 MHz, $CD_3CN$, 300 K): δ [ppm] = 3.72 (s, 12H), 3.43- 3.35 (m, 4H), 1.81-1.67 (m, 4H), 1.43-1.22 (m, 28H), 0.89 (t, $J$ = 6.7 Hz, 6H). $^{13}$C NMR (100 MHz, $CD_3CN$, 300 K): δ [ppm] = 66.41, 52.33, 32.98, 30.51, 30.37, 30.33, 29.96,

26.78, 23.76, 22.97, 14.76. ESI-TOF-HRMS: *m/z* calcd for $[M\text{-}PF_6]^+$ $C_{26}H_{54}F_6N_2P^+$, 539.3923; found 539.3924 (100%).

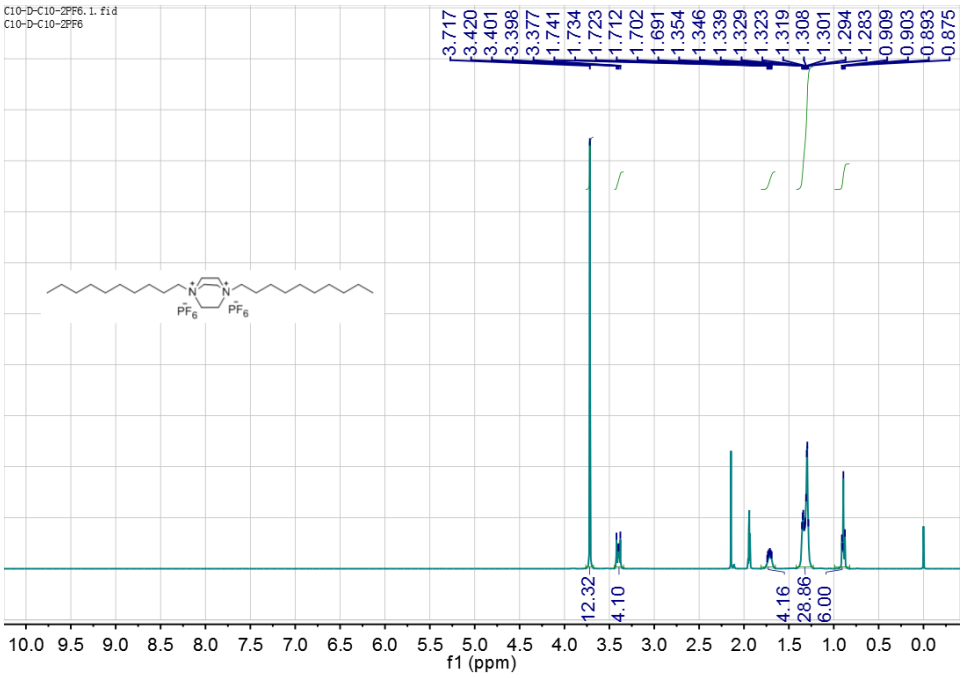


$^1$H NMR spectrum (400 MHz, $CD_3CN$, 300 K) of compound **10D10-2PF$_6$**

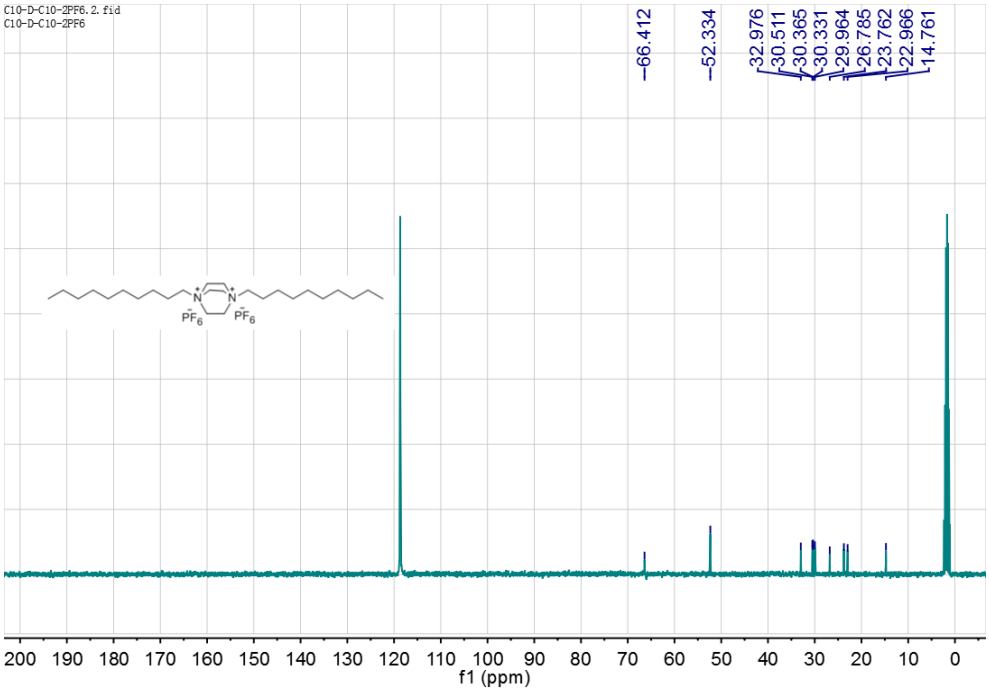


$^{13}$C NMR spectrum (100 MHz, $CD_3CN$, 300 K) of compound **10D10-2PF$_6$**

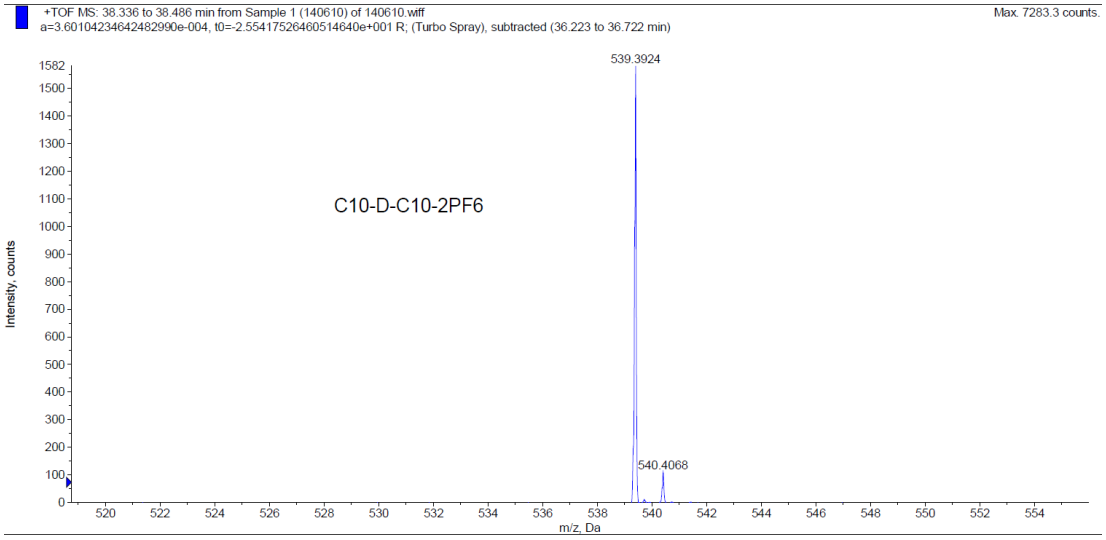


ESI-TOF mass spectrum of **10D10-2PF$_6$**

**12D12-2PF$_6$:** white solid, yield: 75%. $^1$H NMR (400 MHz, $CD_3CN$, 300 K): δ [ppm] = 3.72 (s, 12H), 3.43- 3.35 (m, 4H), 1.75-1.64 (m, 4H), 1.43-1.22 (m, 36H), 0.89 (t, $J$ = 6.7 Hz, 6H). $^{13}$C NMR (100 MHz, $CD_3CN$, 300 K): δ [ppm] = 66.39, 52.31, 33.01, 30.70, 30.54, 30.44, 30.33, 29.96, 26.77, 23.76, 22.95, 14.76. ESI-TOF-HRMS: *m/z* calcd for $[M\text{-}PF_6]^+$ $C_{30}H_{62}F_6N_2P^+$, 595.4549; found 595.4552 (100%).

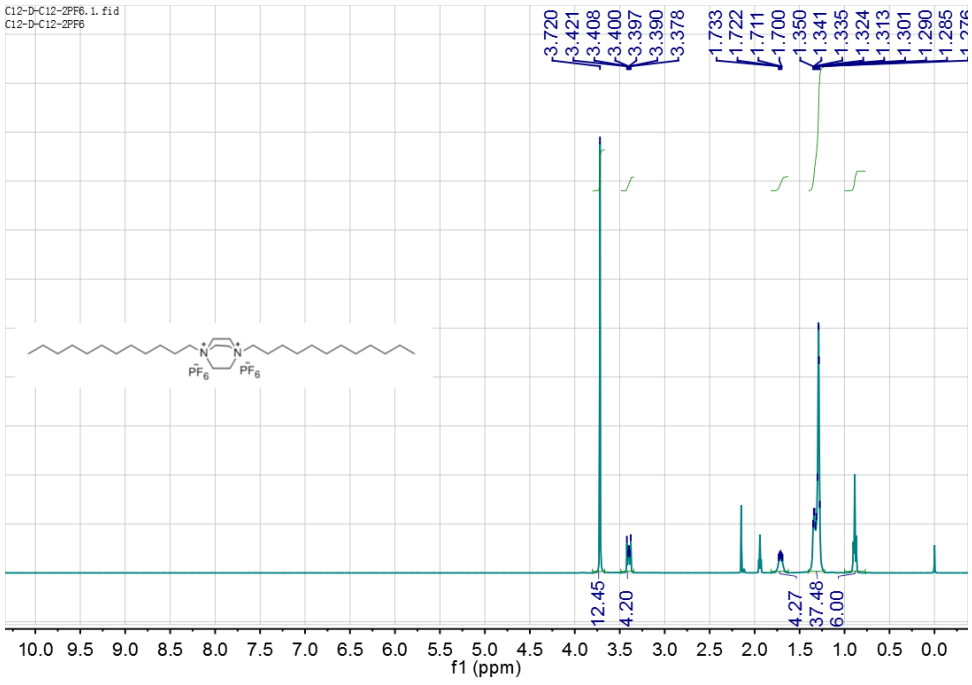


$^1$H NMR spectrum (400 MHz, $CD_3CN$, 300 K) of compound **12D12-2PF$_6$**

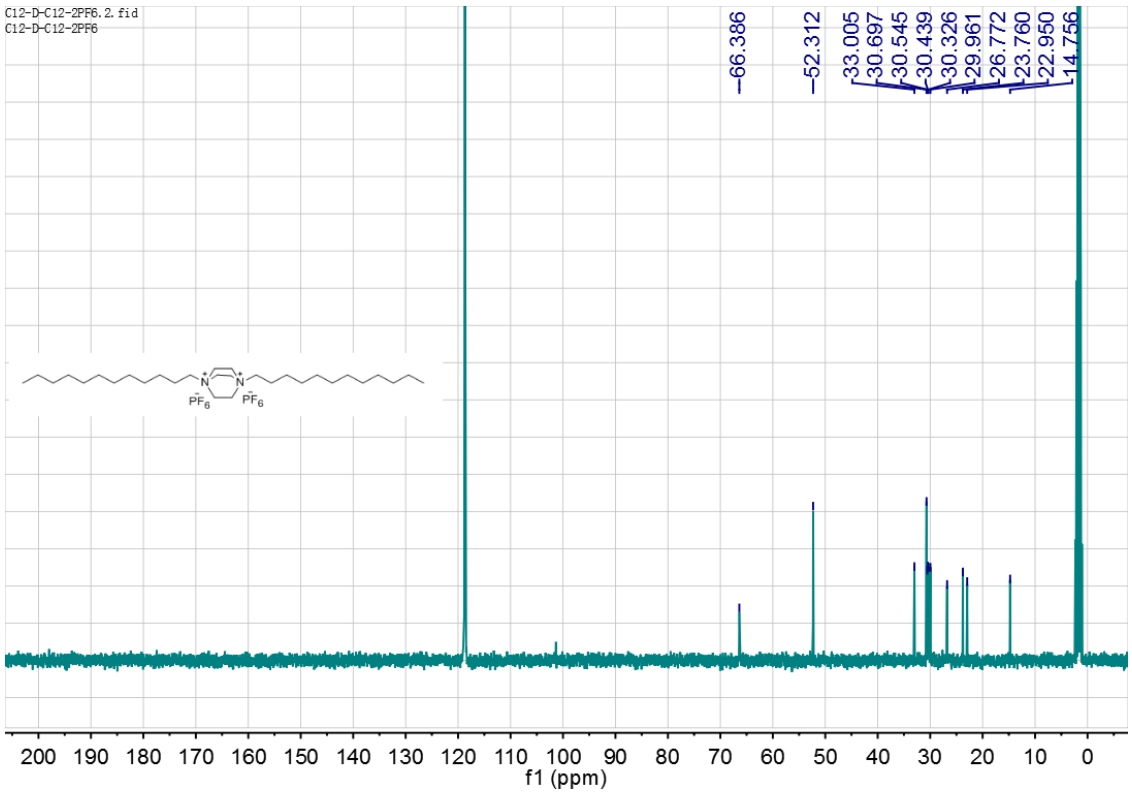


$^{13}$C NMR spectrum (100 MHz, $CD_3CN$, 300 K) of compound **12D12-2PF$_6$.**

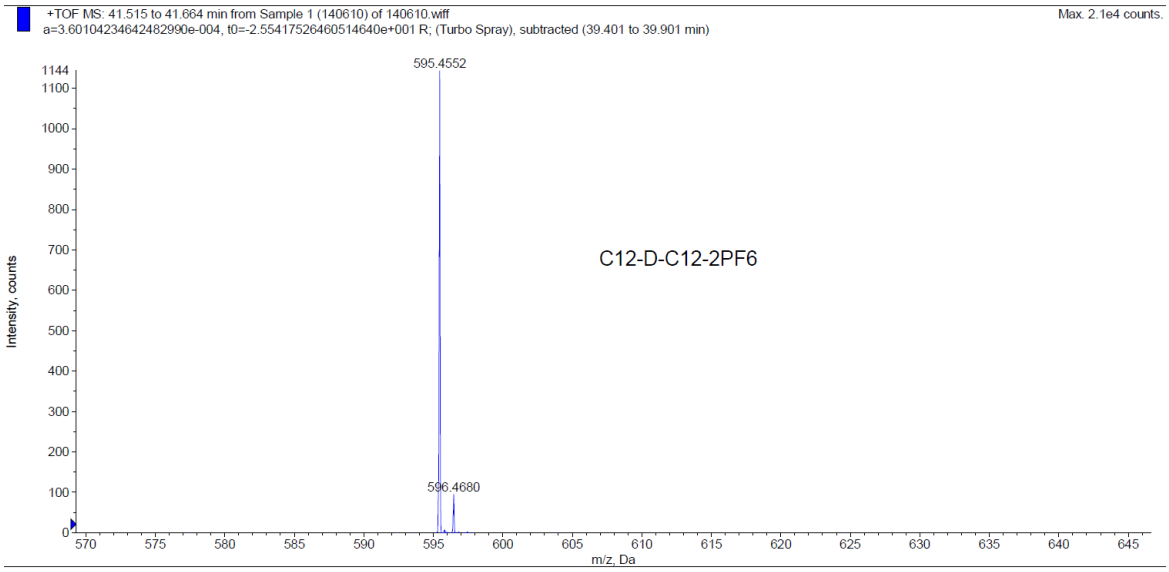


ESI-TOF mass spectrum of **12D12-2PF$_6$**

**General Synthetic Procedure for D10D-2PF$_6$ and D12D-2PF$_6$:**

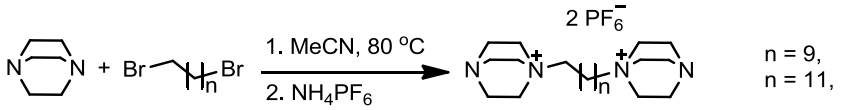


Dibromoalkane (1.0 mmol) in MeCN was dropwised into DABCO (2, 2'-Diazabicyclo [2.2.2] octane, 8.0 mmol) in MeCN (50 mL) at 80 °C. The resulting solution was stirred vigorously overnight. After cooling to room temperature, the solution was concentrated in vacuum. The residue was washed with ethyl ether several times to give compound **DnD-**2Br, which was used directly to the next step. **DnD-**2Br was dissolved in deionized water. The resulting solution was dropwise added into saturated aqueous $NH_4PF_6$. After stirring for 4 h at room temperature, the white precipitate was collected by filtration and washed several times with deionized water. The filter cake was dried to give **DnD-2PF$_6$** as white solids. The detailed characterization data are shown below:

**D10D-2PF$_6$:** white solid, 350 mg, yield: 54%. $^1$H NMR (400 MHz, $CD_3CN$, 300 K): δ [ppm] = 3.26-3.04 (m, 28H), 1.78-1.60 (m, 4H), 1.43-1.25 (m, 12H). $^{13}$C NMR (100 MHz, $CD_3CN$, 300 K): δ [ppm] = 65.90, 65.87, 65.84, 53.77, 53.73, 53.70, 46.17, 30.27, 30.07, 27.30, 22.73. ESI-TOF-HRMS: *m/z* calcd for $[M\text{-}PF_6]^+$ $C_{22}H_{44}F_6N_4P^+$, 509.3202; found 509.3201 (100%).

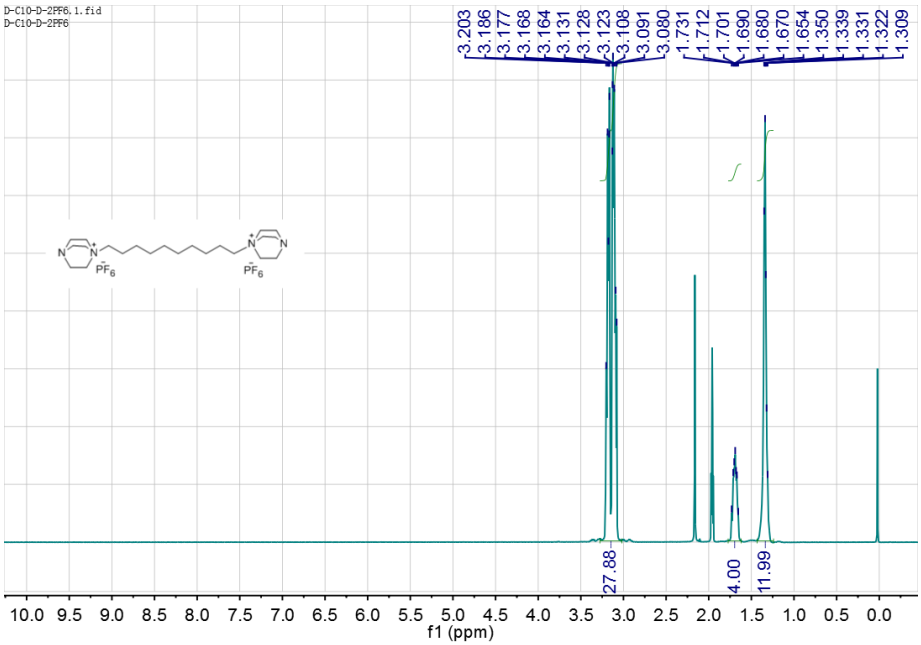


$^1$H NMR spectrum (400 MHz, $CD_3CN$, 300 K) of compound **D10D-2PF$_6$**

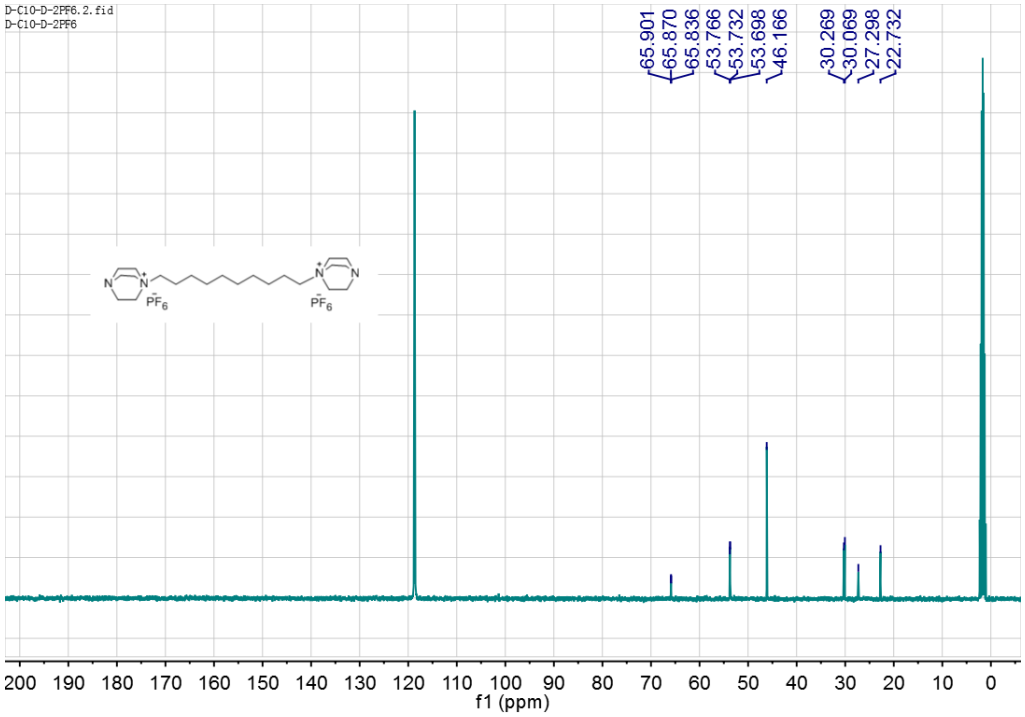


$^{13}$C NMR spectrum (100 MHz, $CD_3CN$, 300 K) of compound **D10D-2PF$_6$**

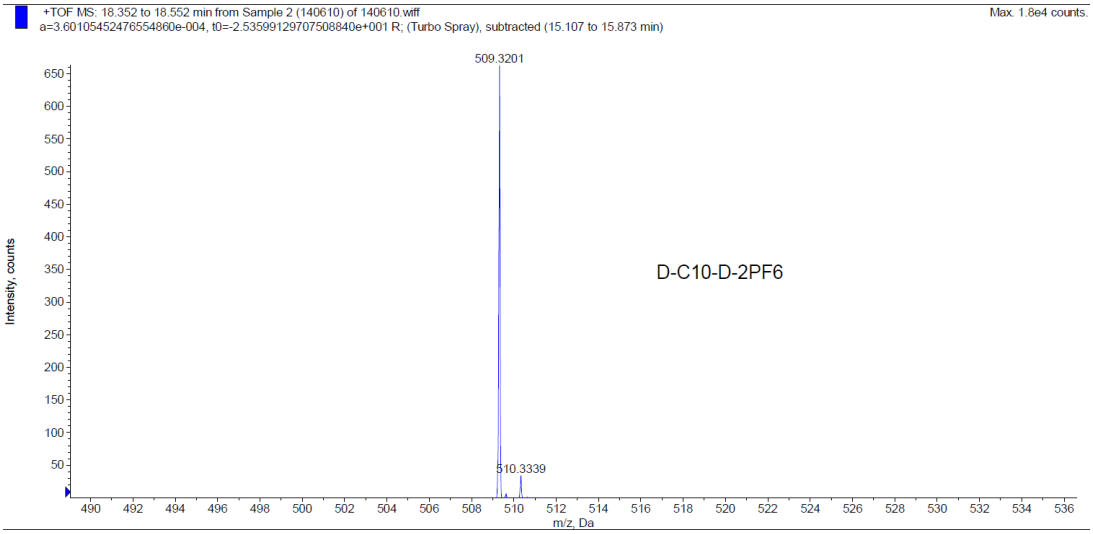


ESI-TOF mass spectrum of **D10D-2PF$_6$**

**D12D-2PF$_6$:** white solid, 490 mg, yield: 72%. $^1$H NMR (400 MHz, $CD_3CN$, 300 K): δ [ppm] = 3.30-2.99 (m, 28H), 1.81-1.62 (m, 4H), 1.46-1.22 (m, 16H). $^{13}$C NMR (100 MHz, $CD_3CN$, 300

K): δ [ppm] = 65.92, 65.86, 65.85, 53.77, 53.74, 53.70, 46.17, 30.59, 30.46, 30.15, 27.34, 22.75.

ESI-TOF-HRMS: *m/z* calcd for $[M\text{-}PF_6]^+$ $C_{24}H_{48}F_6N_4P^+$, 537.3515; found 537.3512 (100%).

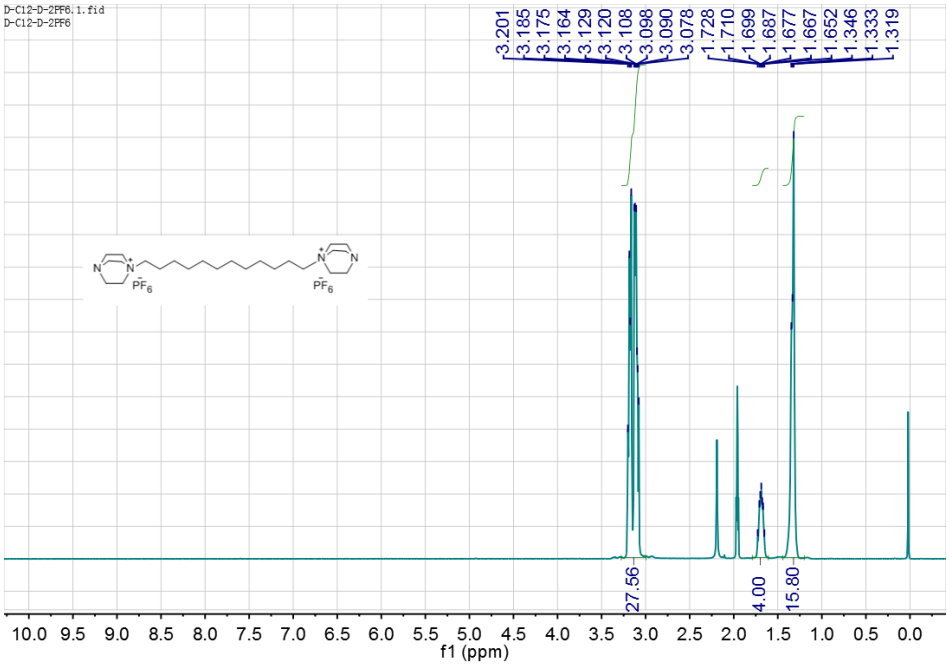


$^{1}$H NMR spectrum (400 MHz, $CD_3CN$, 300 K) of compound **D12D-2PF$_6$**

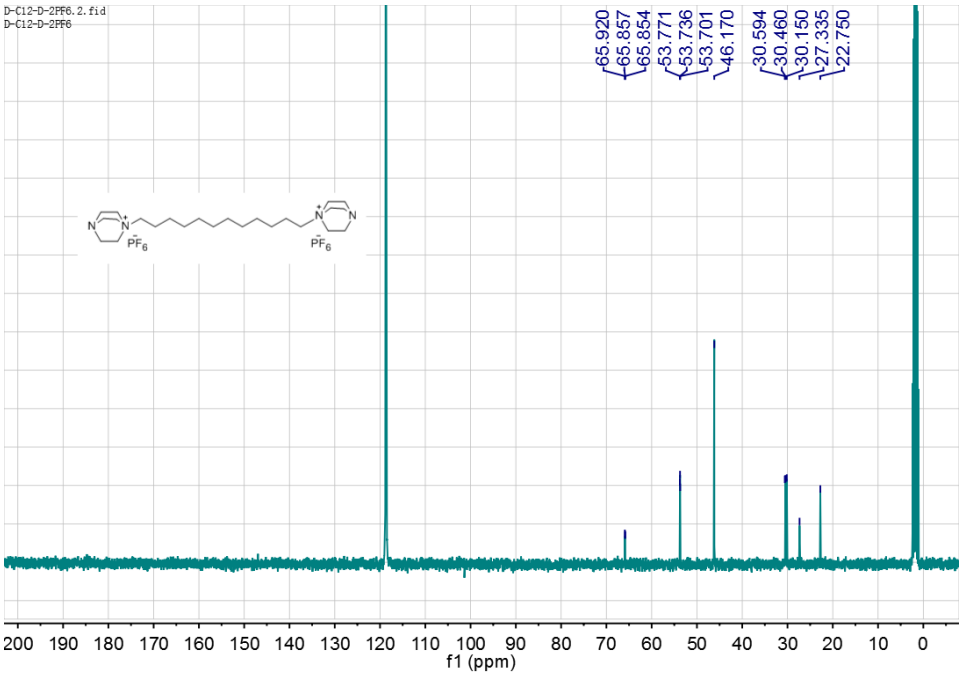


$^{13}$C NMR spectrum (100 MHz, $CD_3CN$, 300 K) of compound **D12D-2PF$_6$**

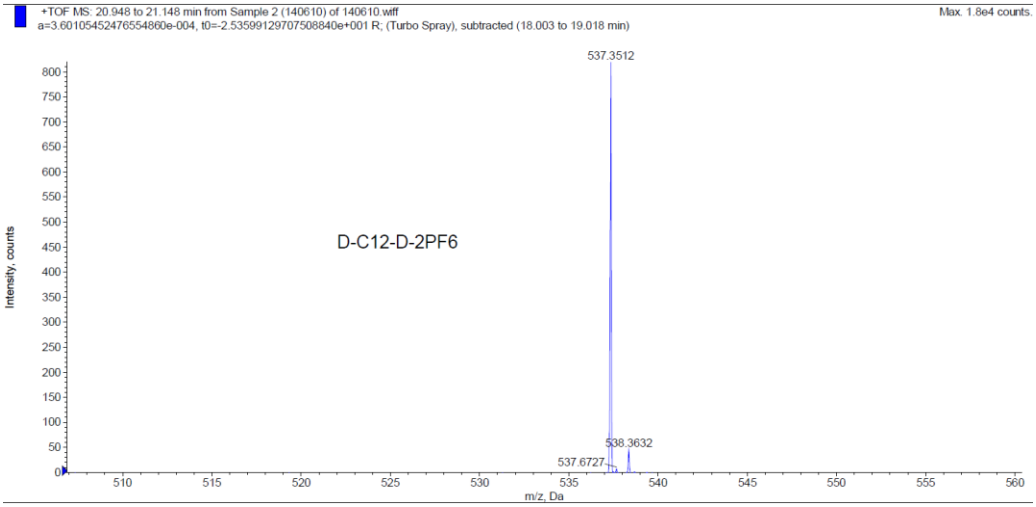


ESI-TOF mass spectrum of **D12D-2PF$_6$**

**Guest ADA-2PF$_6$**

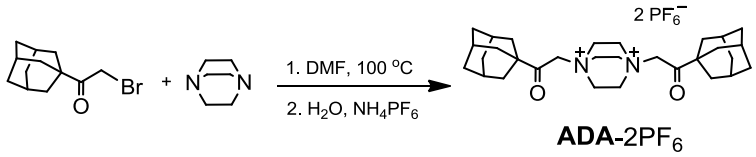


DABCO (100 mg, 0.89 mmol) in DMF (3 mL) was added dropwise into the solution of 1-Adamantyl bromoethyl ketone (687 mg, 2.7 mmol ) in DMF (10 mL) at 100 $^{o}$C in the period of 1 h. The resulting mixture was stirred at the same temperature for another 5 h. The solution was then cooled to room temperature, and the precipitate was filtered off and washed with diethyl ether (50 mL) and $CH_2Cl_2$ (20 mL). The filter cake was then dried in vacuum to give **ADA**-2Br (493 mg, 88%) as a white solid. The solution of $NH_4PF_6$ (650 mg, 4 mmol) in $H_2O$ (10 mL) was added dropwise into the solution of **ADA**-2Br (250 mg, 399 µmol) in $H_2O$ (15 ml). The mixture was stirred at room temperature for 6 h. The precipitate was collected by filtration and dried in vacuum to give **ADA**-2PF$_6$ (270 mg, 89% yield) as a white solid. $^{1}$H NMR (400 MHz, $CD_3CN$, 298 K): δ [ppm] = 4.59 (s, 4H), 4.02 (s, 12H), 2.09 – 2.04 (m, 6H), 1.85 (d, *J* = 2.4 Hz, 12H), 1.82 – 1.68 (m, 12H); $^{13}$C NMR (100 MHz, $CD_3CN$, 298 K): δ [ppm] = 206.84, 66.20, 52.60, 47.72, 37.75, 36.66, 28.52; ESI-TOF-HRMS: *m/z* calcd for $[M\text{-}PF_6]^+$ $C_{30}H_{46}F_6N_2O_2P^+$, 611.3196; found 611.3185 (100%).

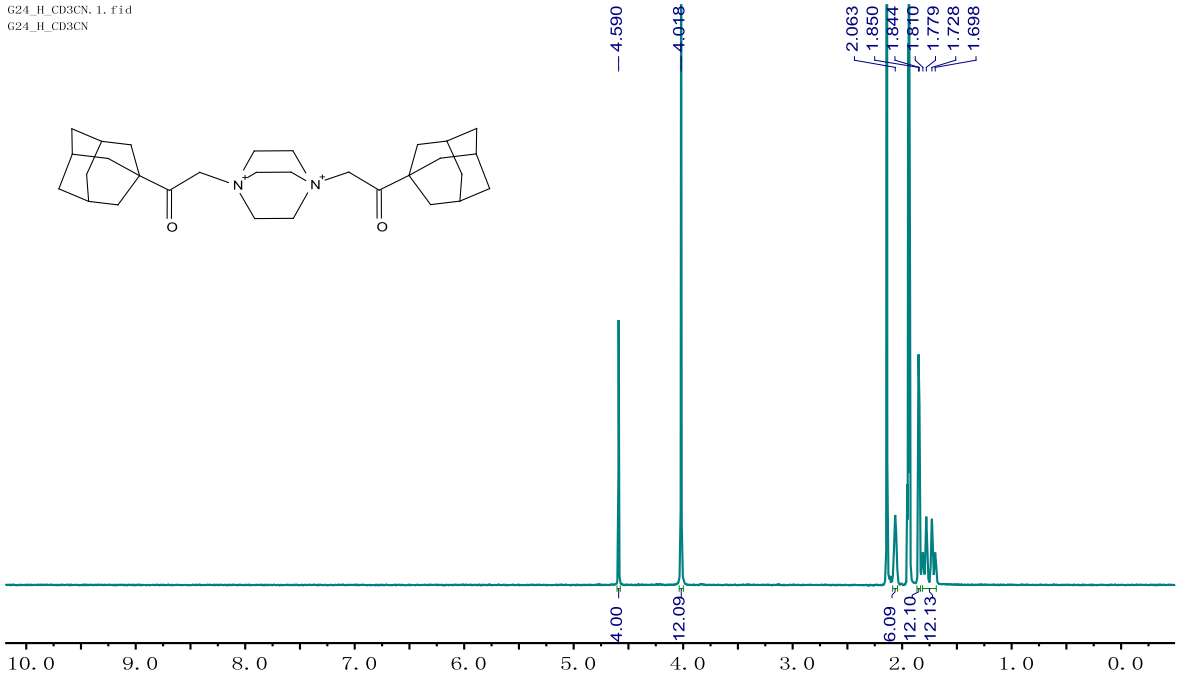


$^{1}$H NMR spectrum (400 MHz, $CD_3CN$, 298 K) of **ADA**-2$PF_6$

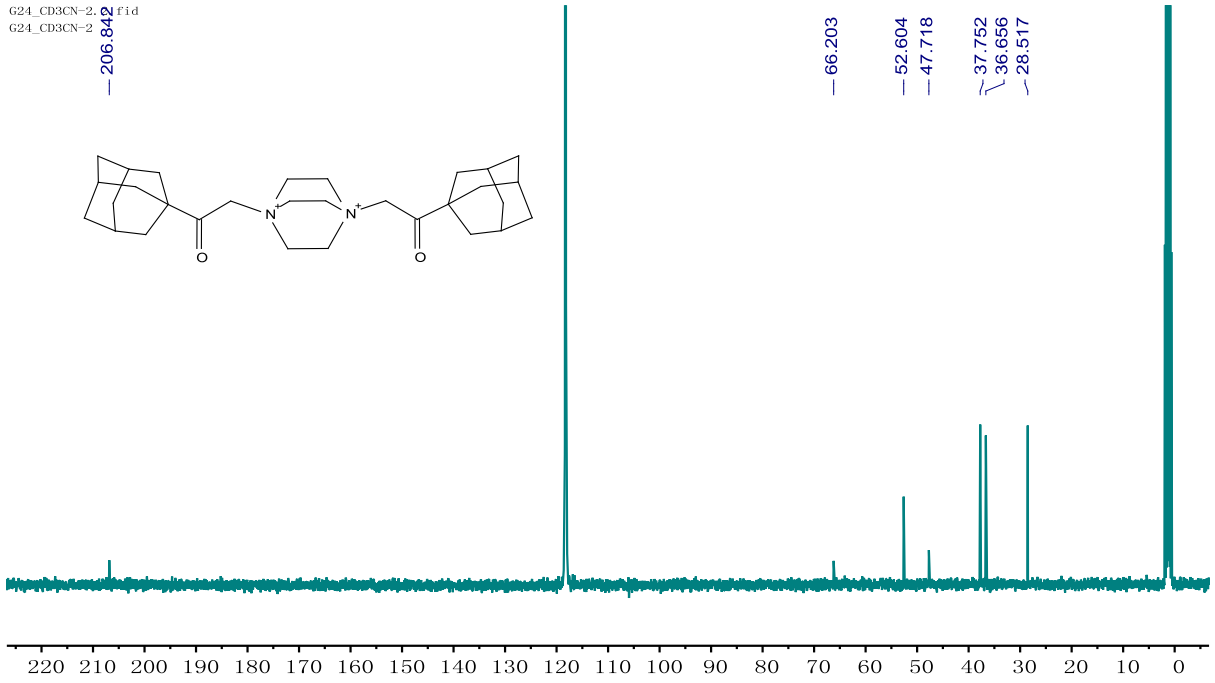


$^{13}$C NMR spectrum (100 MHz, $CD_3CN$, 298 K) of **ADA**-2$PF_6$

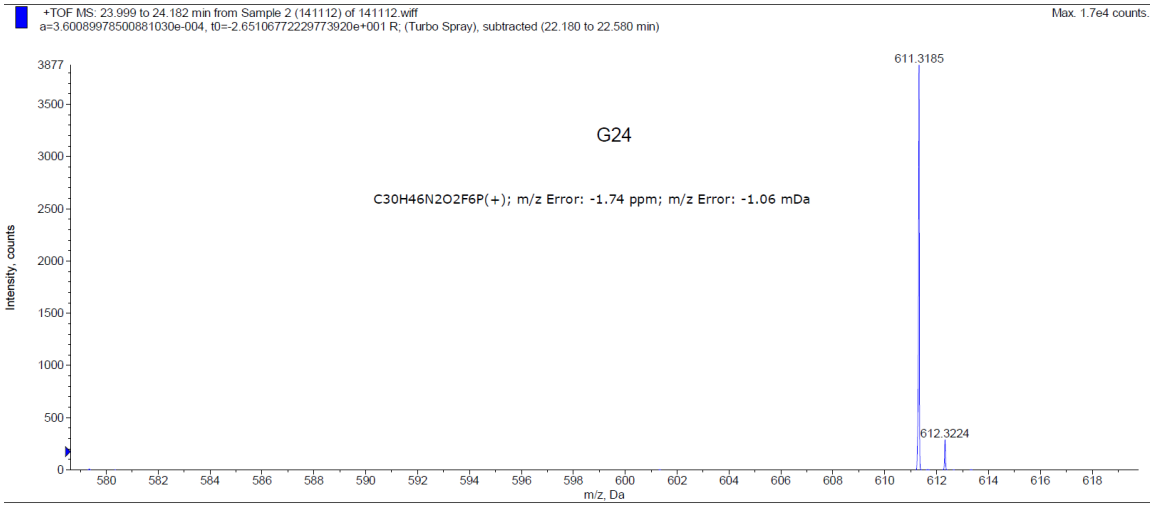


ESI-TOF mass spectrum of **ADA**-2$PF_6$

## 2. Properties of TA4

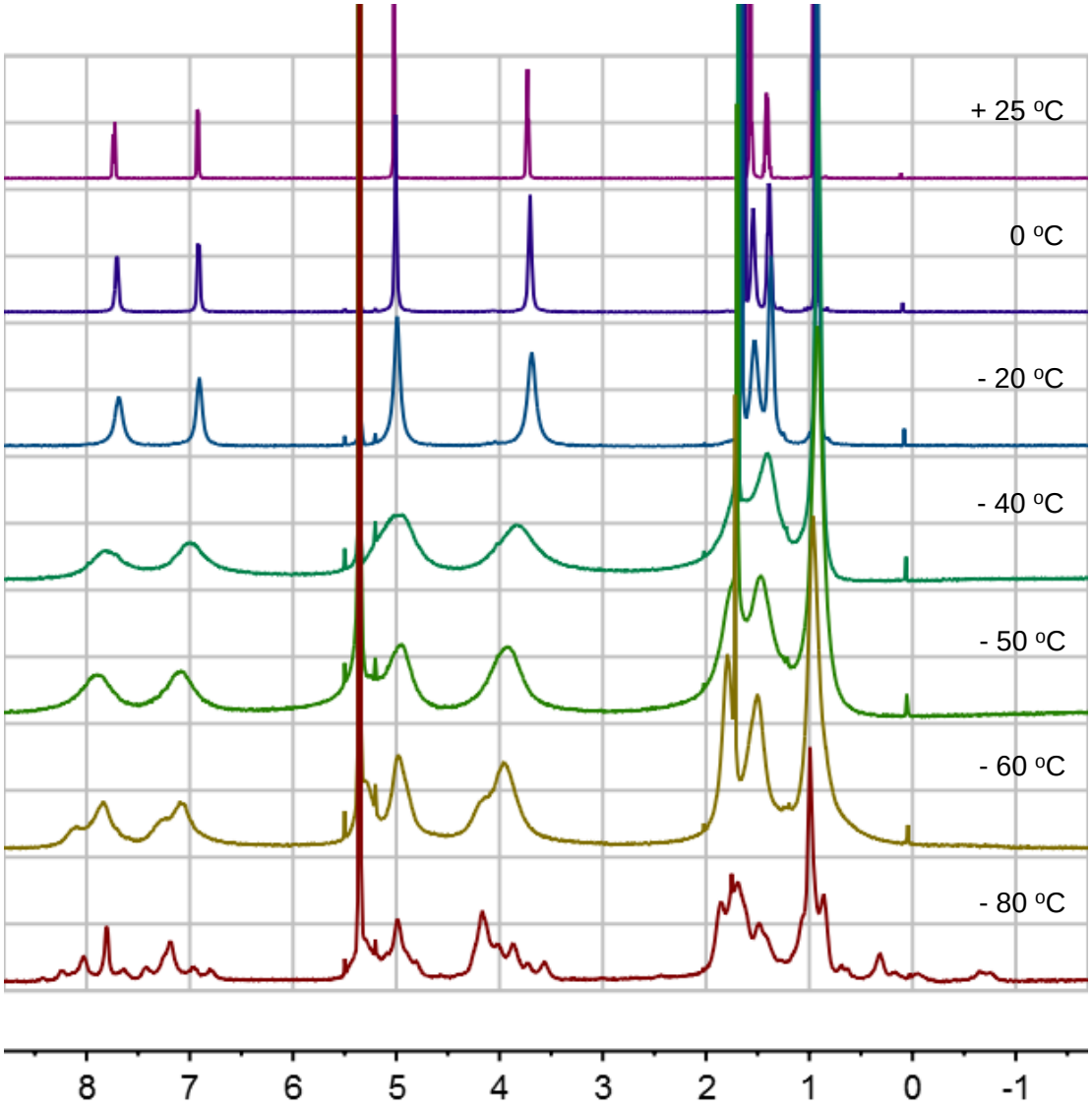


***Fig. S1.*** Variable-temperature $^{1}$H NMR spectra (600 MHz, $CD_2Cl_2$) of **TA4**. At – 40 °C, the peaks start to be broadened. The splitting of peaks is only observable until – 60 °C. At – 80 °C, more peaks are detected and the peaks become slightly sharper. This is not due to aggregated structures (see Fig. S2). Although the flexible **TA4** has numerous conformations, the four conformers, resulting from the naphthalene ring flipping, should have much higher interconversion barriers. Therefore, the peak broadening and splitting of **TA4** at low temperatures is presumably due to the slower interconversion among the four conformers. However, due to the complexity of NMR spectra, it is difficult to determine the activation barrier. But we know the ring flipping for **TA4** with butyl groups is every quick at room temperature, affording quick conformational interconversion.

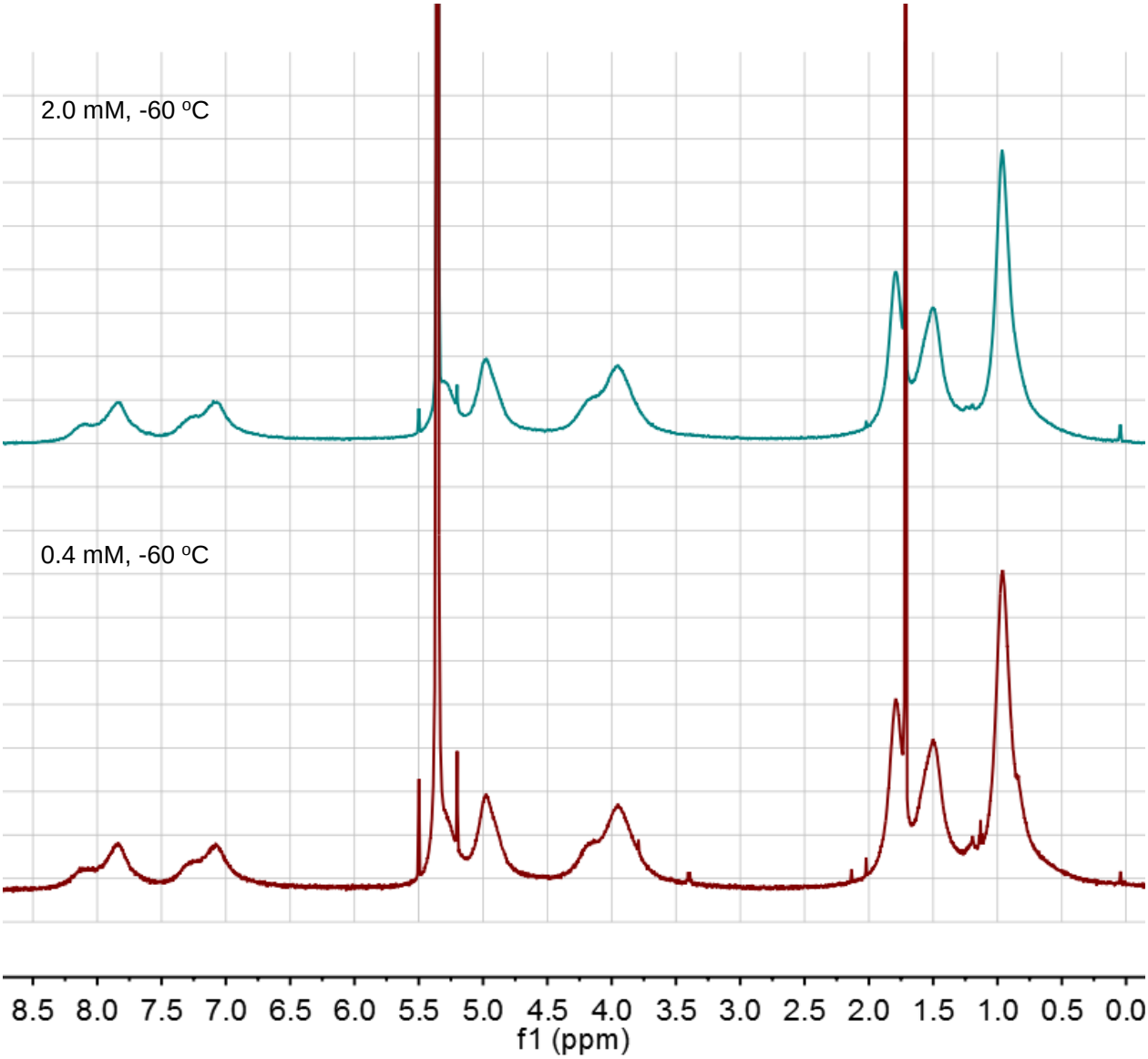


***Fig. S2.*** $^{1}$H NMR spectra (600 MHz, $CD_2Cl_2$, – 60 $^{o}$C) of **TA4** at two different concentrations. The peak numbers and peak shapes are exactly the same, suggesting the peak splitting and broadening of **TA4** at low temperatures (Fig. S1) is not due to aggregated structures (dimeric, trimeric, etc.). Therefore, these experiments support the existence of four conformers resulting from the flipping of naphthalene ring.

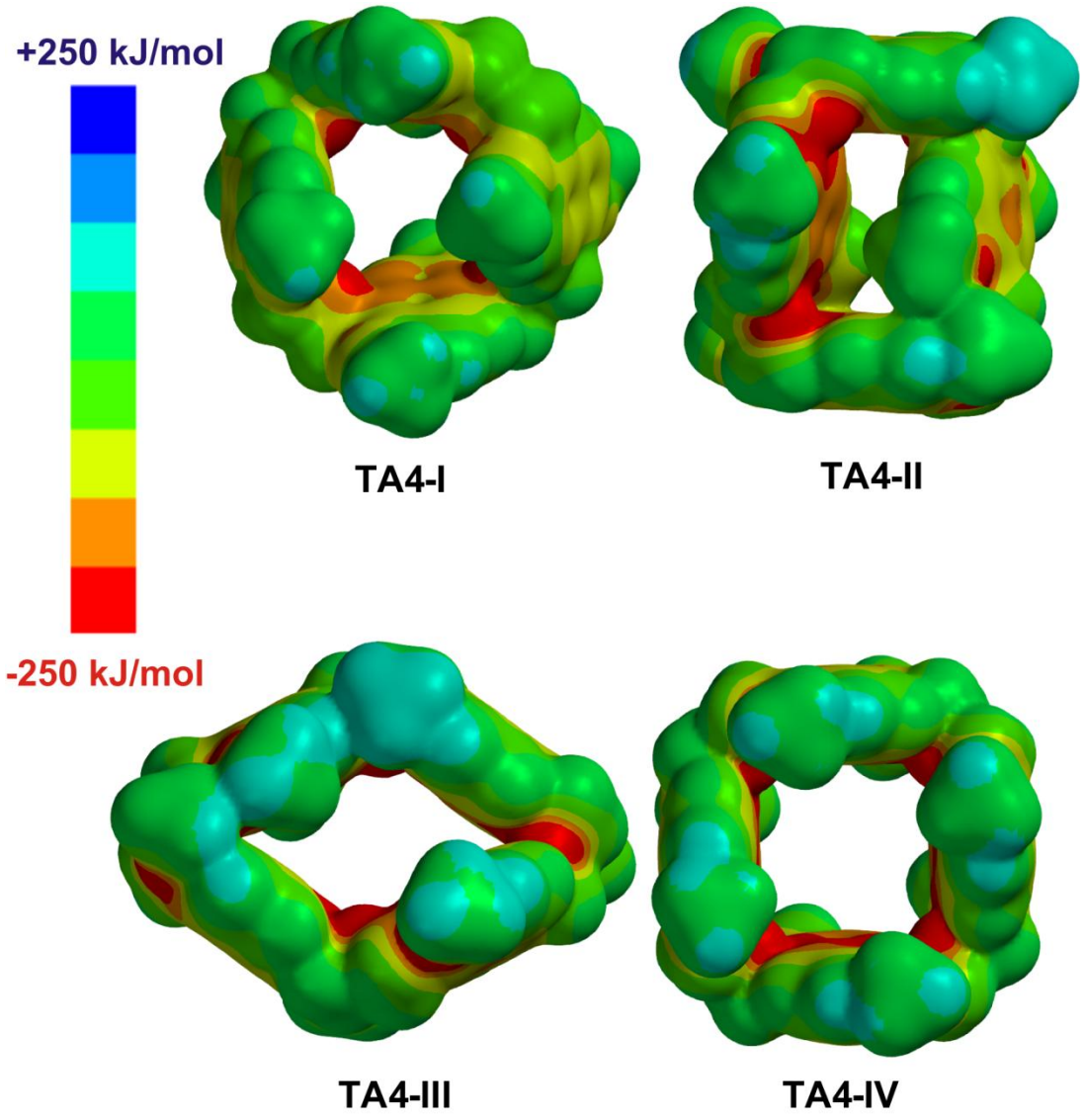


***Fig. S3.*** Electrostatic potential surfaces of four conformers of **TA4**. These structures were optimized at the AM1 level of theory by using Spartan ’14 (Wavefunction, Inc.). Methyl groups were used instead of butyl groups in the models for viewing clarity. Obviously, all the conformers of **TA4** are electron-rich in their cavities, providing good host environment for organic cations.

## 3. Guesting Binding Property of TA4

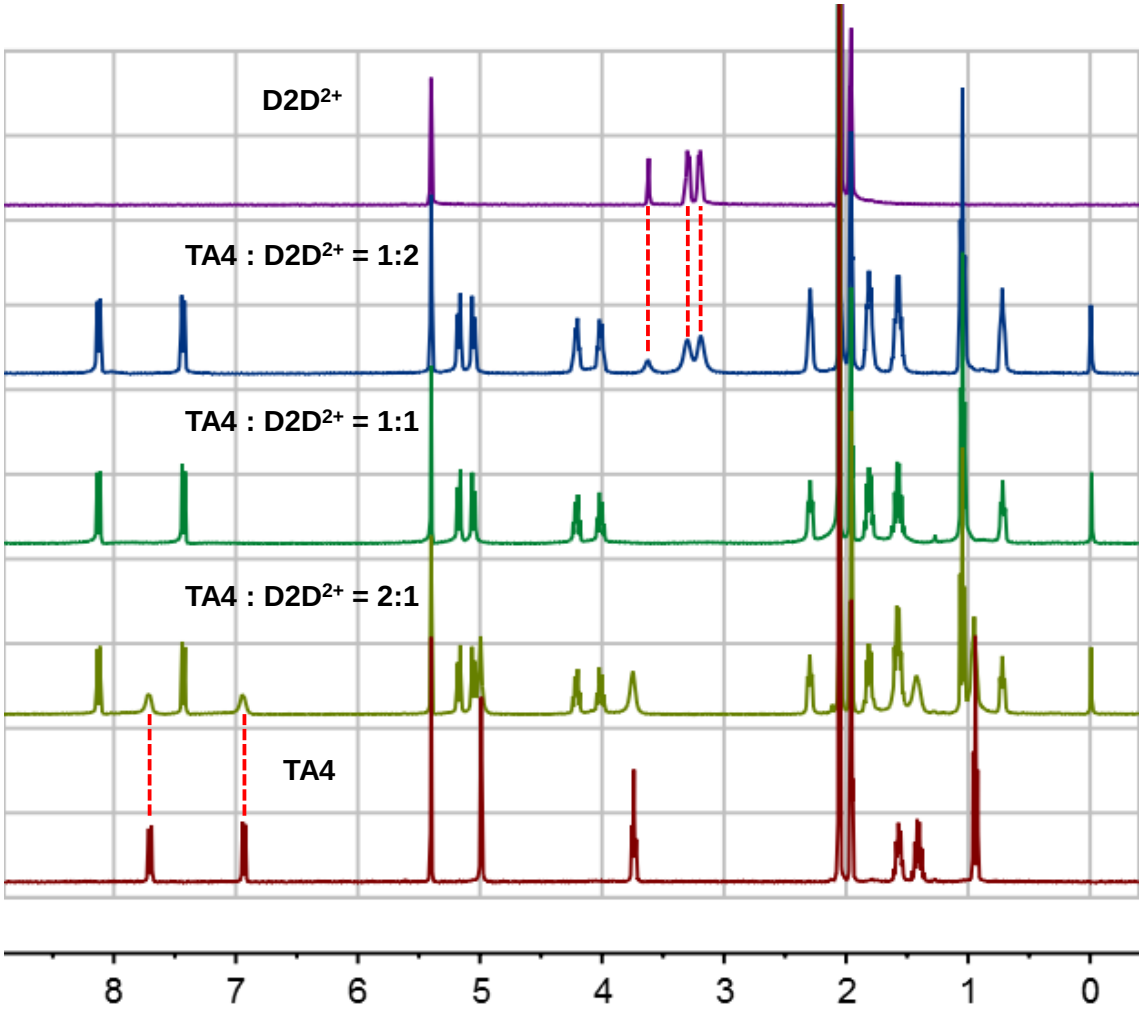


***Fig. S4.*** Full $^{1}$H NMR spectra (400 MHz, $CD_2Cl_2$:$CD_3CN$=1:1, 2.0 mM, 298 K) of **TA4**, **D2D**$^{2+}$, and their mixture in 2:1, 1:1, and 1:2 ratio. These experiments suggest that the complex between **TA4** and **D2D**$^{2+}$ undergoes slow exchange at the current NMR timescale. Thus, the complete disappearance of free host and free guest in the 1:1 mixture of **TA4** and **D2D**$^{2+}$ indicates a very strong binding between them. We assume that the detection limit of the NMR instrument to be 10%, and use the current concentration 2.0 mM. We may estimate the binding constant to be $(0.90\times2.0\text{mM})/(0.10\times2.0\text{mM})^2 = 4.5\times10^4$ $M^{-1}$. Thus, the binding constant between **TA4** and **D2D**$^{2+}$ should be bigger than $10^4$ $M^{-1}$, which is beyond the measuring limit by $^{1}$H NMR spectroscopy. This binding strength is true for the complex between **TA4** and the corresponding guests involved in this research, since no free host or guest is detected in the corresponding equimolar mixture.

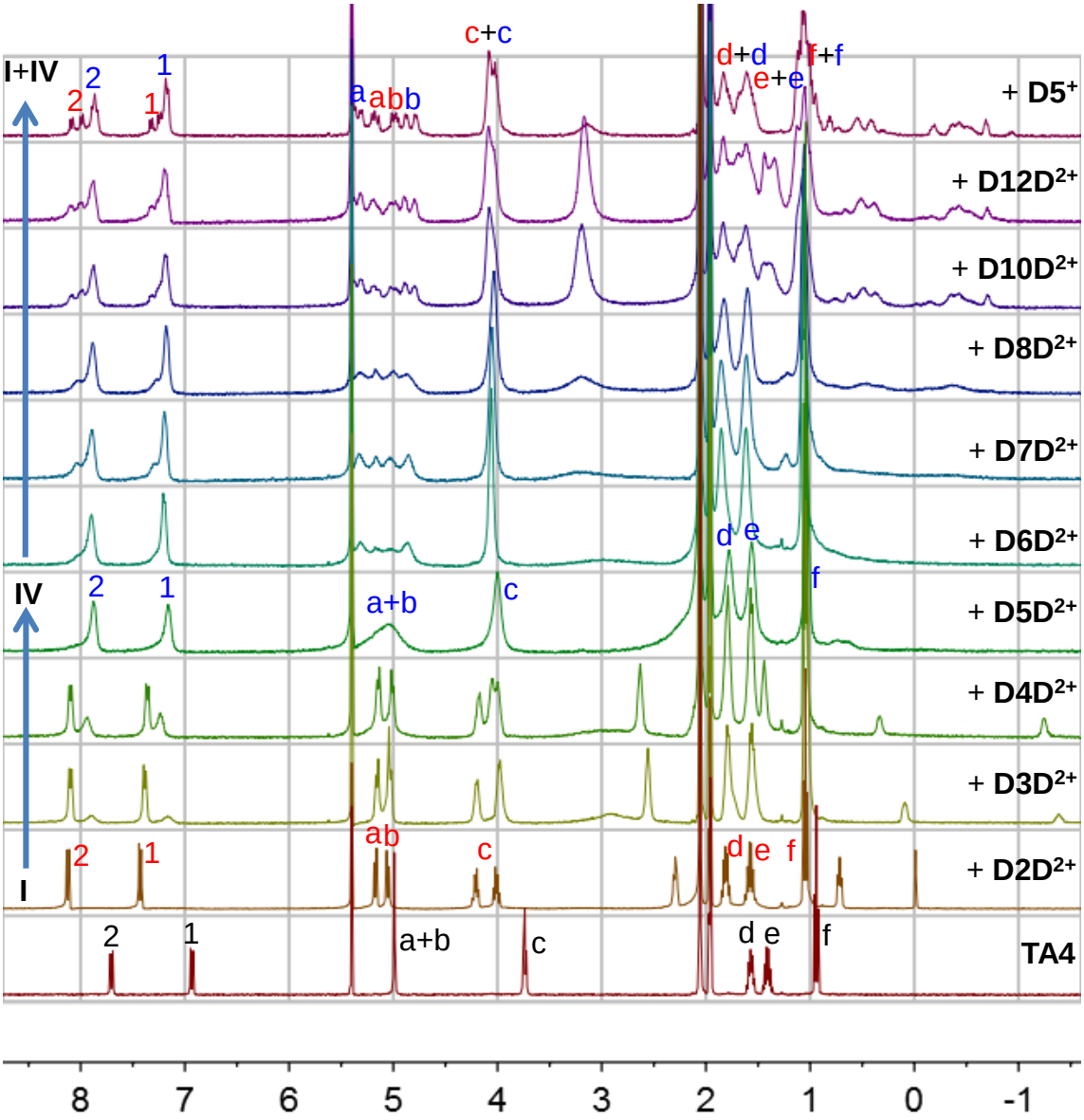


***Fig. S5.*** Full $^{1}$H NMR spectra (400 MHz, $CD_2Cl_2$:$CD_3CN$=1:1, 2.0 mM, 298 K) of **TA4** in the absence and the presence of one equivalent of individual guest **D2D**$^{2+}$ - **D12D**$^{2+}$ or **D5**$^{+}$. The assignments of conformers are based on 2D NMR and single crystal structure. From guest **D2D**$^{2+}$ to **D5D**$^{2+}$, **TA4** gradually change from conformer **I** to conformer **IV**; from **D5D**$^{2+}$ to **D12D**$^{2+}$, conformer **I** re-appear with conformer **IV** still present. For the guest with long linker between two DABCO groups, only one DABCO is encapsulated in the cavity of **TA4**. Thus, this guest is similar to guest **D5**$^{+}$, which is supported by the similar appearance of NMR spectra. In addition, these guests can bind to two TA4 through two DABCO (see below for NMR and MS evidence). All the complexes are confirmed by ESI-HRMS experiments (see below).

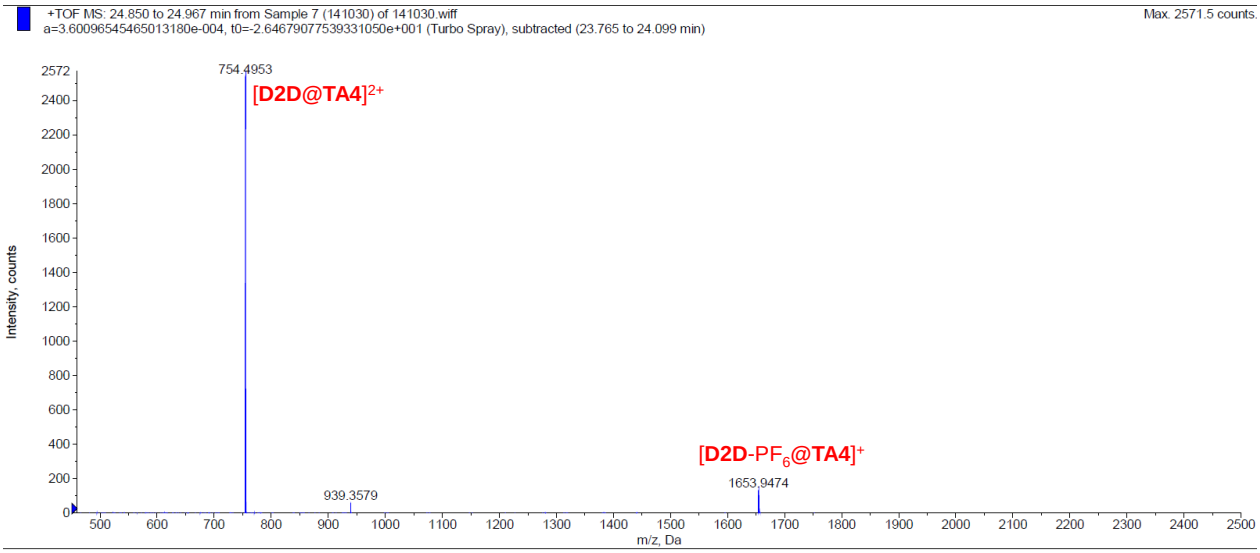


***Fig. S6.*** ESI-TOF mass spectrum of **D2D**-2$PF_6$**@TA4**. The result indicates **D2D**-2$PF_6$ and **TA4** form a 1:1 complex.

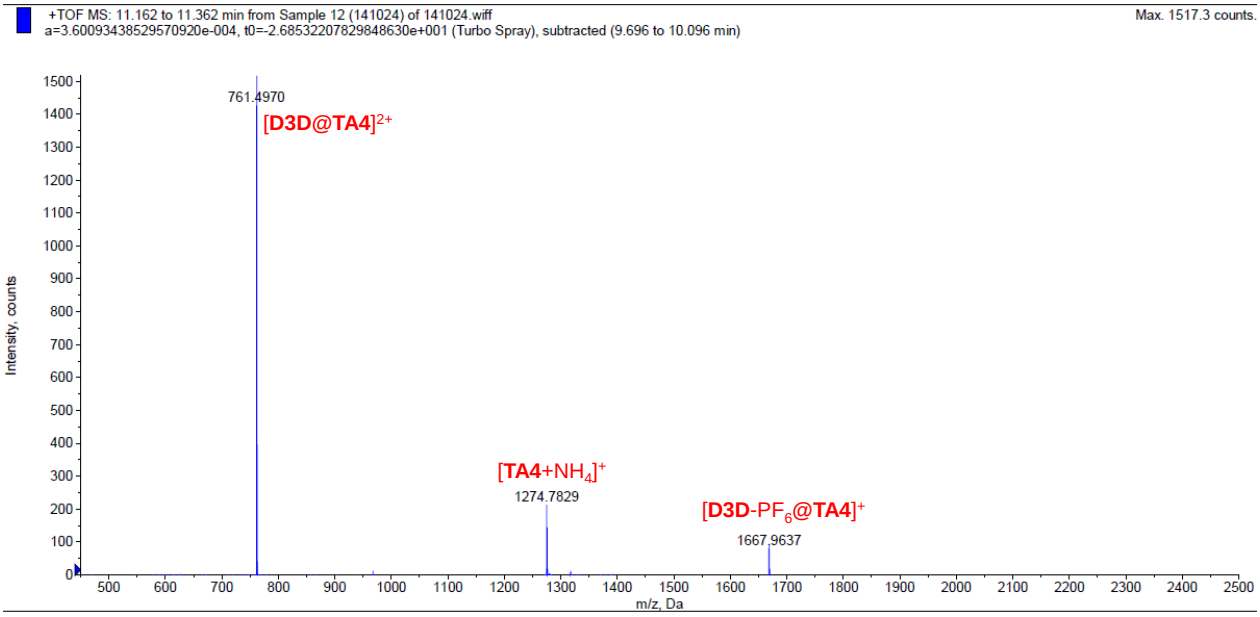


***Fig. S7.*** ESI-TOF mass spectrum of **D3D**-2$PF_6$**@TA4**. The result indicates **D3D**-2$PF_6$ and **TA4** form a 1:1 complex.

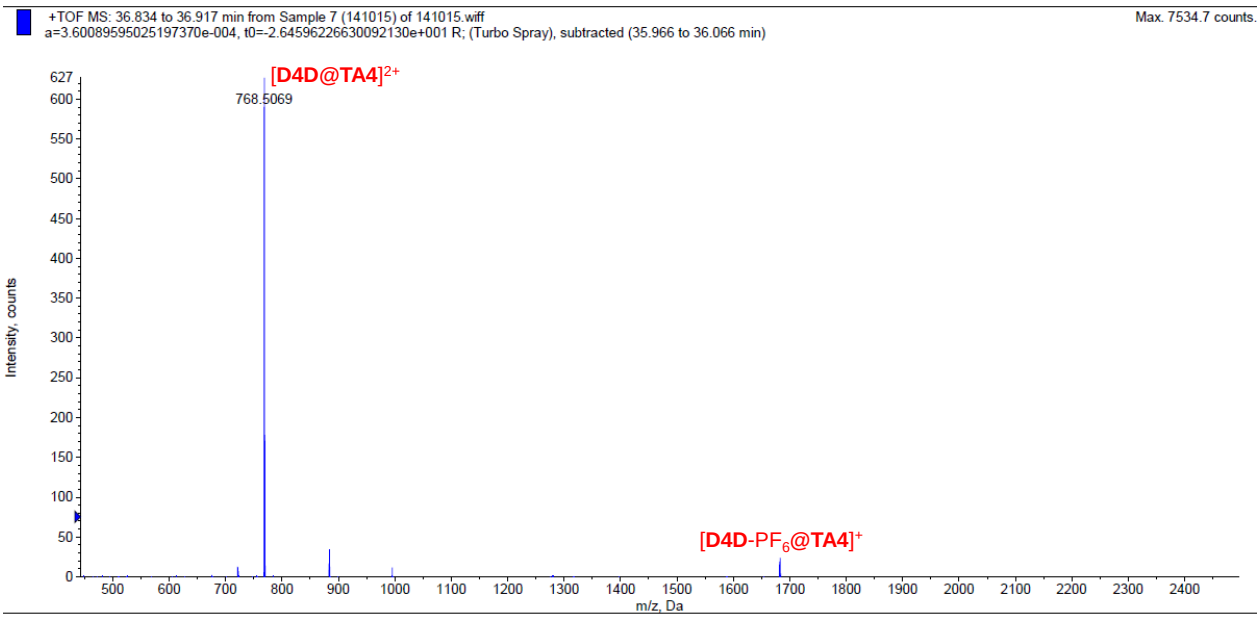


***Fig. S8.*** ESI-TOF mass spectrum of **D4D-**2$PF_6$**@TA4**. The result indicates **D4D-**2$PF_6$ and **TA4** form a 1:1 complex.

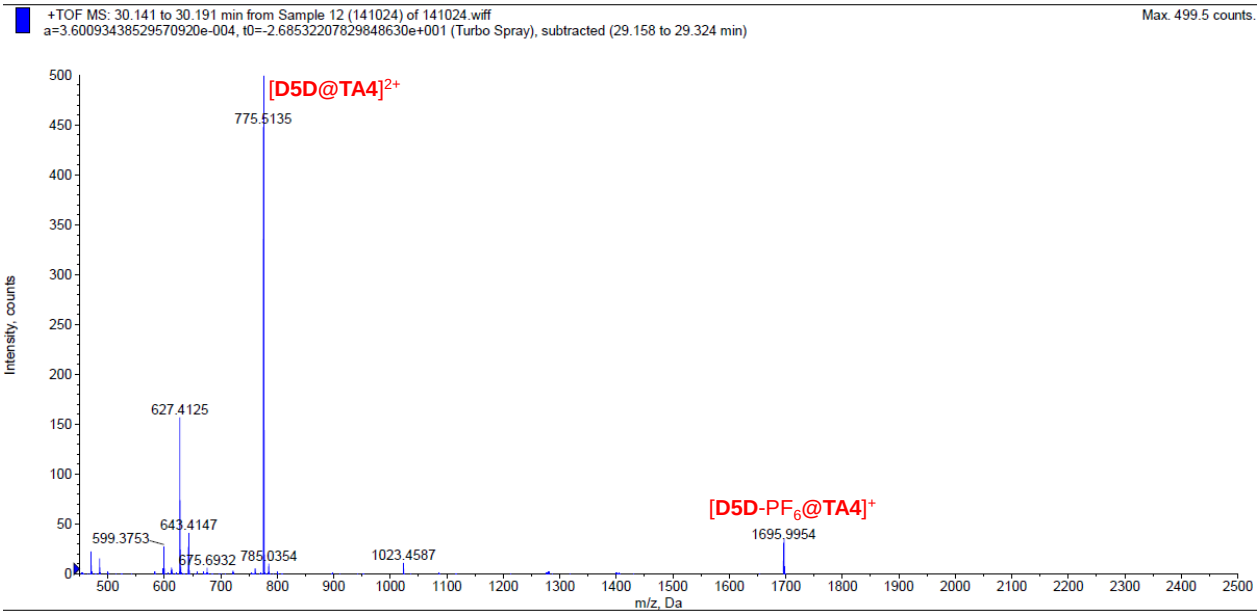


***Fig. S9.*** ESI-TOF mass spectrum of the 1:1 mixture of **TA4** and **D5D-**2$PF_6$. The result indicates **D5D-**2$PF_6$ and **TA4** only form a 1:1 complex in this solution.

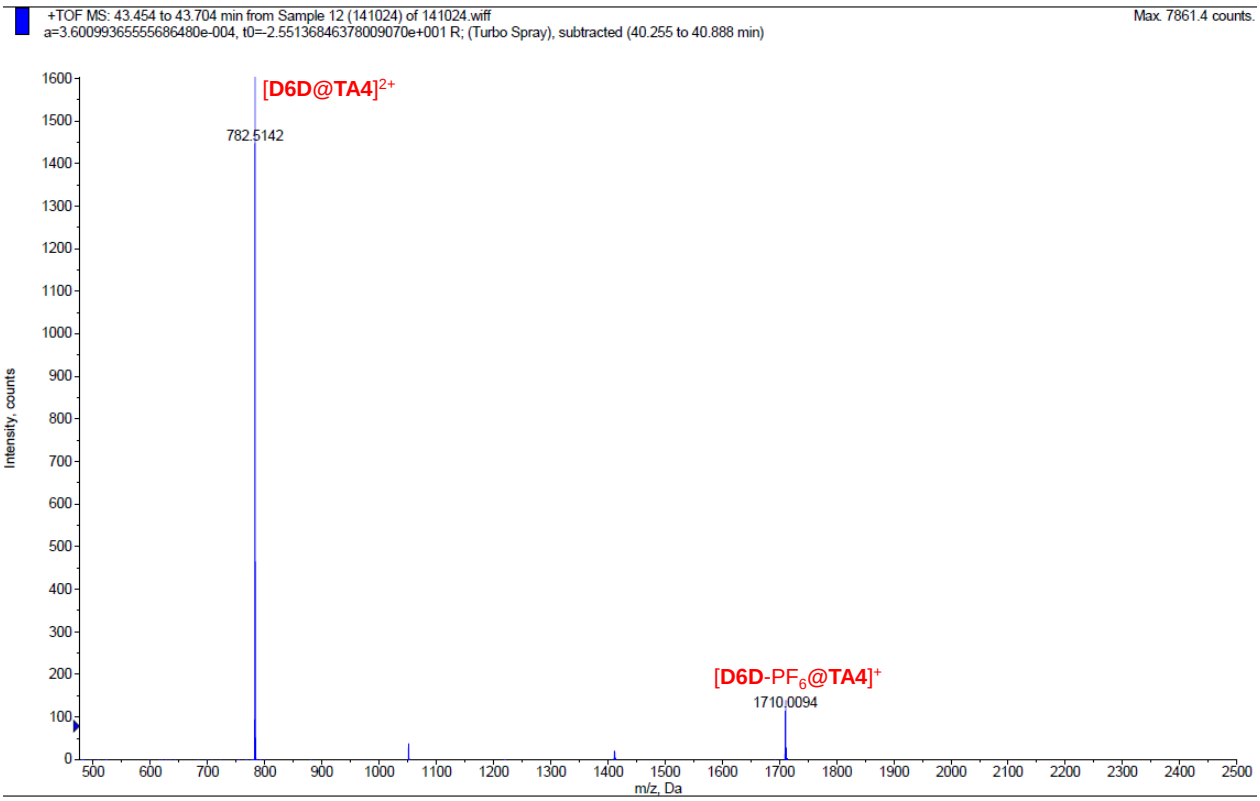


***Fig. S10.*** ESI-TOF mass spectrum of the 1:1 mixture of **TA4** and **D6D-**$2PF_6$. The result indicates **D6D-**$2PF_6$ and **TA4** mainly form a 1:1 complex in this solution.

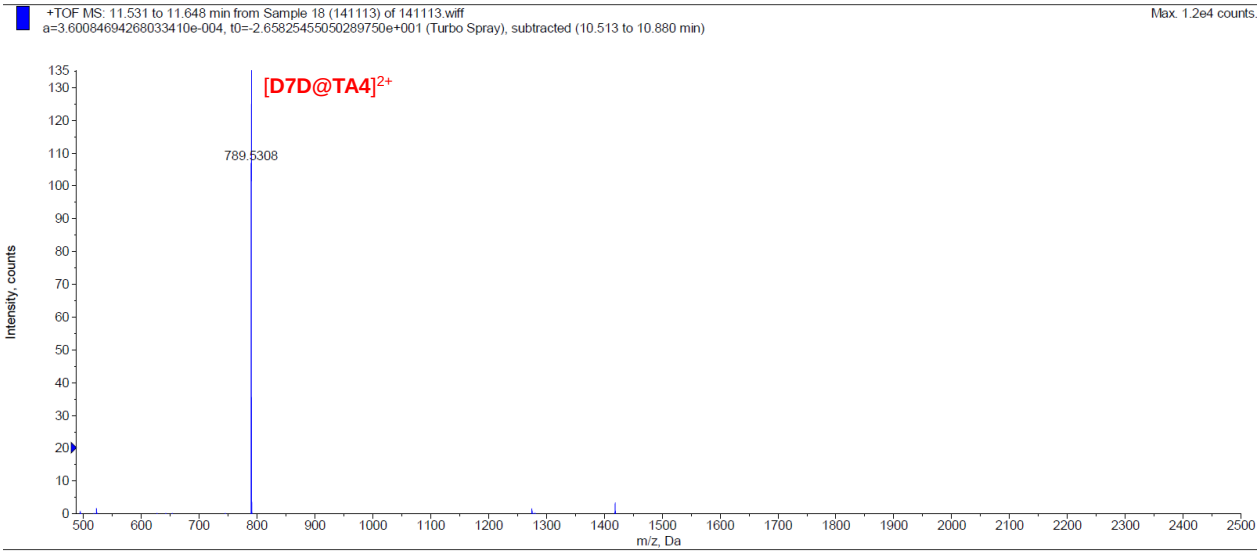


***Fig. S11.*** ESI-TOF mass spectrum of the 1:1 mixture of **TA4** and **D7D-**$2PF_6$. The result indicates **D7D-**$2PF_6$ and **TA4** mainly form a 1:1 complex in this solution.

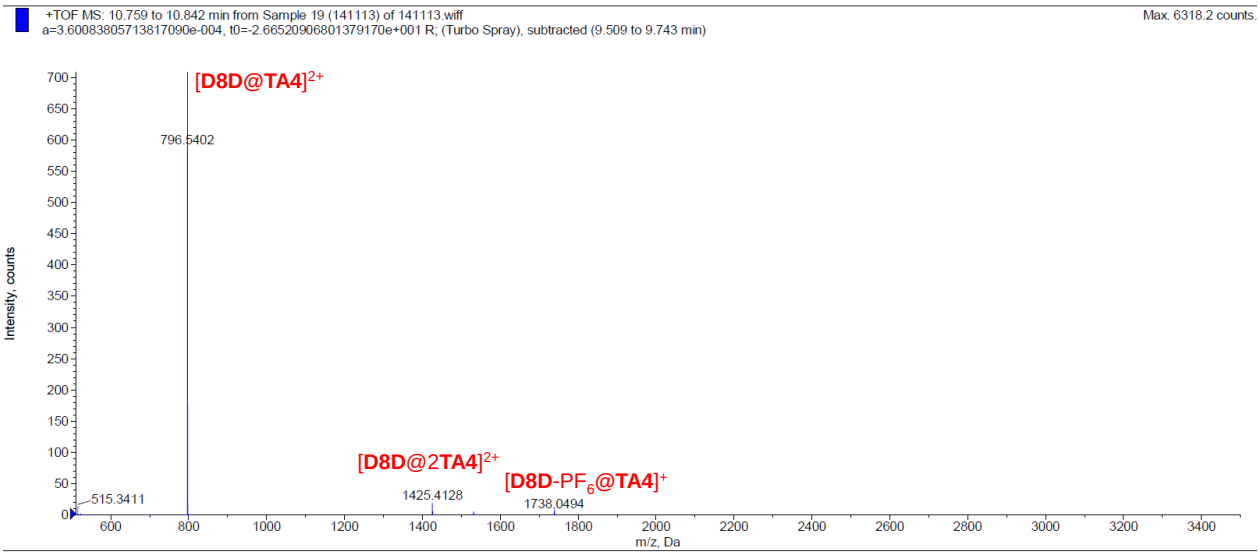


***Fig. S12.*** ESI-TOF mass spectrum of the 1:1 mixture of **TA4** and **D8D-**$2PF_6$. The result indicates **D8D-**$2PF_6$ and **TA4** mainly form a 1:1 complex, but 1:2 complex also exist.

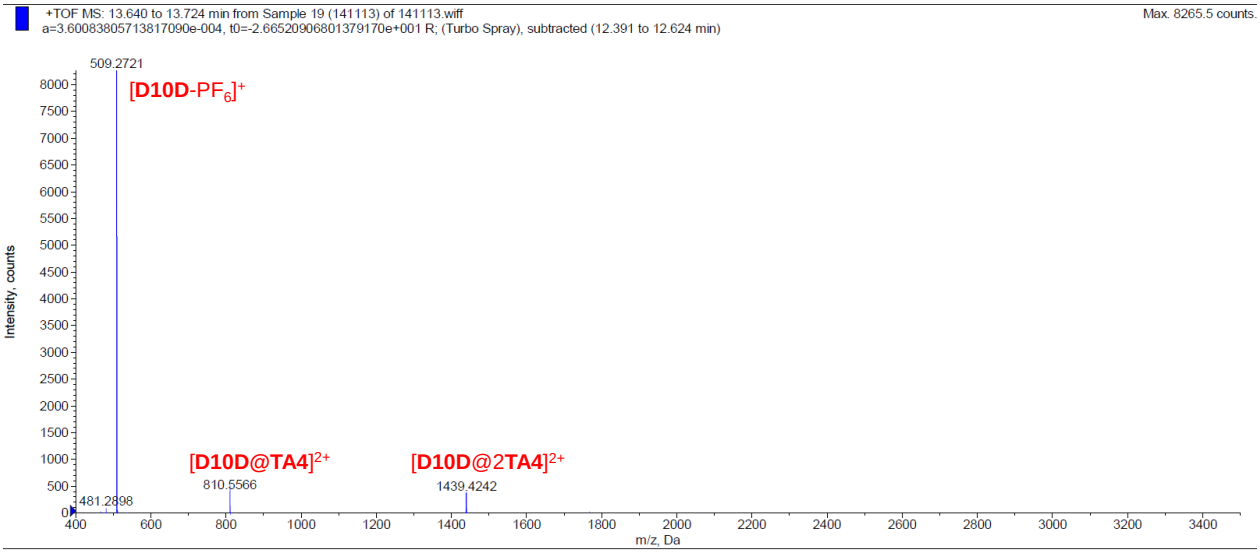


***Fig. S13.*** ESI-TOF mass spectrum of the 1:1 mixture of **TA4** and **D10D-**$2PF_6$. The result indicates **D10D-**$2PF_6$ and **TA4** form a 1:1 complex, but 1:2 complex also exist.

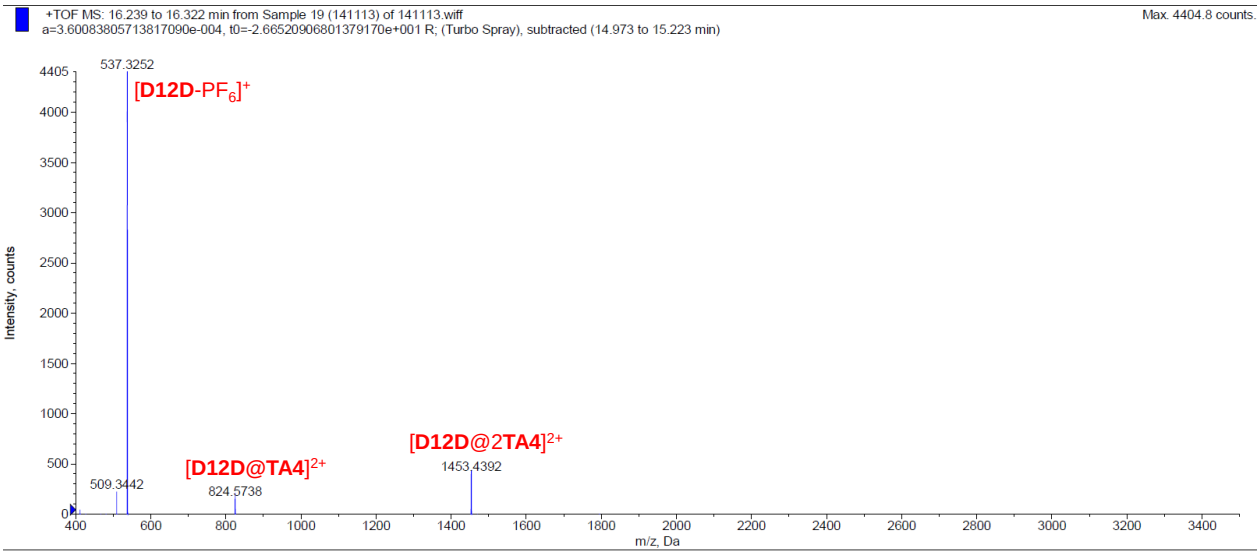


***Fig. S14.*** ESI-TOF mass spectrum of the 1:1 mixture of **TA4** and **D12D**-$2PF_6$. The result indicates **D12D**-$2PF_6$ and **TA4** form a 1:1 complex, but 1:2 complex also exist.

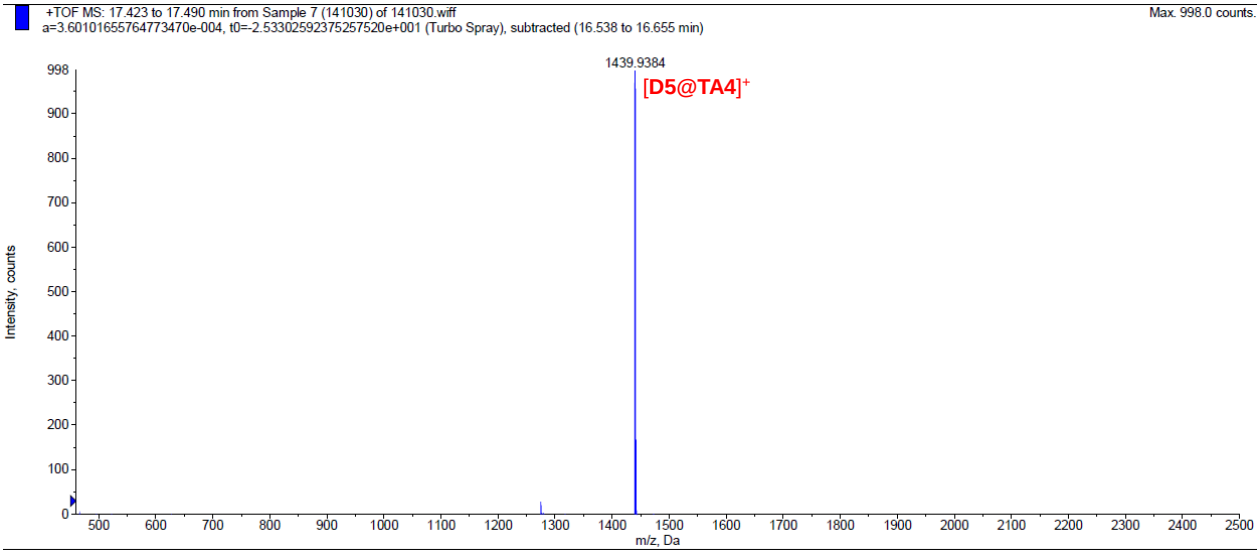


***Fig. S15.*** ESI-TOF mass spectrum of **D5**-$PF_6$**@TA4**. The result indicates **D5**-$PF_6$ and **TA4** form a 1:1 complex.

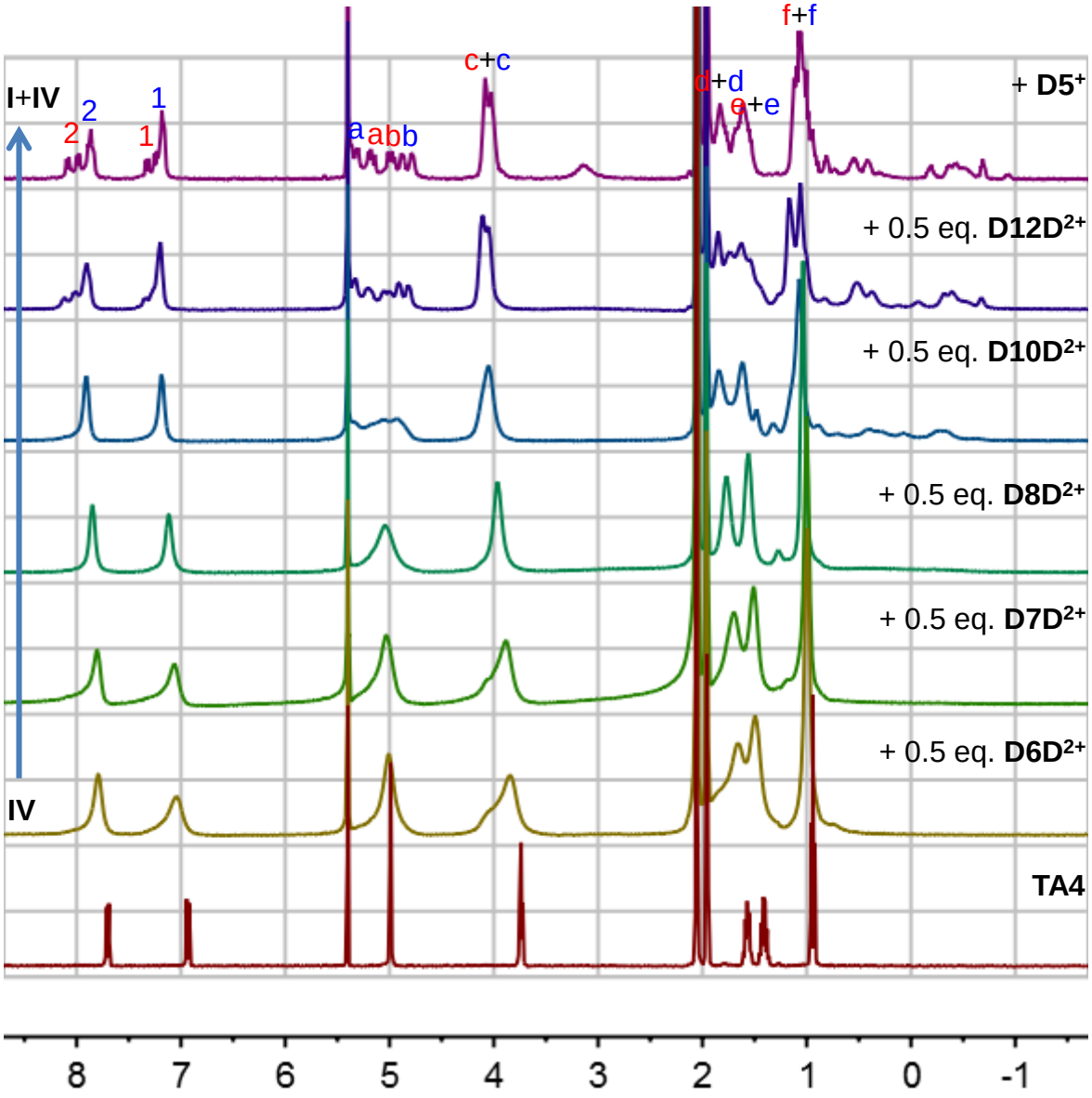


***Fig. S16.*** Full $^{1}$H NMR spectra (400 MHz, $CD_2Cl_2$:$CD_3CN$=1:1, 2.0 mM, 298 K) of **TA4** in the absence and the presence of $\mathbf{D5}^{+}$ or 0.5 equivalent of individual guest $\mathbf{D6D}^{2+}$ - $\mathbf{D12D}^{2+}$. The appearances of these NMR spectra are different from those with one equivalent of guest. In addition, no free host was detected. These results suggest each of the two DABCOs on these guests can take one TA4 to form a ternary complex, which is supported by ESI-HRMS experiments (see below).

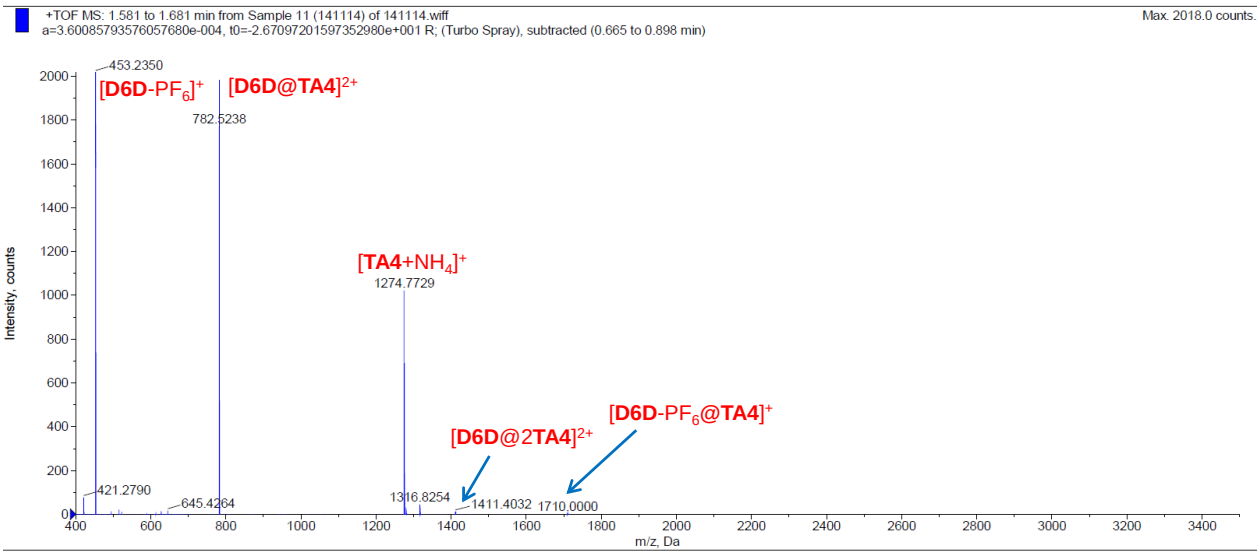


***Fig. S17.*** ESI-TOF mass spectrum of the 2:1 mixture of **TA4** and **D6D-**$2PF_6$. The result indicates **TA4** and **D6D-**$2PF_6$ mainly form a 1:1 complex in this solution, but the 2:1 complex also exists.

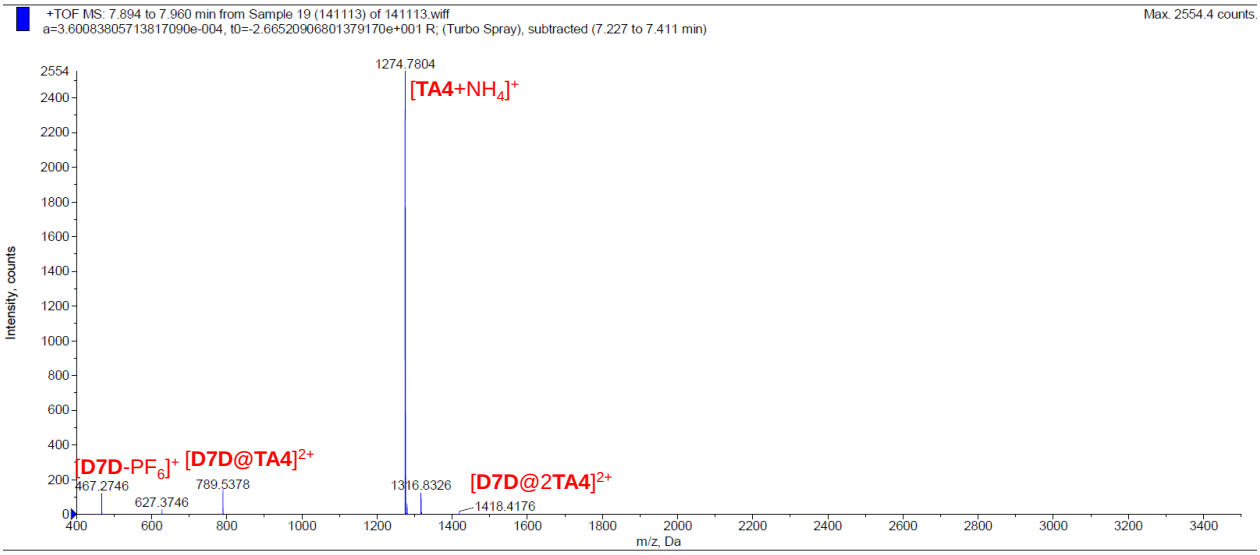


***Fig. S18.*** ESI-TOF mass spectrum of the 2:1 mixture of **TA4** and **D7D-**$2PF_6$. The result indicates the 2:1 complex between **TA4** and **D7D-**$2PF_6$ may exist in significant amount.

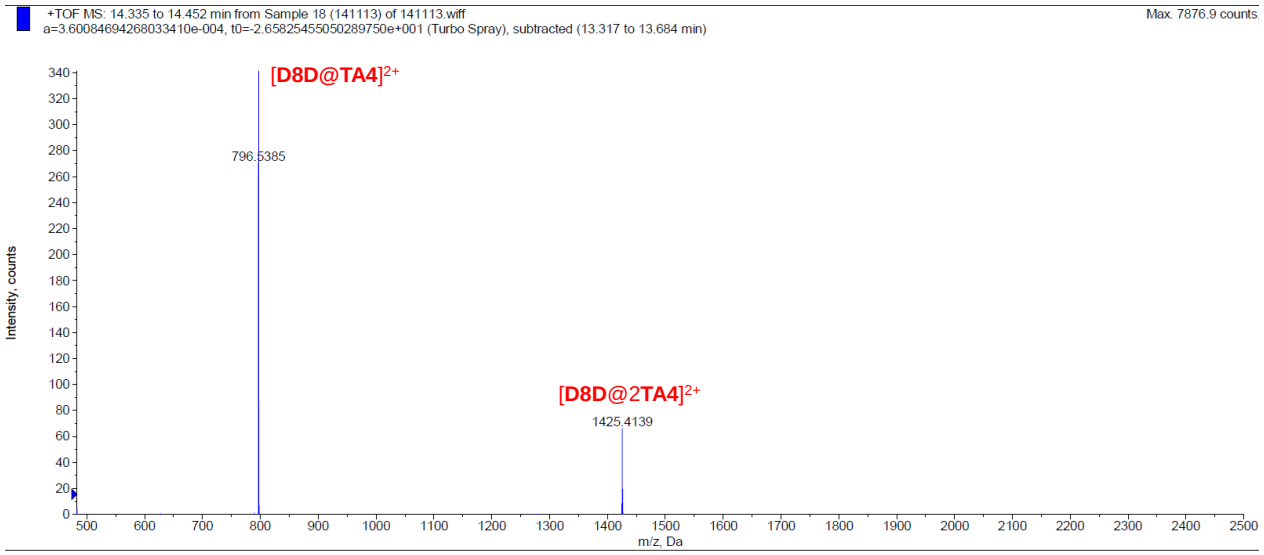


***Fig. S19.*** ESI-TOF mass spectrum of the 2:1 mixture of **TA4** and **D8D-**$2PF_6$. The result indicates the 2:1 complex between **TA4** and **D8D-**$2PF_6$ may exist in significant amount.

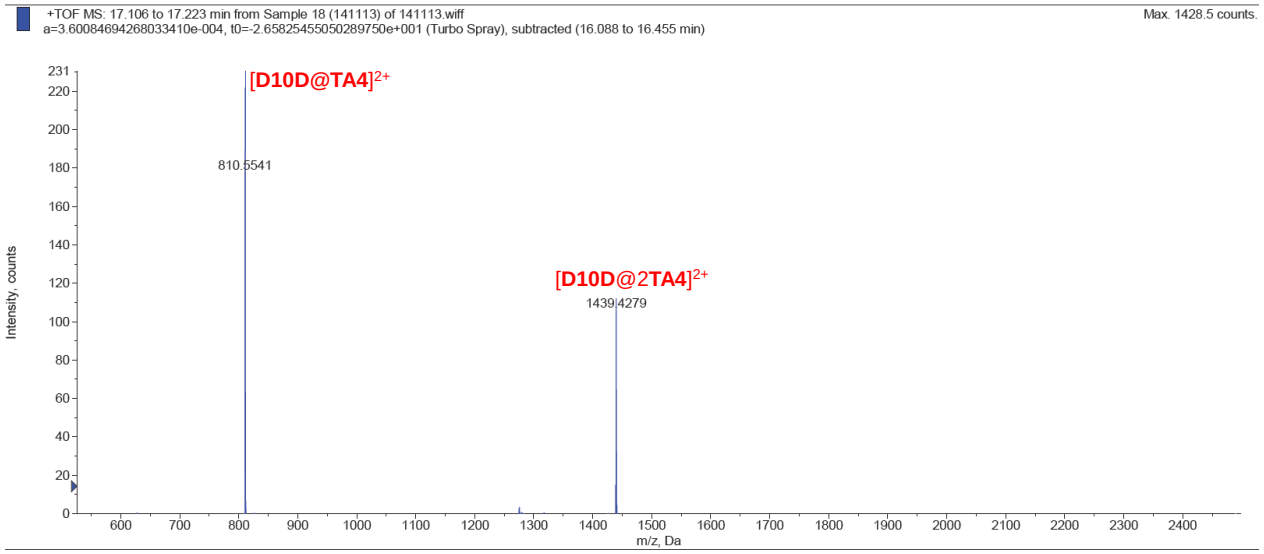


***Fig. S20.*** ESI-TOF mass spectrum of the 2:1 mixture of **TA4** and **D10D-**$2PF_6$. The result indicates the 2:1 complex between **TA4** and **D10D-**$2PF_6$ may exist in significant amount.

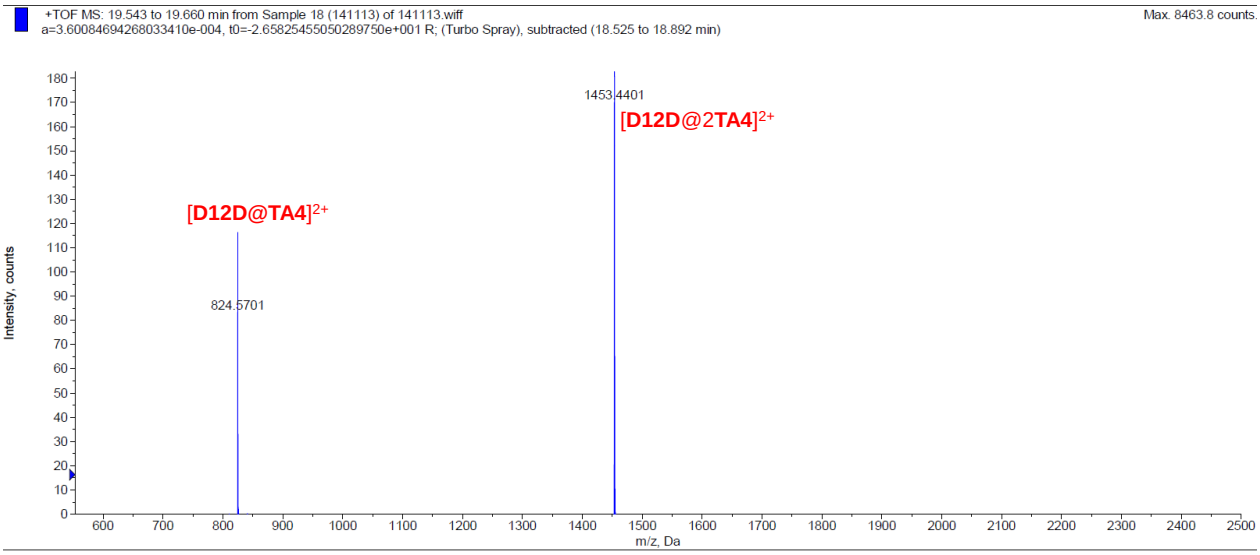


***Fig. S21.*** ESI-TOF mass spectrum of the 2:1 mixture of **TA4** and **D12D**-$2PF_6$. The result indicates the 2:1 complex between **TA4** and **D12D**-$2PF_6$ may exist in significant amount.

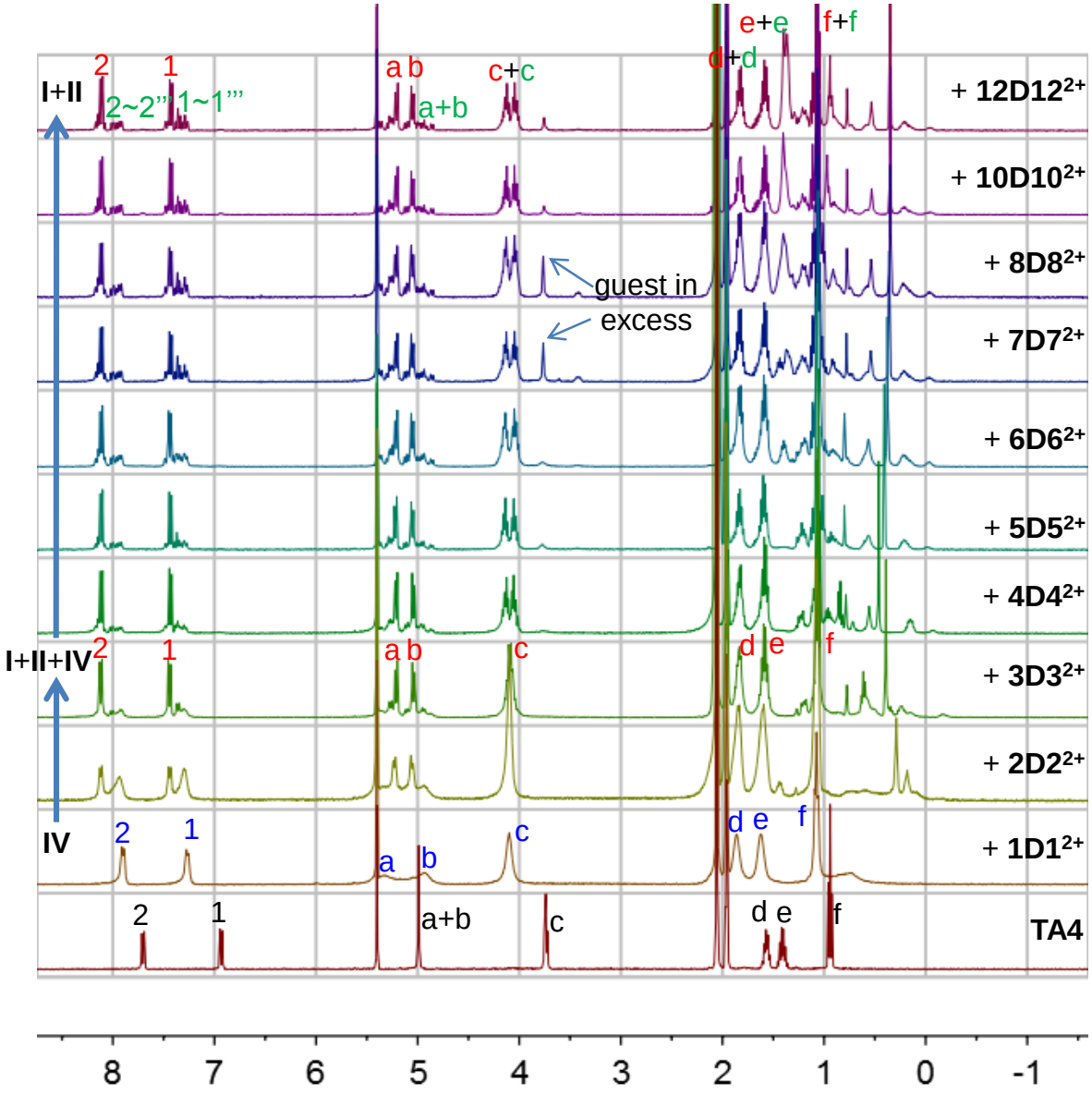


***Fig. S22.*** Full $^{1}$H NMR spectra (400 MHz, $CD_2Cl_2$:$CD_3CN$=1:1, 2.0 mM, 298 K) of **TA4** in the absence and the presence of one equivalent of individual guest **1D1**$^{2+}$ - **12D12**$^{2+}$. The assignments of conformers are based on 2D NMR, single crystal structure, and the symmetry of the host conformers. From guest **1D1**$^{2+}$ to **3D2**$^{2+}$, **TA4** gradually change from conformer **IV** to conformer **I**+**IV**; for **3D3**$^{2+}$ to **12D12**$^{2+}$, conformer **I** coexists with conformer **II**. ESI-HRMS experiments (see below) indicate these guests all form 1:1 complex with **TA4**, suggesting the DABCO is the binding site. This is in line with the large chemical shift of the protons on DABCO upon complexation.

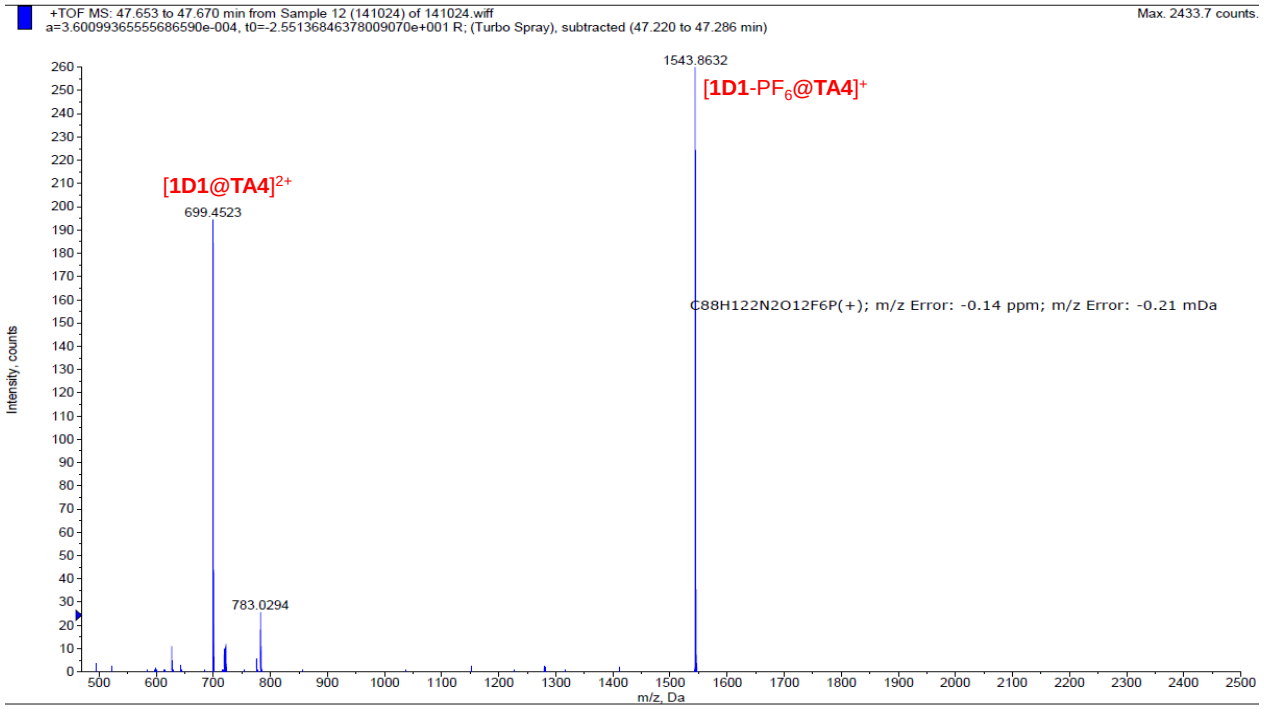


***Fig. S23.*** ESI-TOF mass spectrum of **1D1-**$2PF_6$**@TA4**. The result indicates **1D1-**$2PF_6$ and **TA4** form a 1:1 complex.

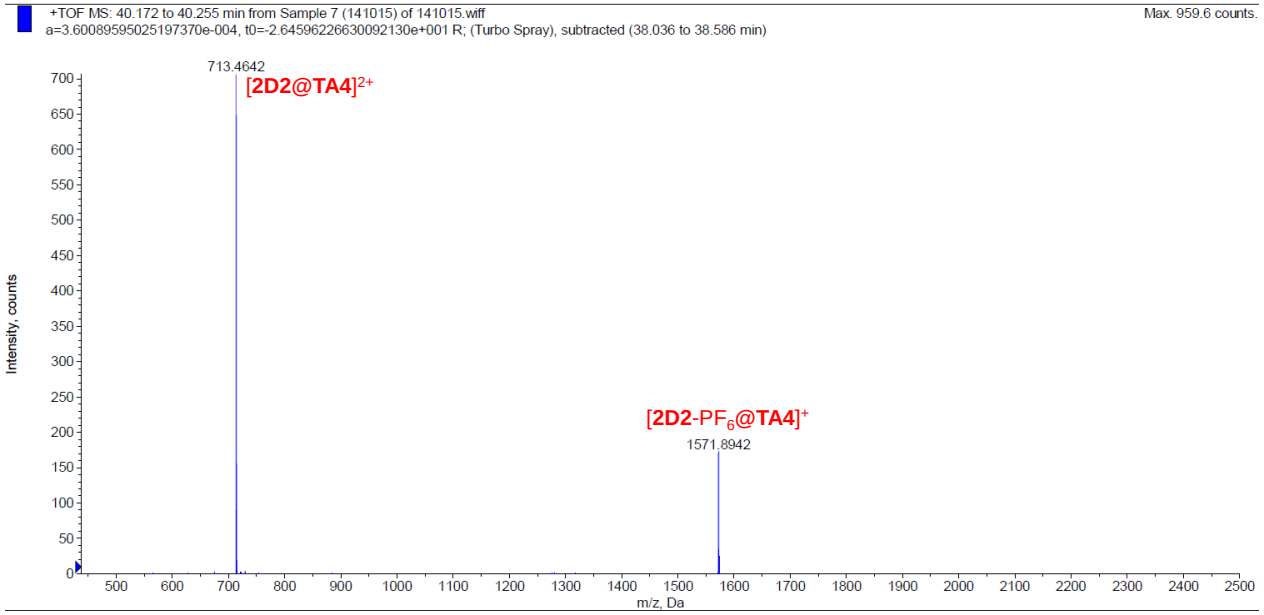


***Fig. S24.*** ESI-TOF mass spectrum of **2D2-**$2PF_6$**@TA4**. The result indicates **2D2-**$2PF_6$ and **TA4** form a 1:1 complex.

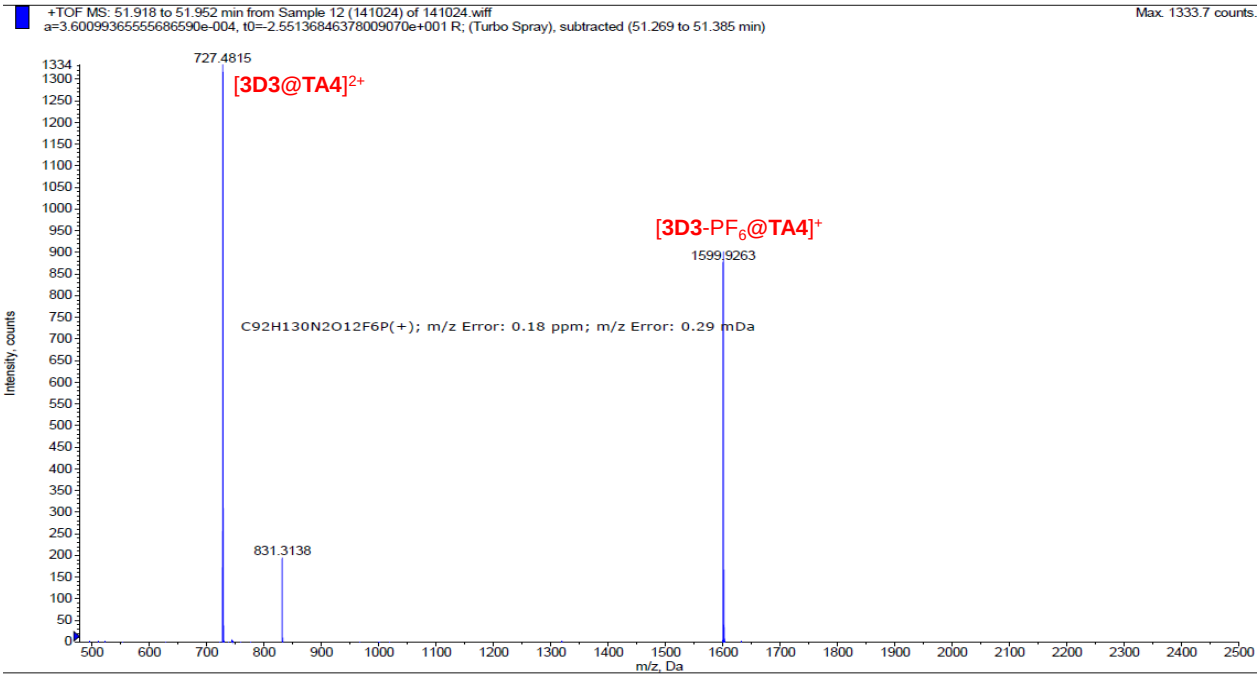


***Fig. S25.*** ESI-TOF mass spectrum of **3D3**-2$PF_6$**@TA4**. The result indicates **3D3**-2$PF_6$ and **TA4** form a 1:1 complex.

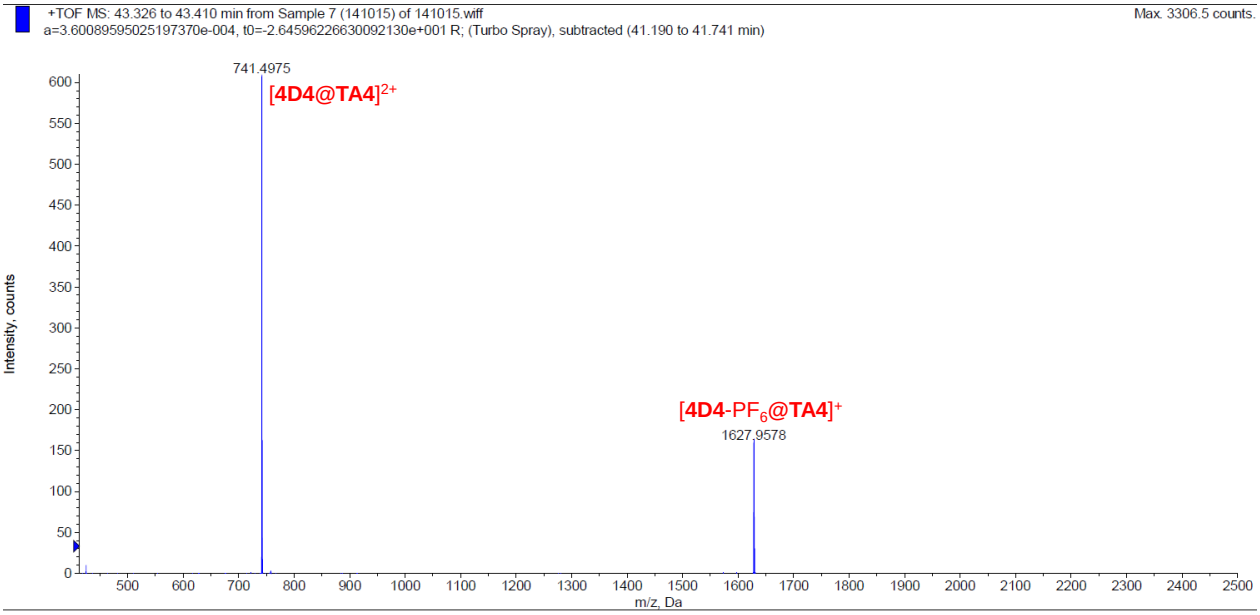


***Fig. S26.*** ESI-TOF mass spectrum of **4D4**-2$PF_6$**@TA4**. The result indicates **4D4**-2$PF_6$ and **TA4** form a 1:1 complex.

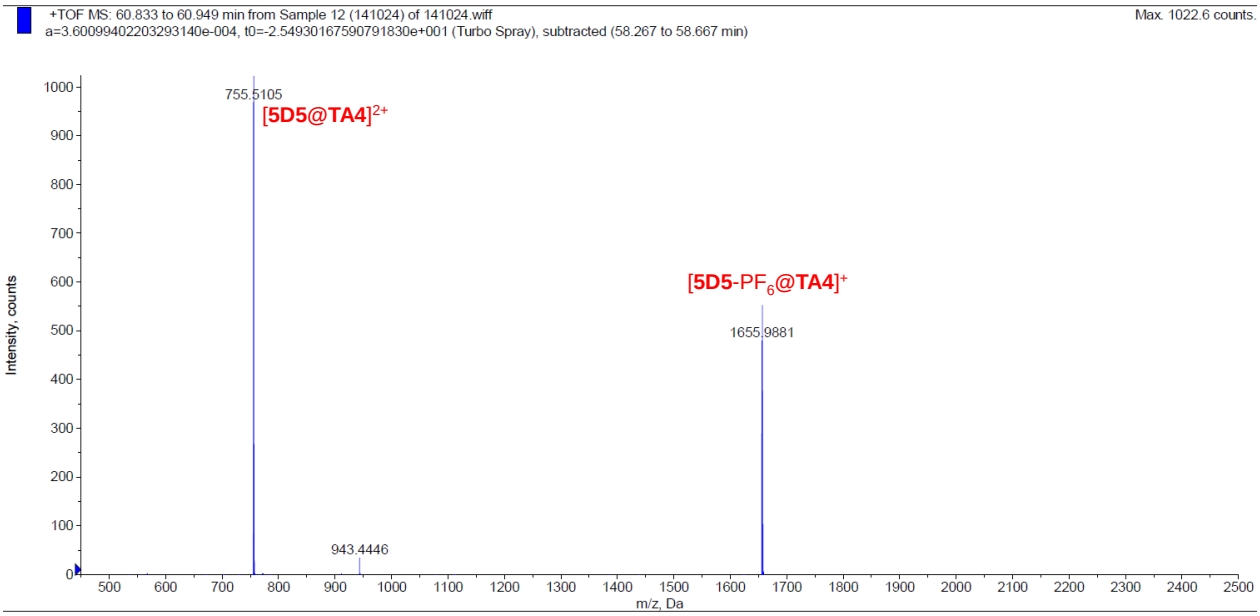


***Fig. S27.*** ESI-TOF mass spectrum of **5D5-**$2PF_6$**@TA4**. The result indicates **5D5-**$2PF_6$ and **TA4** form a 1:1 complex.

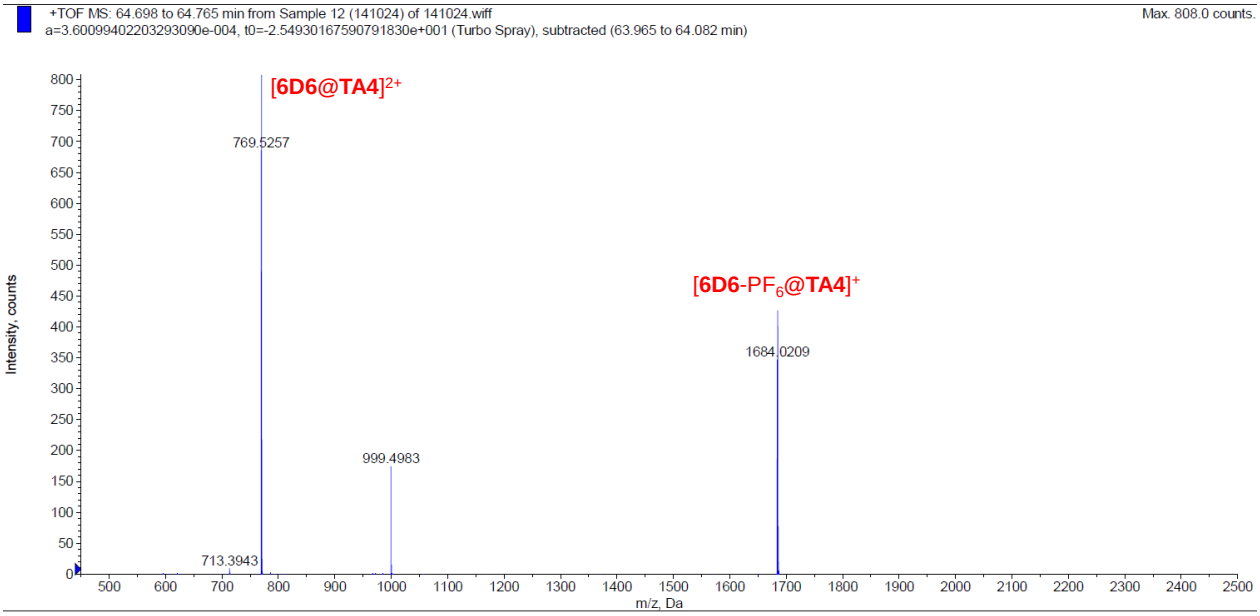


***Fig. S28.*** ESI-TOF mass spectrum of **6D6-**$2PF_6$**@TA4**. The result indicates **6D6-**$2PF_6$ and **TA4** form a 1:1 complex.

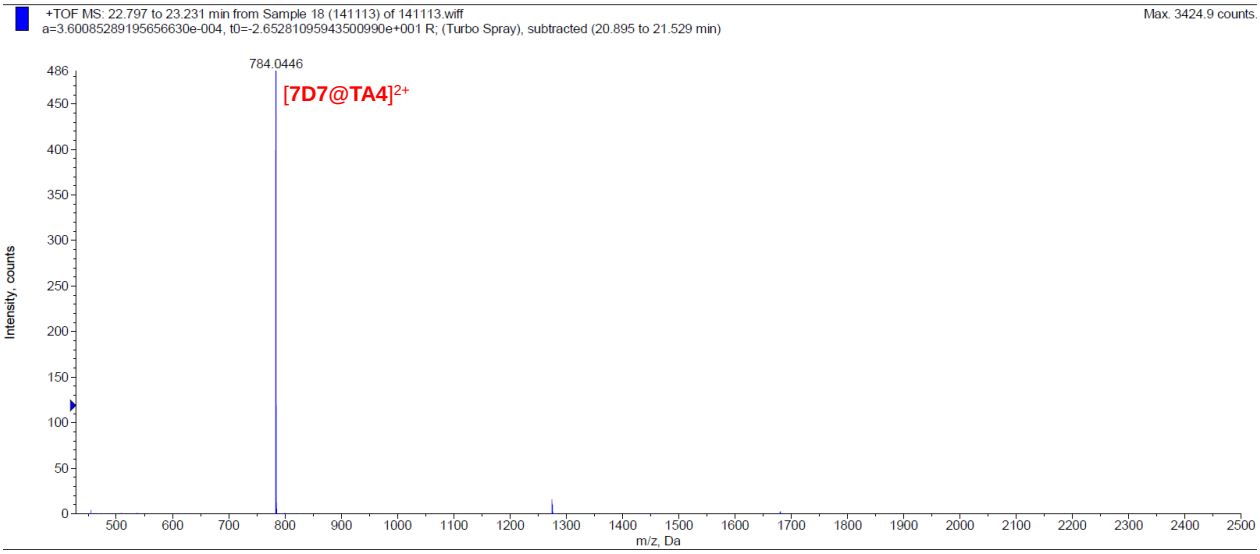


***Fig. S29.*** ESI-TOF mass spectrum of **7D7**-2$PF_6$**@TA4**. The result indicates **7D7**-2$PF_6$ and **TA4** form a 1:1 complex.

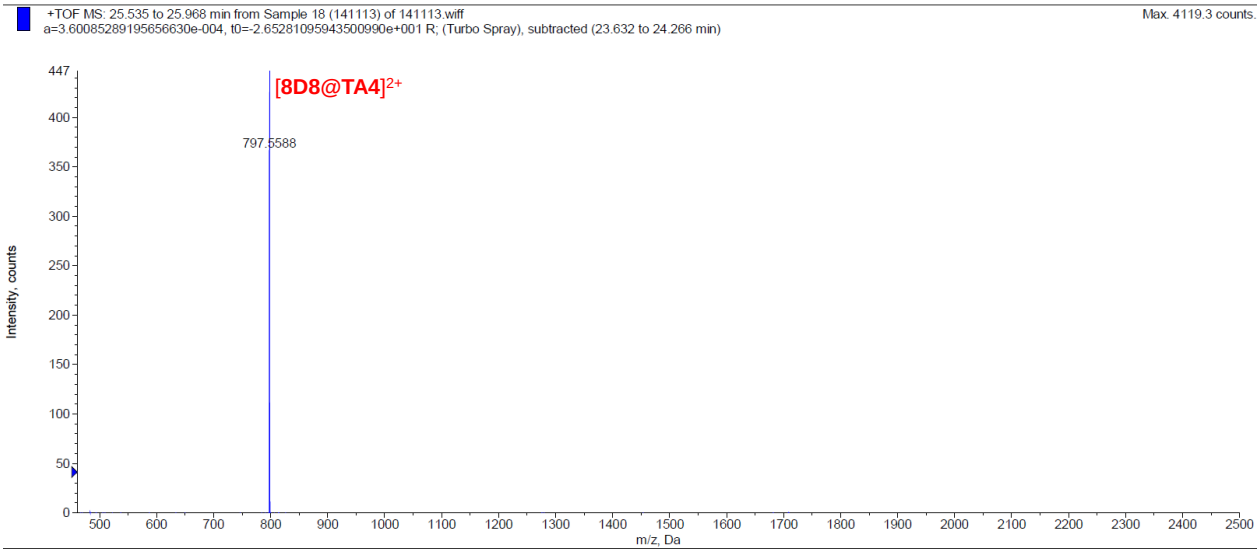


***Fig. S30.*** ESI-TOF mass spectrum of **8D8**-2$PF_6$**@TA4**. The result indicates **8D8**-2$PF_6$ and **TA4** form a 1:1 complex.

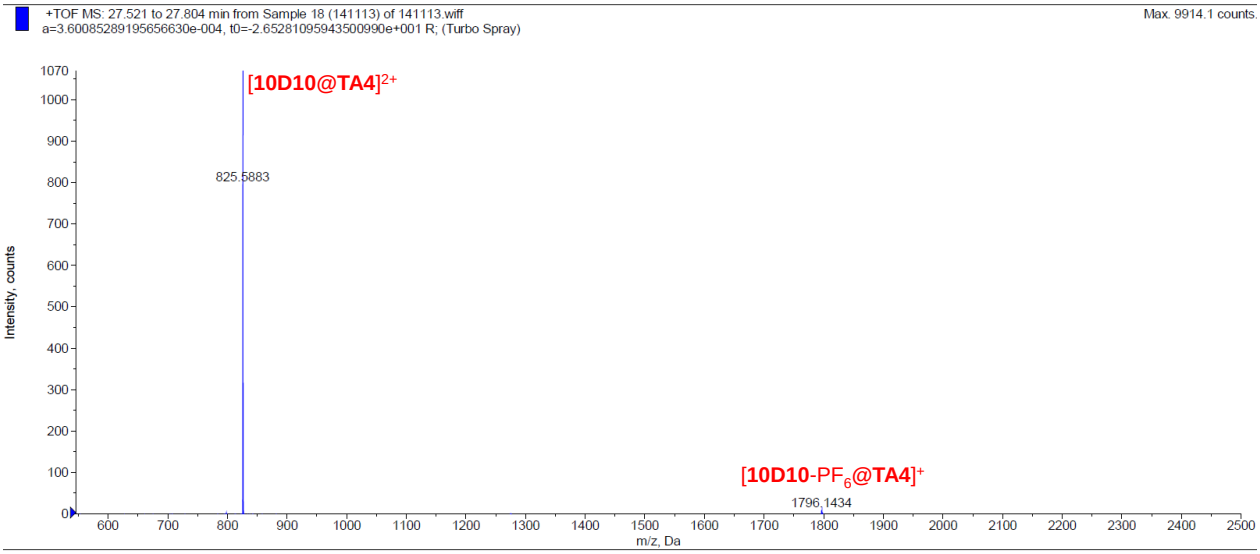


***Fig. S31.*** ESI-TOF mass spectrum of **10D10-**$2PF_6$**@TA4**. The result indicates **10D10-**$2PF_6$ and **TA4** form a 1:1 complex.

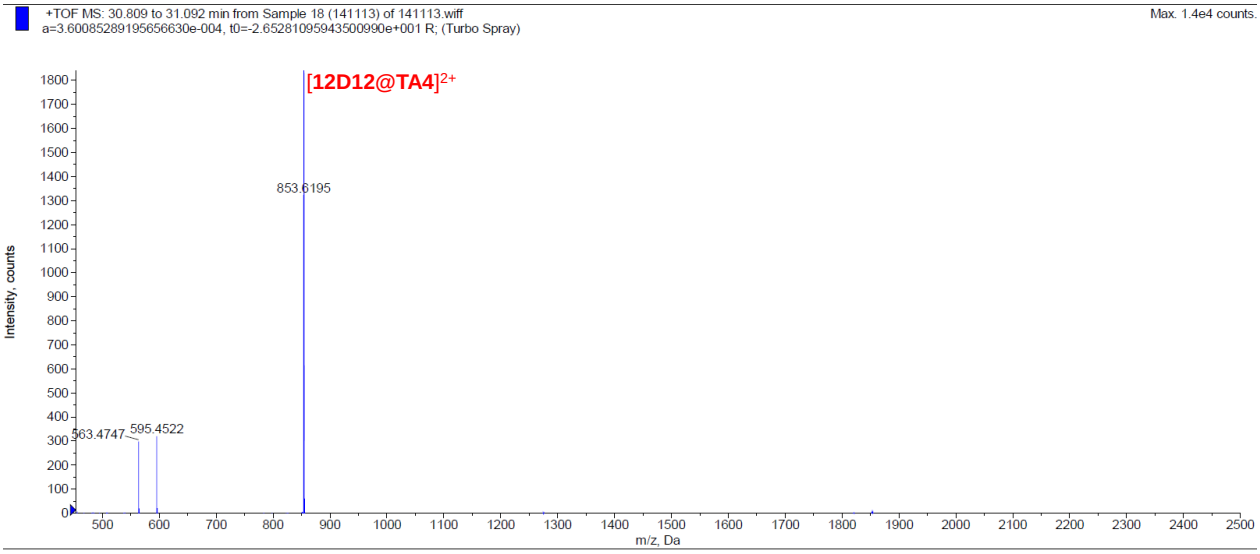


***Fig. S32.*** ESI-TOF mass spectrum of **12D12-**$2PF_6$**@TA4**. The result indicates **12D12-**$2PF_6$ and **TA4** form a 1:1 complex.

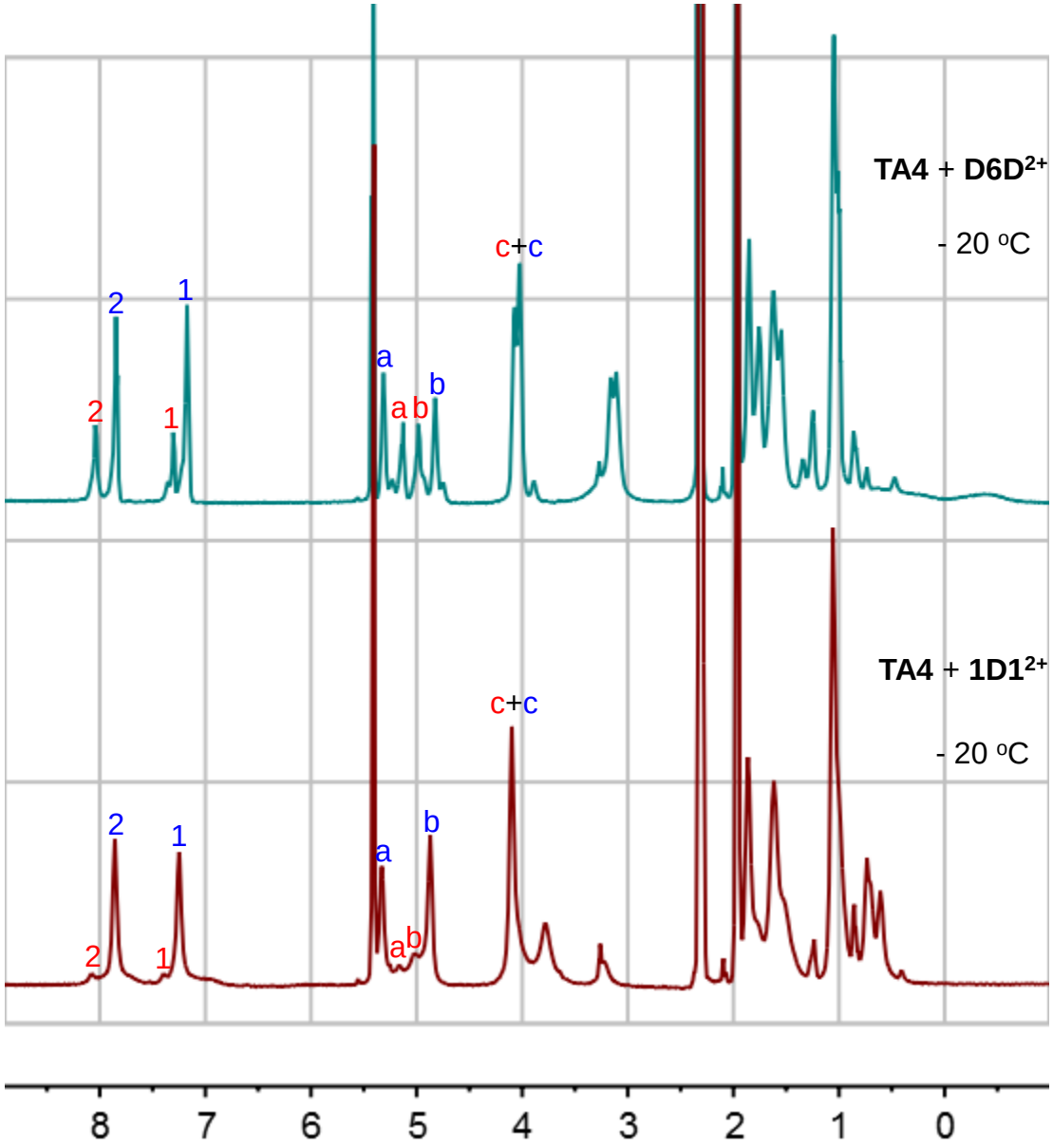


***Fig. S33.*** Full $^{1}$H NMR spectra (600 MHz, $CD_2Cl_2$:$CD_3CN$=1:1, 2.0 mM) of **1D1**$^{2+}$**@TA4** and **D6D**$^{2+}$**@TA4** at – 20 $^{o}$C. These results indicate that in the presence of **D6D**$^{2+}$, **TA4** exists as both conformer **I** (33%) and conformer **IV** (67%), but conformer **IV** (67%) is still the major conformer. For guest **1D1**$^{2+}$**,** conformer **IV** is predominant conformer, accompanied by tiny amount of conformer **I** (less than 5%).

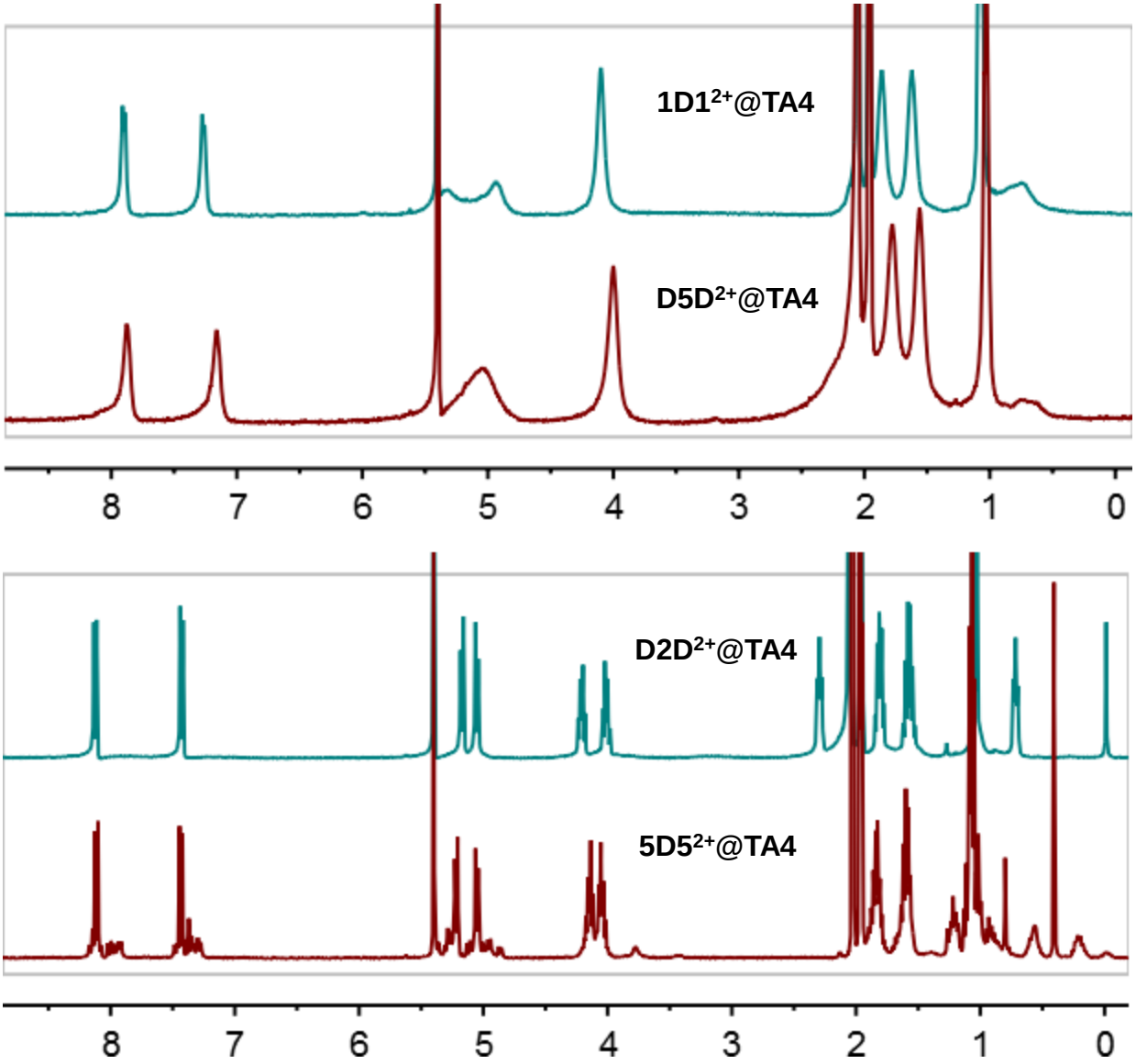


***Fig. S34.*** Comparison of $^{1}$H NMR spectra (400 MHz, $CD_2Cl_2$:$CD_3CN$=1:1, 2.0 mM, 298 K) of **1D1$^{2+}$@TA4** and **D5D$^{2+}$@TA4, 5D5$^{2+}$@TA4** and **D2D$^{2+}$@TA4**. Clearly, these two pairs have very similar peak shift and pattern, highly suggesting that their host structures share the same conformation, respectively. This is supported by 2D NMR spectra (see below).

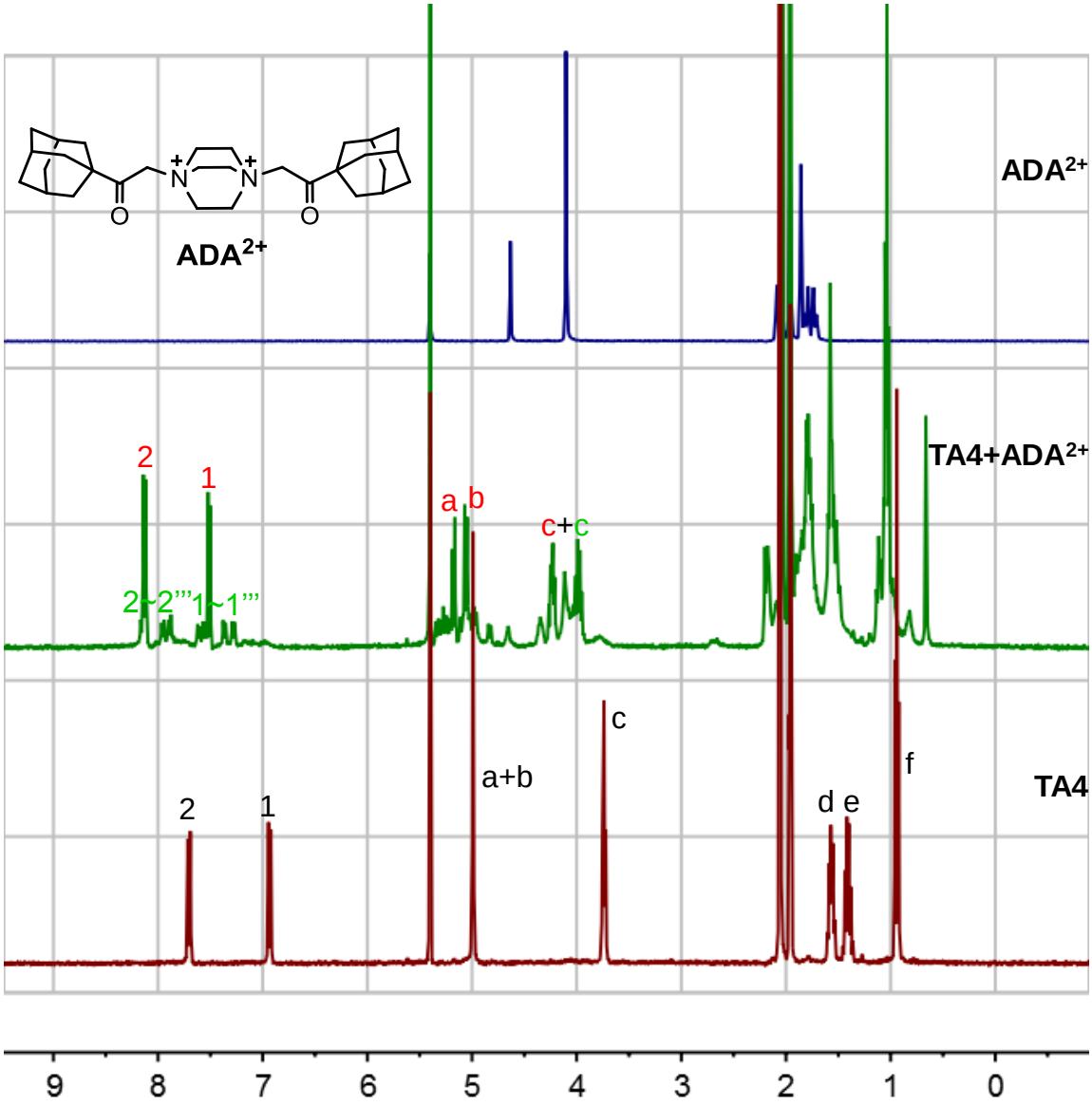


***Fig. S35.*** Full $^{1}$H NMR spectra (400 MHz, $CD_2Cl_2$:$CD_3CN$=1:1, 2.0 mM, 298 K) of **TA4** (bottom), **ADA**$^{2+}$ (top), and their equimolar mixture (middle). ROESY NMR experiment confirms that conformation **TA4-I** (45%) is one of the conformer in the 1:1 mixture of **TA4** and **ADA**$^{2+}$; At least 7 small doublets at 7.2 ~ 8.2 ppm strongly suggest the existence of conformer **TA4-II** (55%) with the lowest C2 symmetry.

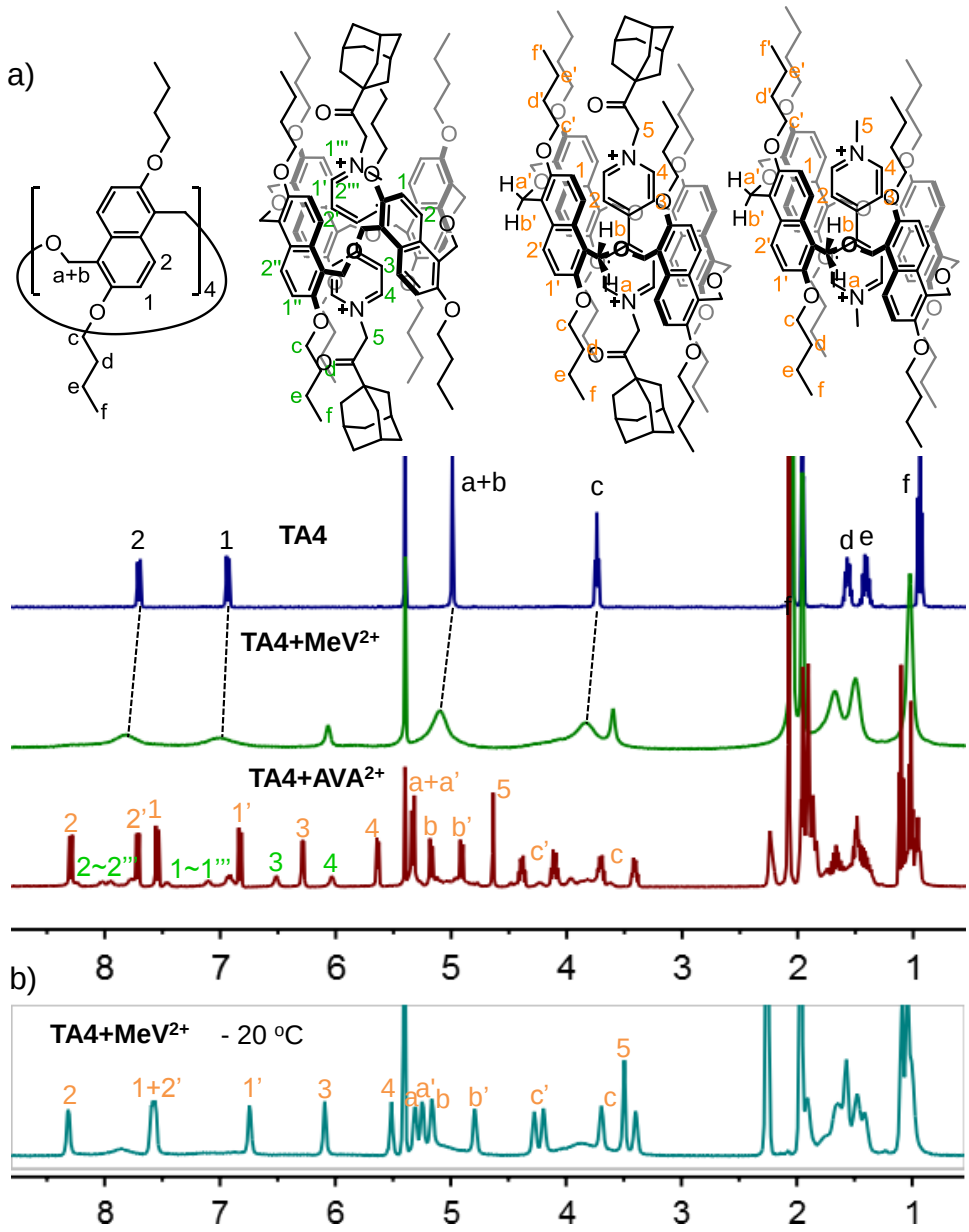


***Fig. S36.*** (a) Full $^{1}$H NMR spectra (400 MHz, $CD_2Cl_2$:$CD_3CN$=1:1, 2.0 mM, 298 K) of **TA4** (top), **MeV$^{2+}$@TA4** (middle), and **AVA$^{2+}$@TA4** (bottom). The NMR peak pattern and ROESY NMR experiment confirms that conformation **TA4-III** (70%) is the major conformer in the 1:1 mixture of **TA4** and **AVA$^{2+}$**; But the 8 small doublets at 6.8 ~ 8.3 ppm also suggest the existence of conformer **TA4-II** (30%); (b) Full $^{1}$H NMR spectra (600 MHz, $CD_2Cl_2$:$CD_3CN$=1:1, 2.0 mM, - 20 $^{o}$C) of **MeV$^{2+}$@TA4**. The peak pattern is in line with conformer **III**, and conformer **II** was not obviously detected. Hypothetically, the bulky adamantane group on **AVA$^{2+}$** may favor the formation of conformer **II**. This is similar for guest **ADA$^{2+}$**, with which conformer **II** contributes 55% of the population of **TA4**.

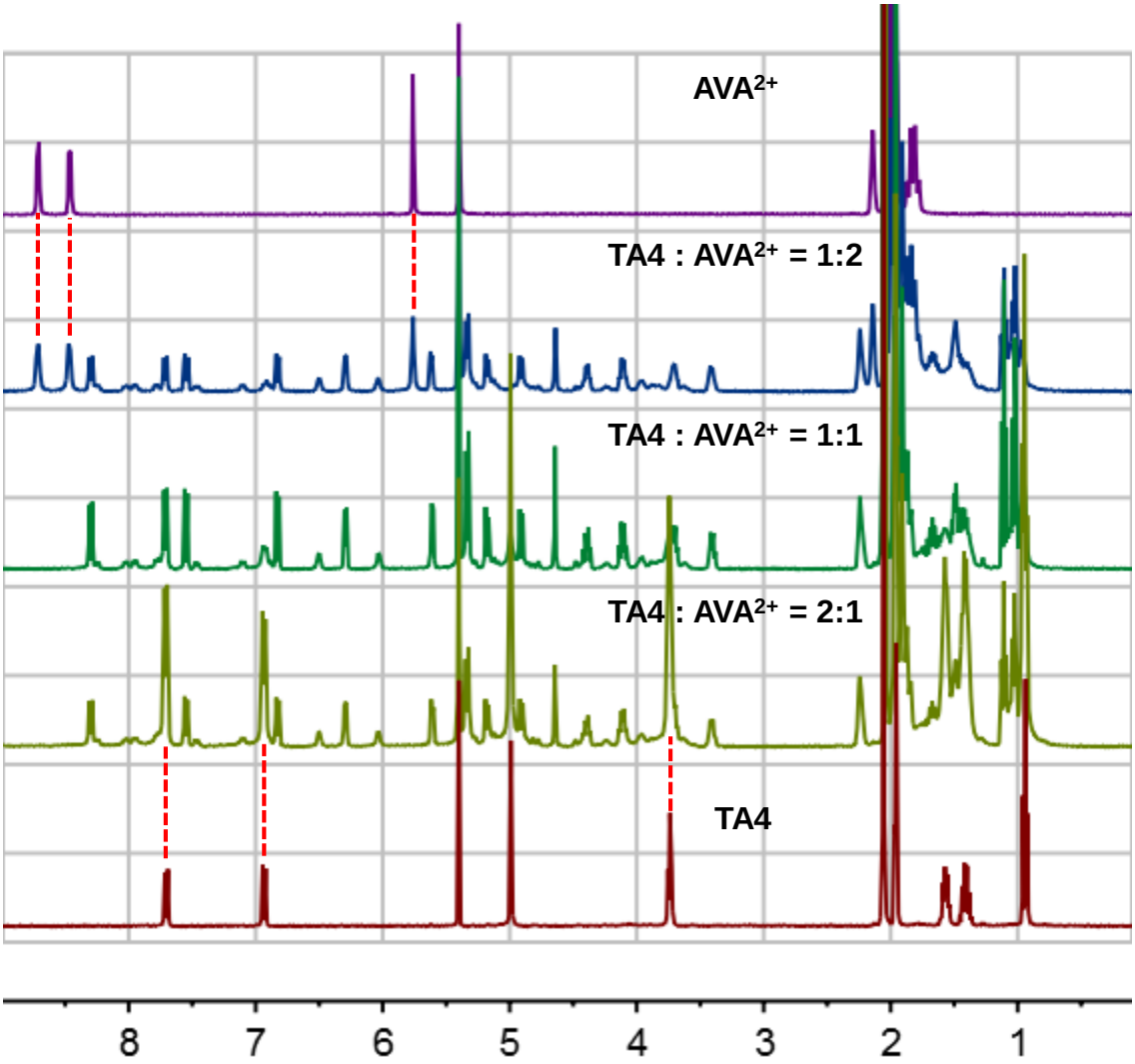


***Fig. S37.*** Full $^{1}$H NMR spectra (400 MHz, $CD_2Cl_2$:$CD_3CN$=1:1, 2.0 mM, 298 K) of **TA4**, **AVA**$^{2+}$, and their mixture in 2:1, 1:1, and 1:2 ratio. These experiments suggest that the complex between **TA4** and **AVA**$^{2+}$ undergoes slow exchange at the current NMR timescale. Thus, the complete disappearance of free host and free guest in the 1:1 mixture of **TA4** and **AVA**$^{2+}$ indicates a very strong binding between them. In analogy to **D2D**$^{2+}$**@TA4**, we can estimate that the binding constant between **TA4** and **AVA**$^{2+}$ should be bigger than $10^5$ $M^{-1}$.

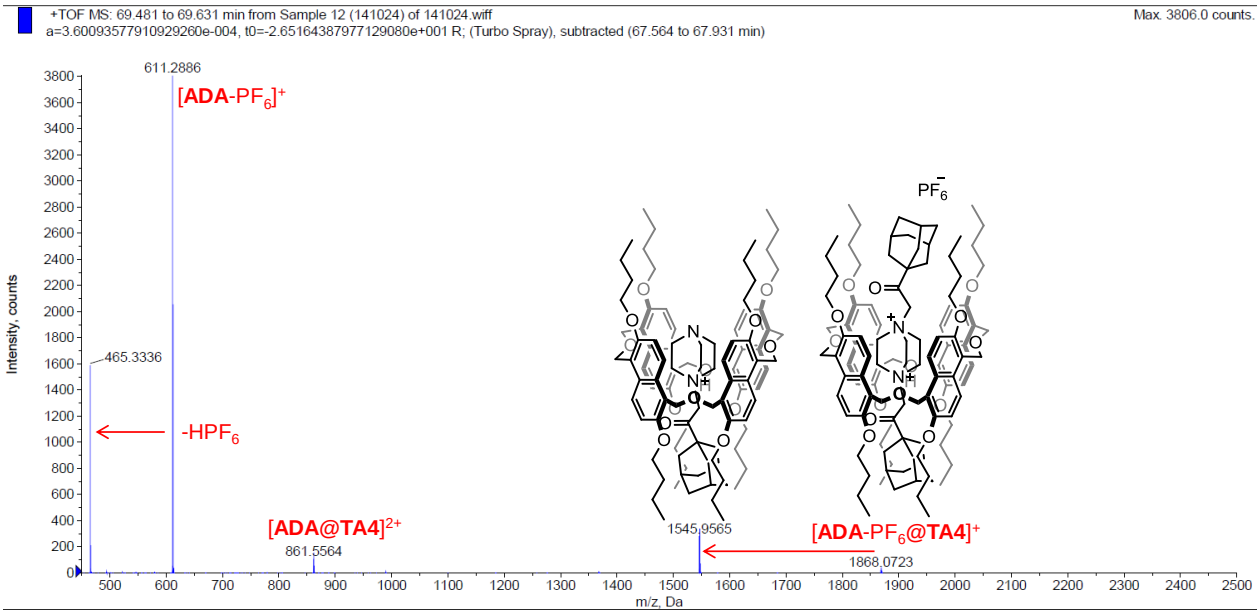


***Fig. S38.*** ESI-TOF mass spectrum of **ADA**-2$PF_6$**@TA4**. The result indicates **ADA**-2$PF_6$ and **TA4** form a 1:1 complex.

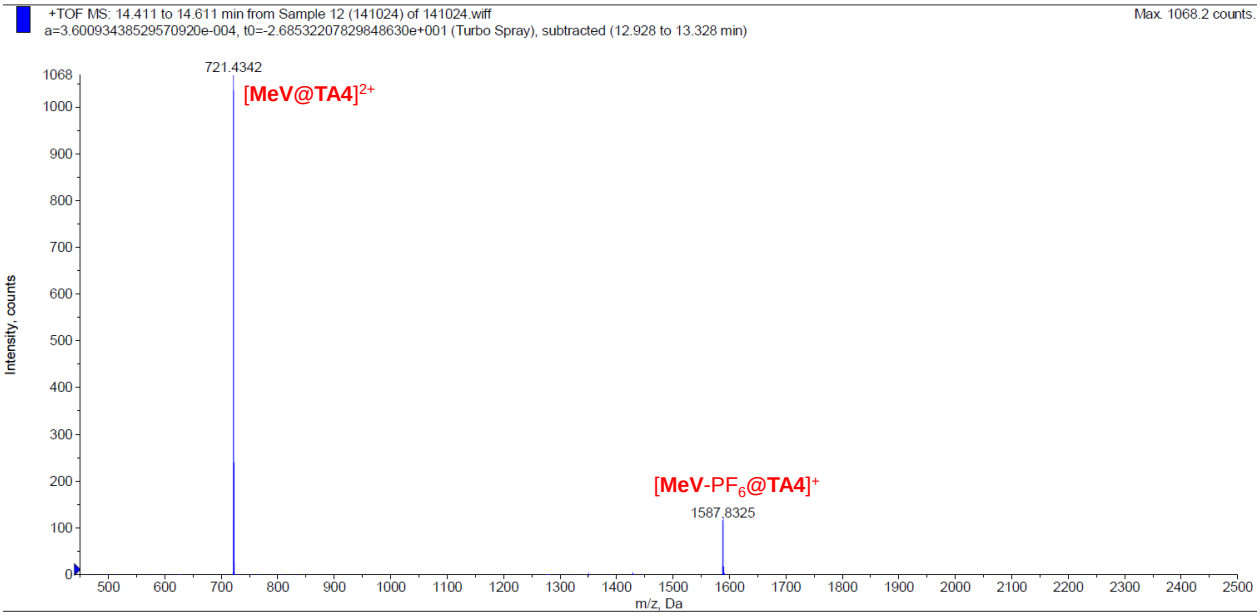


***Fig. S39.*** ESI-TOF mass spectrum of **MeV**-2$PF_6$**@TA4**. The result indicates **MeV**-2$PF_6$ and **TA4** form a 1:1 complex.

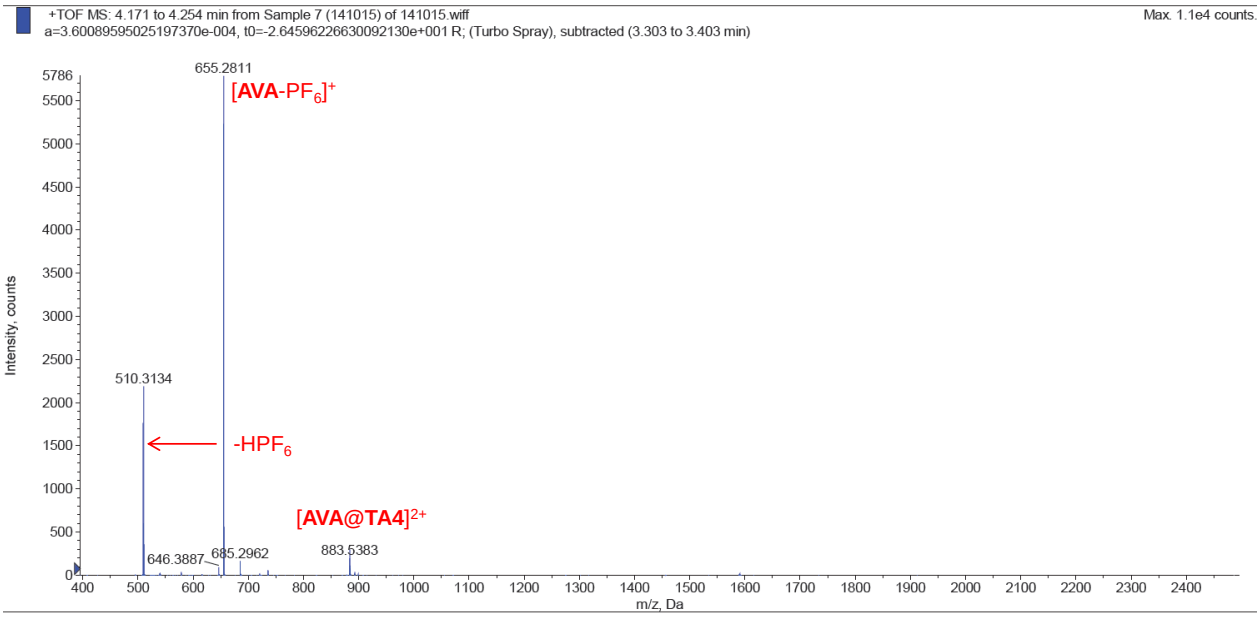


***Fig. S40.*** ESI-TOF mass spectrum of **AVA**-2$PF_6$**@TA4**. The result indicates **AVA**-2$PF_6$ and **TA4** form a 1:1 complex.

## 4. 2D NMR Spectra of the Complexes

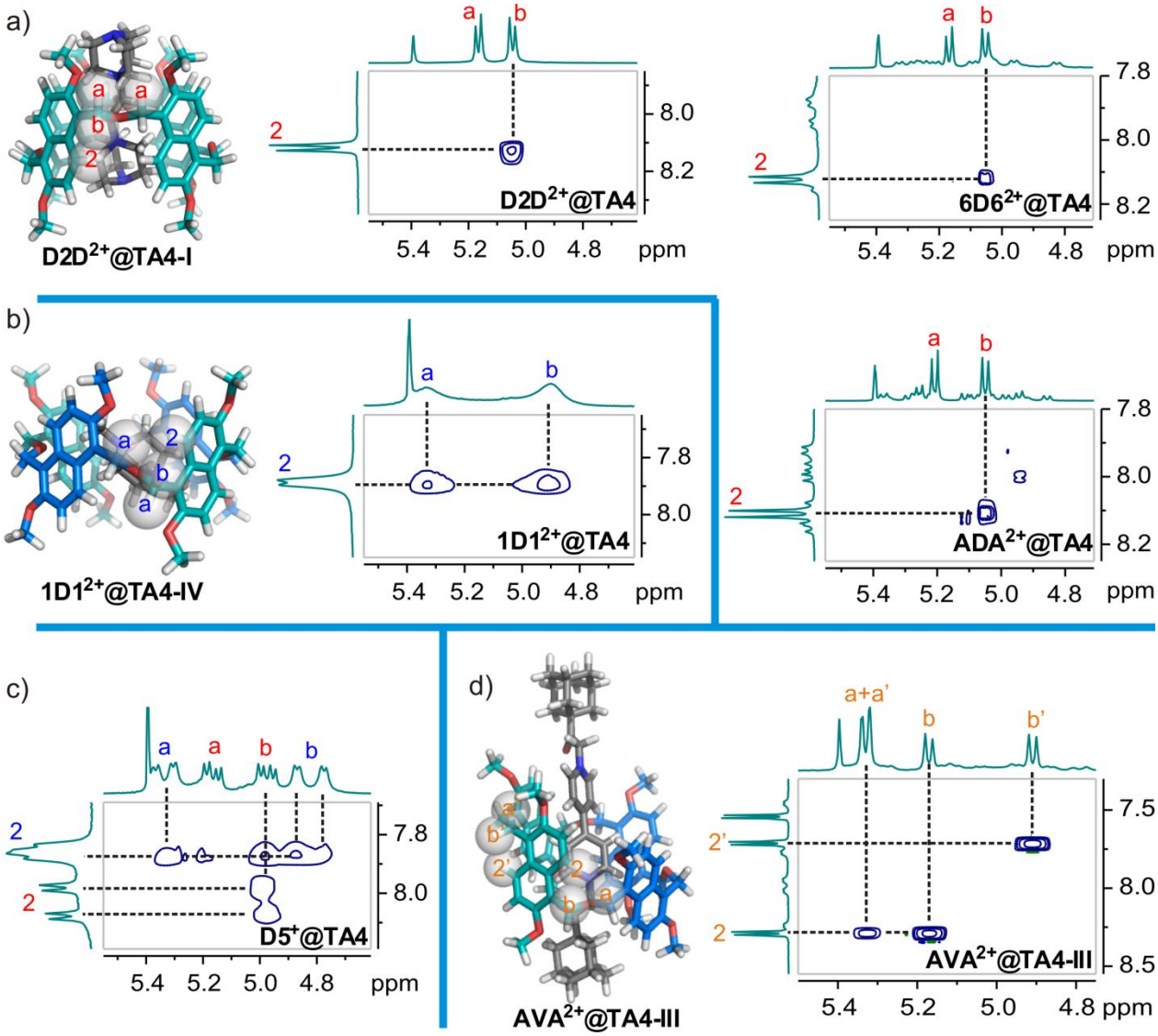


***Fig. S41.*** Partial $^{1}$H, $^{1}$H-ROESY NMR spectra (500 MHz, $CD_2Cl_2$:$CD_3CN$=1:1, 6.0 mM, 298 K) of (a) **D2D$^{2+}$@TA4**, **6D6$^{2+}$@TA4**, and **ADA$^{2+}$@TA4**; (b) **1D1$^{2+}$@TA4**; (c) **D5$^{+}$@TA4**; and (d) **AVA$^{2+}$@TA4**. The results in Fig. a all support the conformer **I**, while the NOE effect in Fig. b suggest conformer **IV** to be predominant. In the case of **D5$^{+}$@TA4**, both conformer **I** and **IV** coexist, and their NOE effects are indeed different, supporting the above assignments. A more clear-cut support is from the ROESY NMR spectrum of **AVA$^{2+}$@TA4**: we know from the peak pattern that conformer **III** is predominant in this solution. In conformer **III**, protons 2, a, and b exist in both the situations for conformer **I** and conformer **IV**. Their NOE effects are indeed consistent with what is observed for conformer **I** and **IV**, strongly support the above assignments.

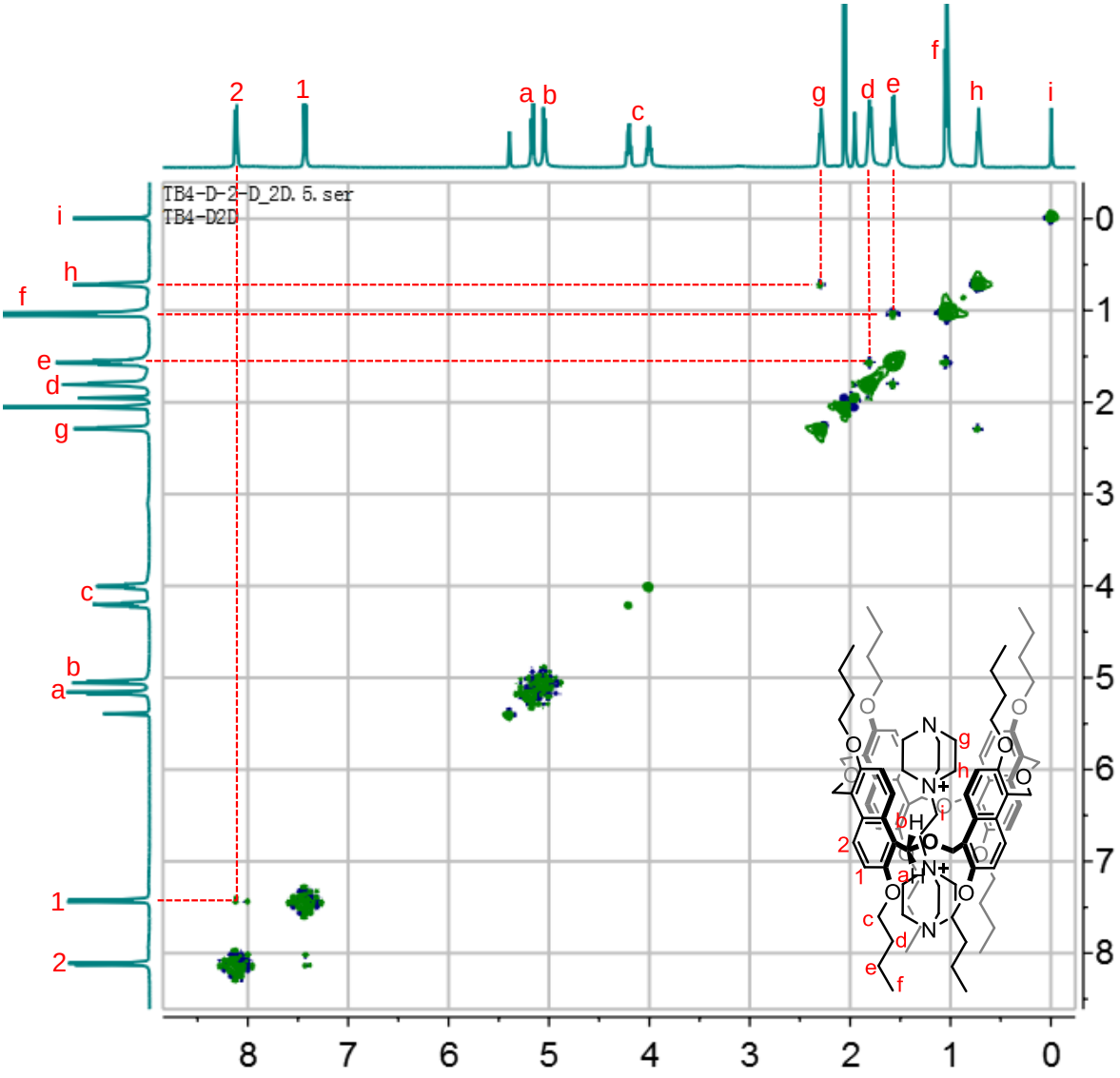


***Fig. S42.*** Full $^{1}$H, $^{1}$H-COSY NMR spectrum (500 MHz, $CD_2Cl_2$:$CD_3CN$=1:1, 6.0 mM, 298 K) of **D2D**-2$PF_6$**@TA4**.

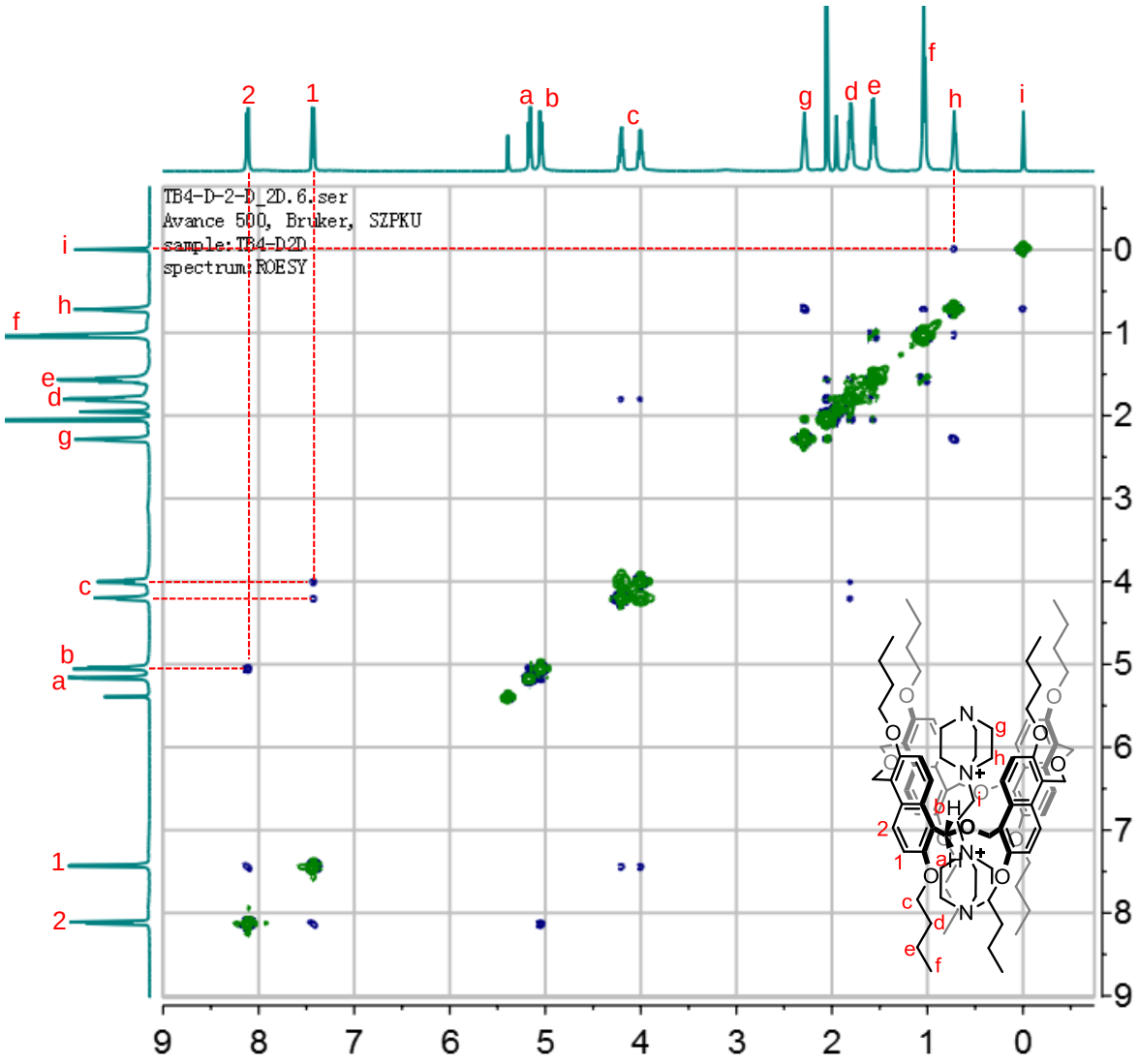


***Fig. S43.*** Full $^{1}$H, $^{1}$H-ROESY NMR spectrum (500 MHz, $CD_2Cl_2$:$CD_3CN$=1:1, 6.0 mM, 298 K) of **D2D**-2$PF_6$**@TA4**.

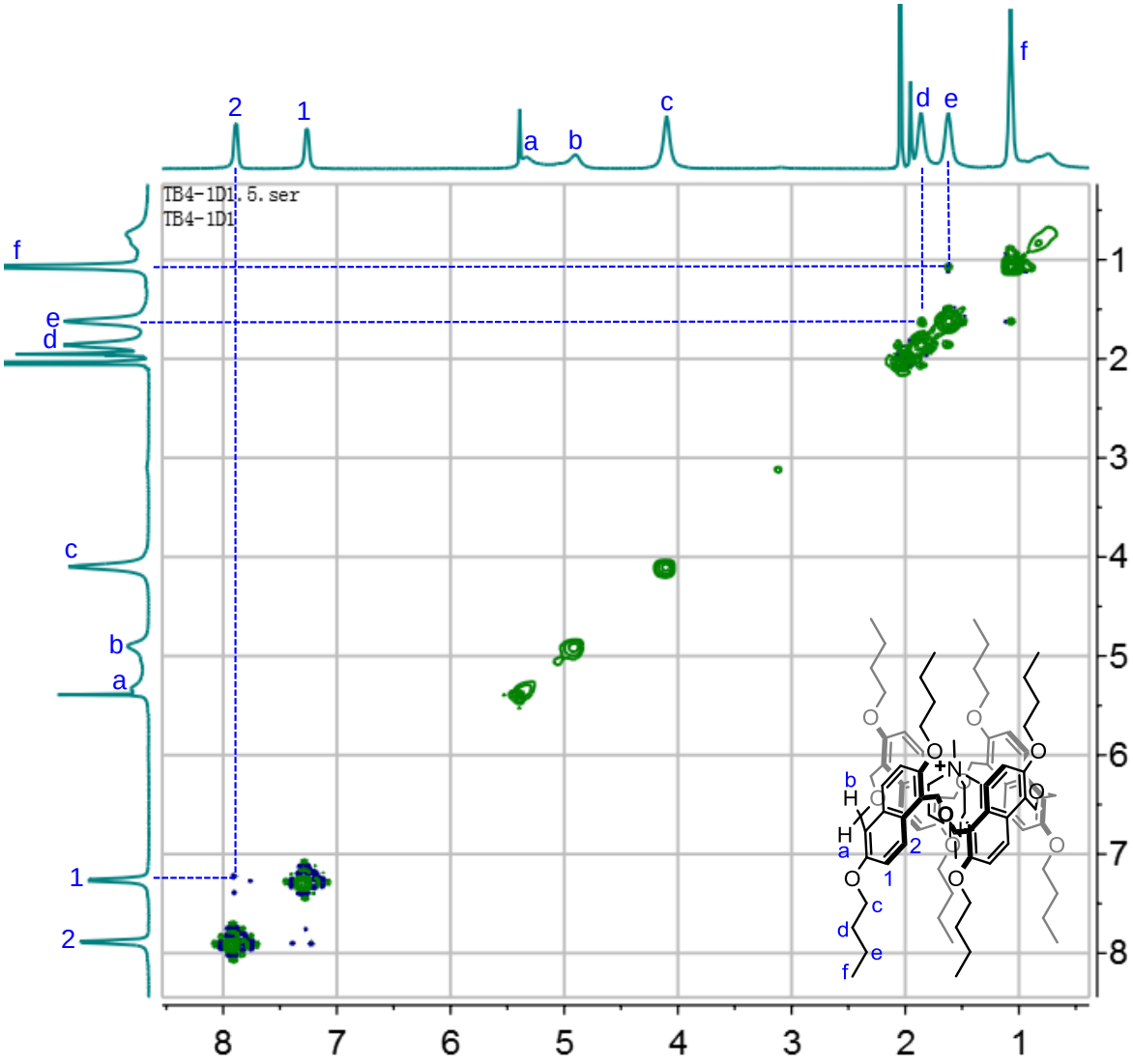


***Fig. S44.*** Full $^{1}$H, $^{1}$H-COSY NMR spectrum (500 MHz, $CD_2Cl_2$:$CD_3CN$=1:1, 6.0 mM, 298 K) of **1D1**-2$PF_6$**@TA4**.

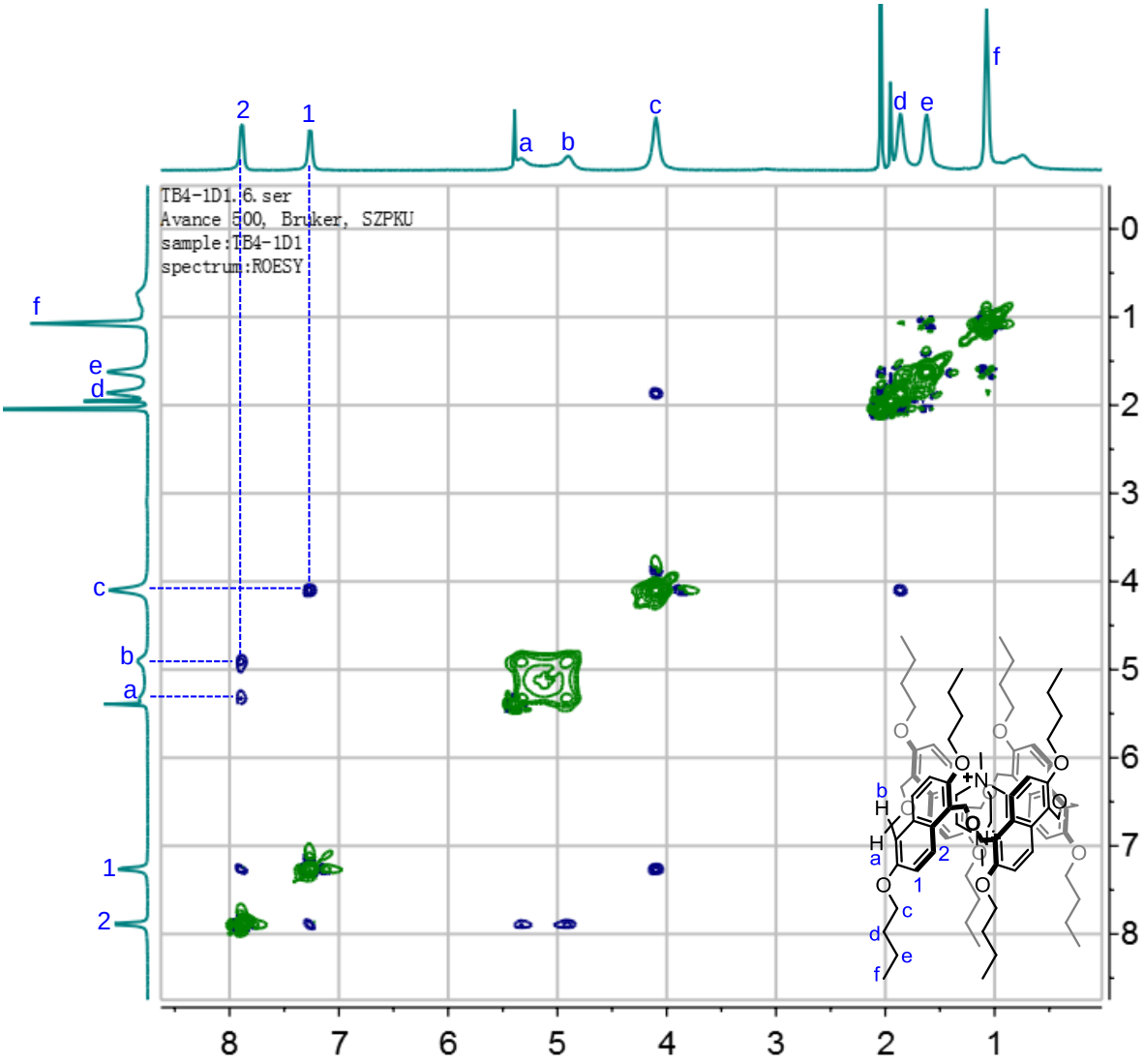


***Fig. S45.*** Full $^{1}$H, $^{1}$H-ROESY NMR spectrum (500 MHz, $CD_2Cl_2$:$CD_3CN$=1:1, 6.0 mM, 298 K) of **1D1**-2$PF_6$**@TA4**.

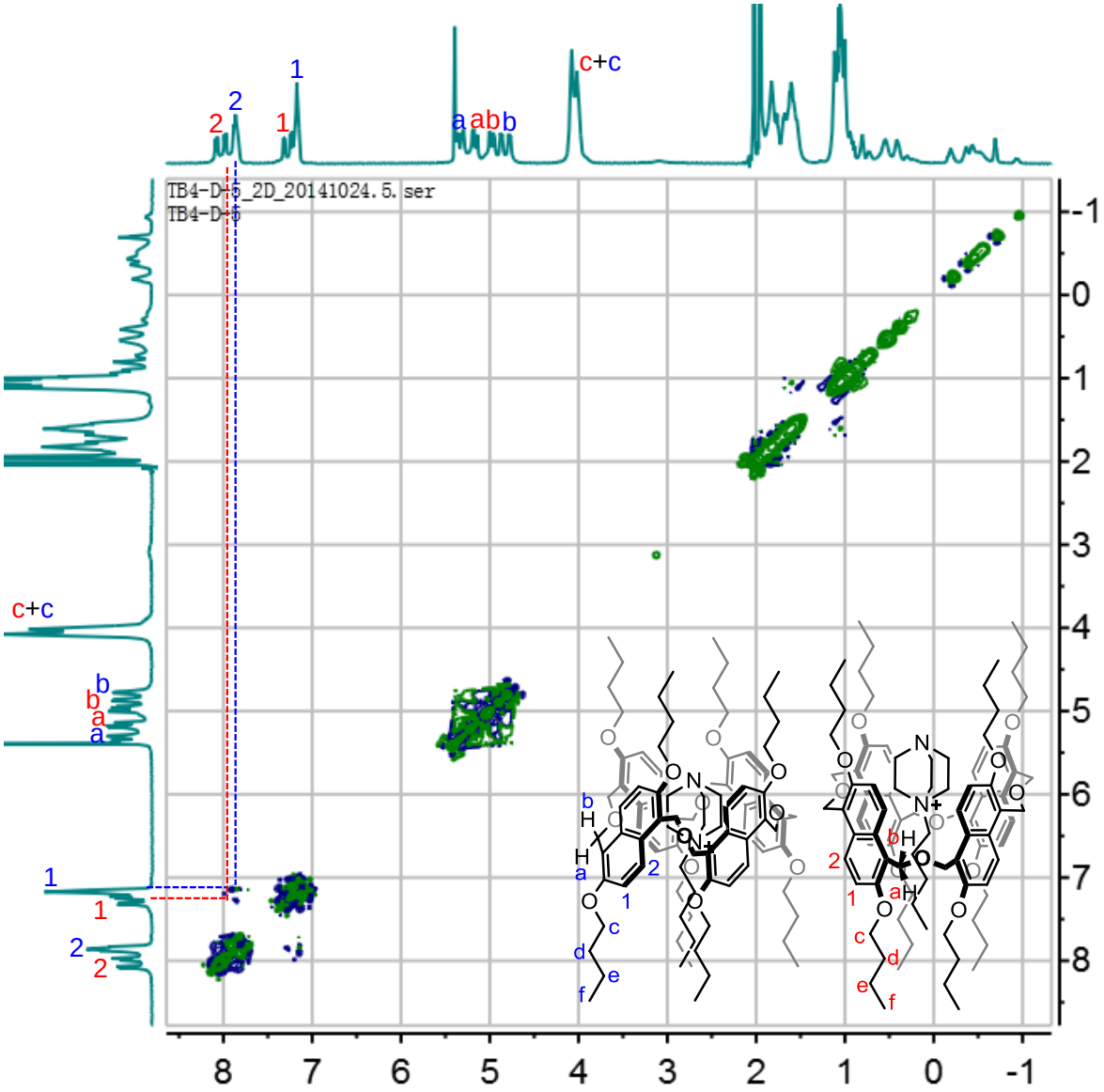


***Fig. S46.*** Full $^{1}$H, $^{1}$H-COSY NMR spectrum (500 MHz, $CD_2Cl_2$:$CD_3CN$=1:1, 6.0 mM, 298 K) of **D5**-$PF_6$**@TA4**.

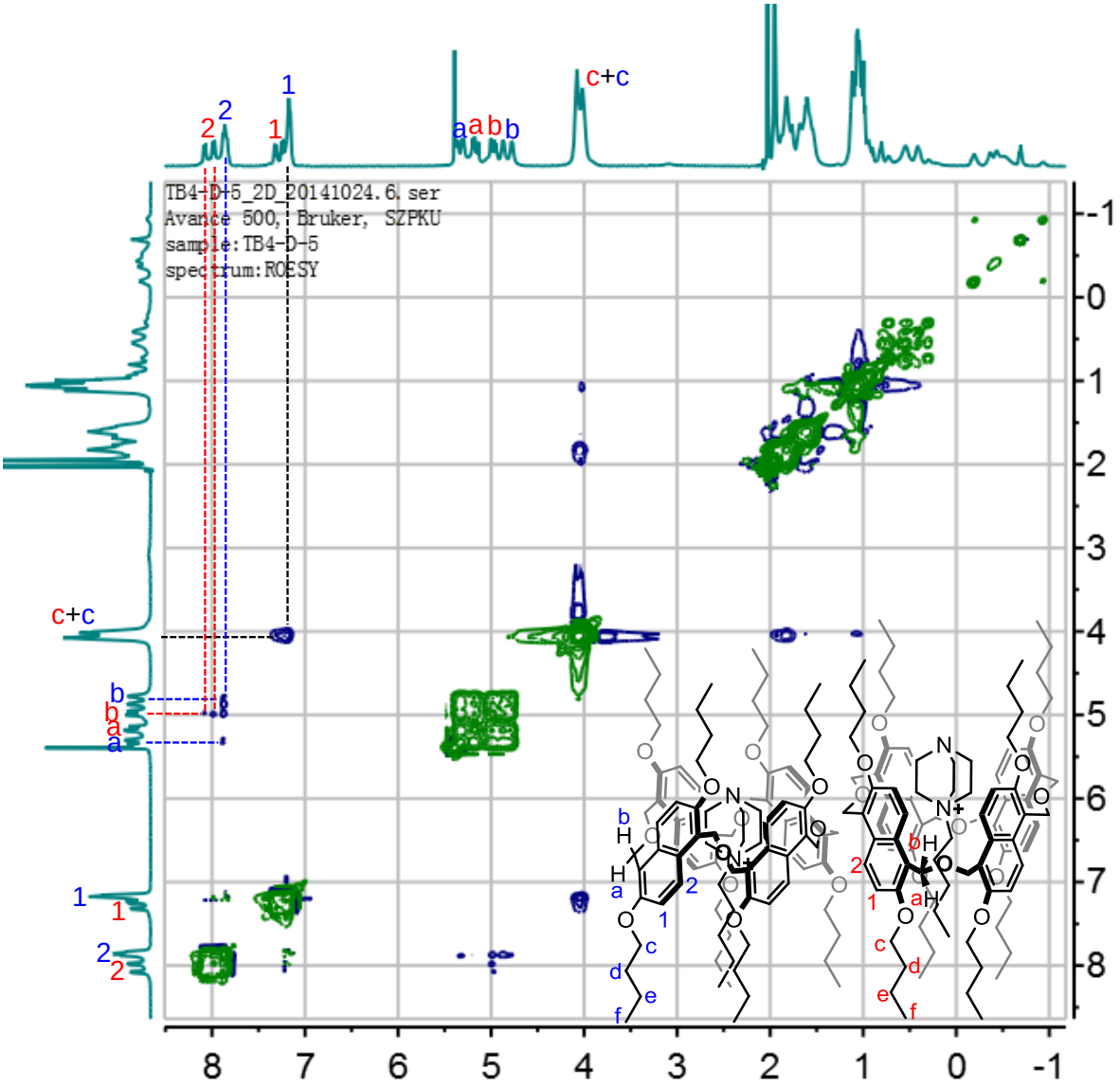


***Fig. S47.*** Full $^{1}$H, $^{1}$H-ROESY NMR spectrum (500 MHz, $CD_2Cl_2$:$CD_3CN$=1:1, 6.0 mM, 298 K) of **D5**-$PF_6$**@TA4**.

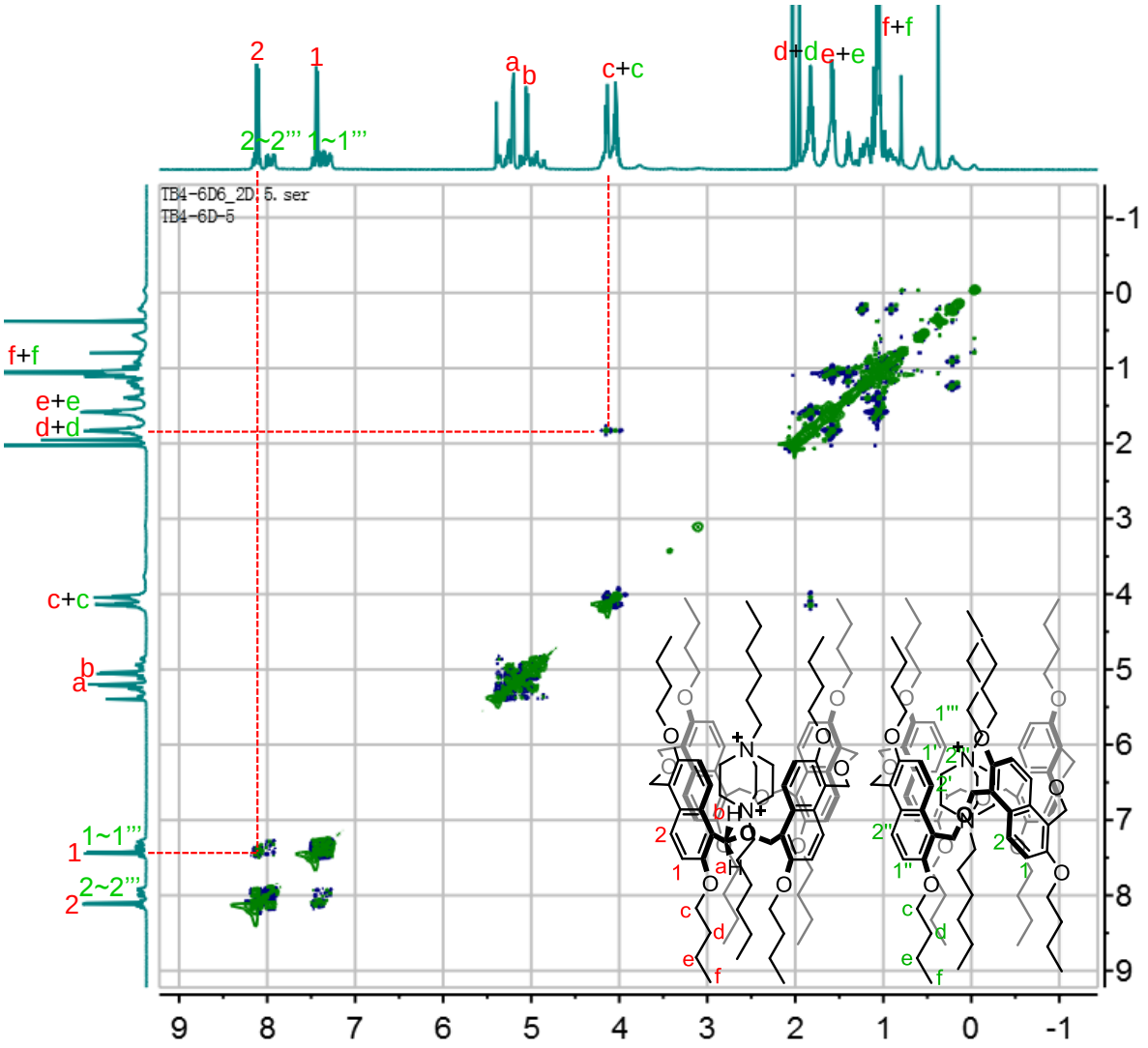


***Fig. S48.*** Full $^{1}$H, $^{1}$H-COSY NMR spectrum (500 MHz, $CD_2Cl_2$:$CD_3CN$=1:1, 6.0 mM, 298 K) of **6D6**-2$PF_6$**@TA4**.

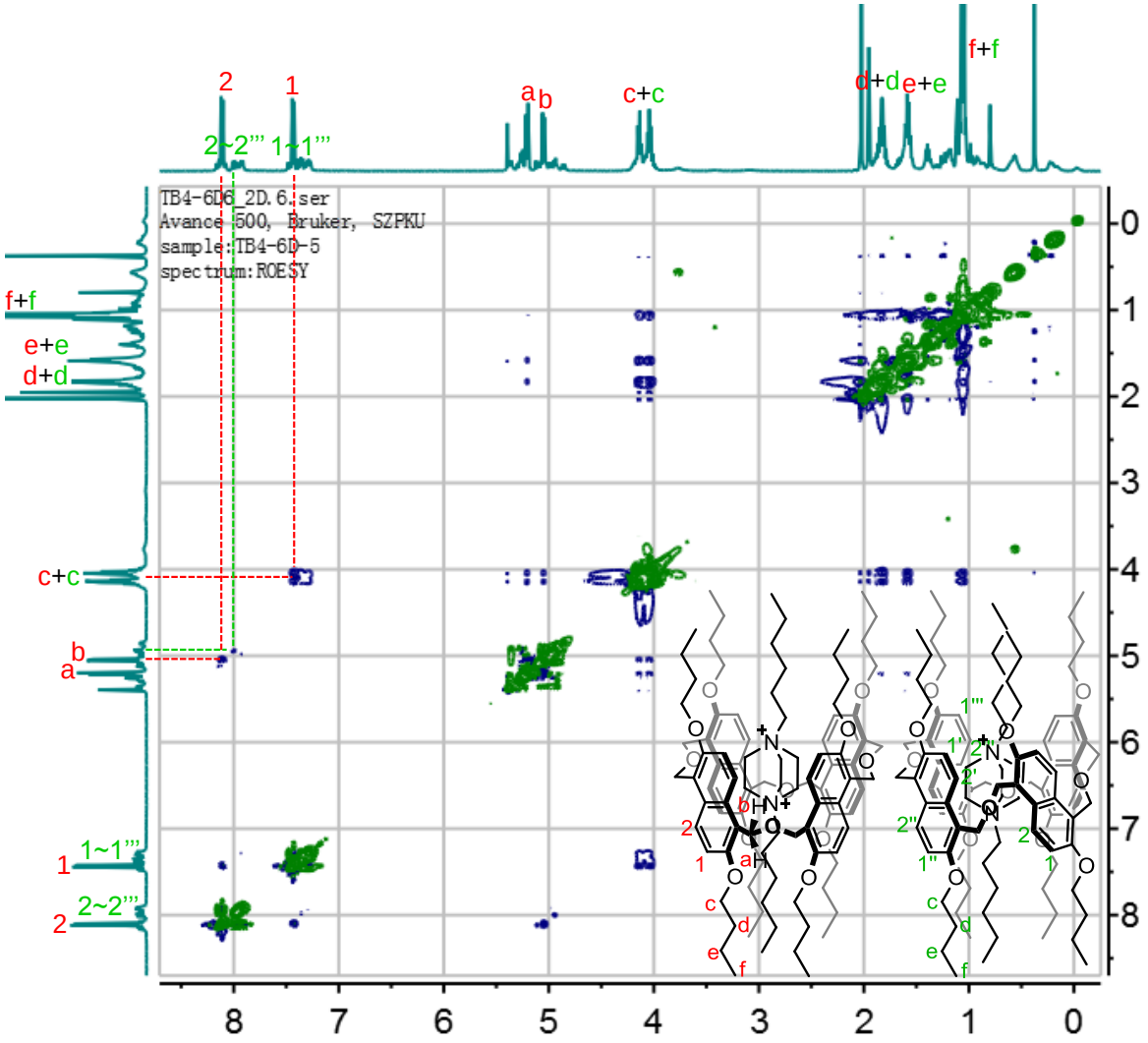


***Fig. S49.*** Full $^{1}$H, $^{1}$H-ROESY NMR spectrum (500 MHz, $CD_2Cl_2$:$CD_3CN$=1:1, 6.0 mM, 298 K) of **6D6**-2$PF_6$**@TA4**.

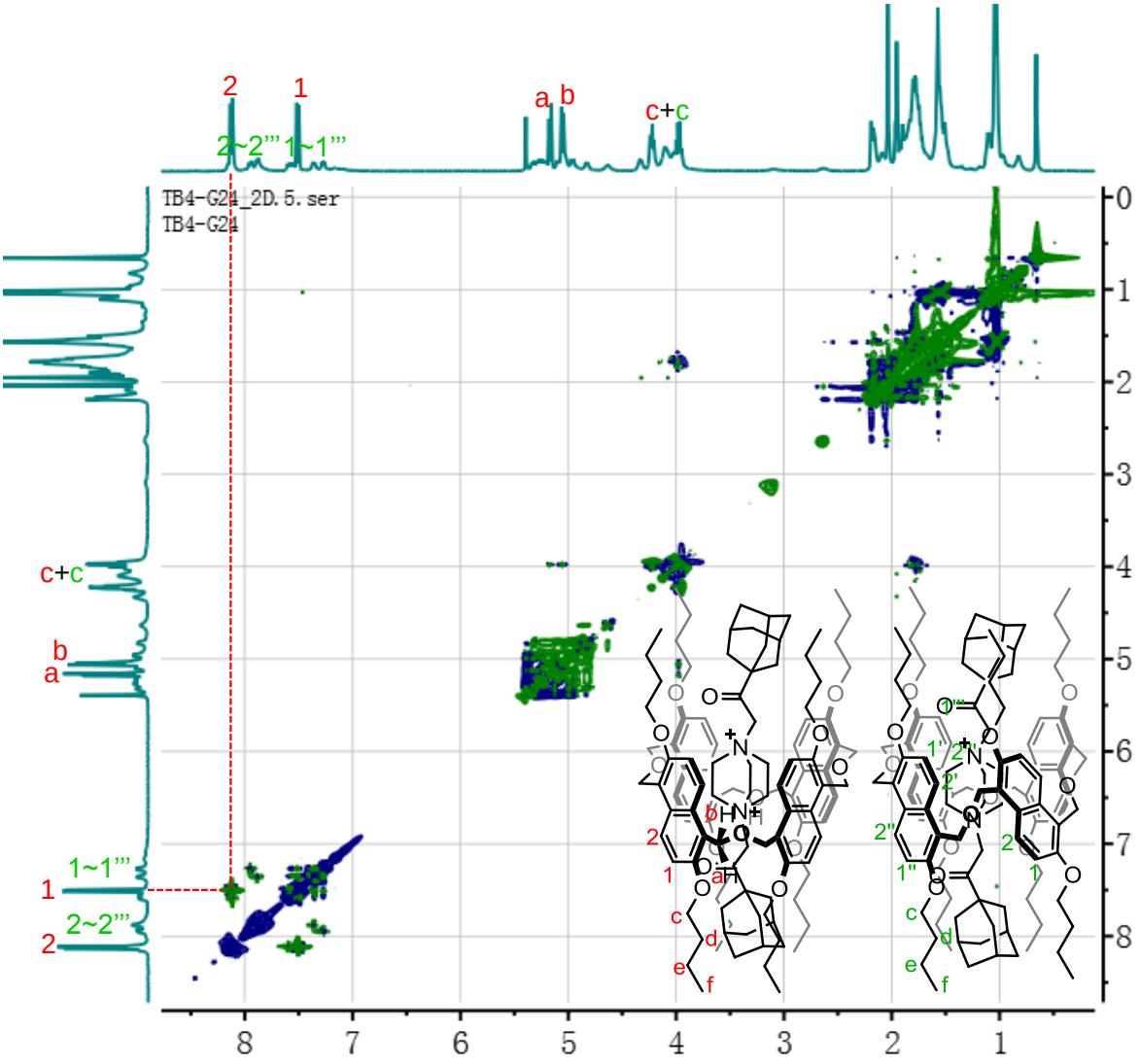


***Fig. S50.*** Full $^{1}$H, $^{1}$H-COSY NMR spectrum (500 MHz, $CD_2Cl_2$:$CD_3CN$=1:1, 6.0 mM, 298 K) of **ADA-**$2PF_6$**@TA4**.

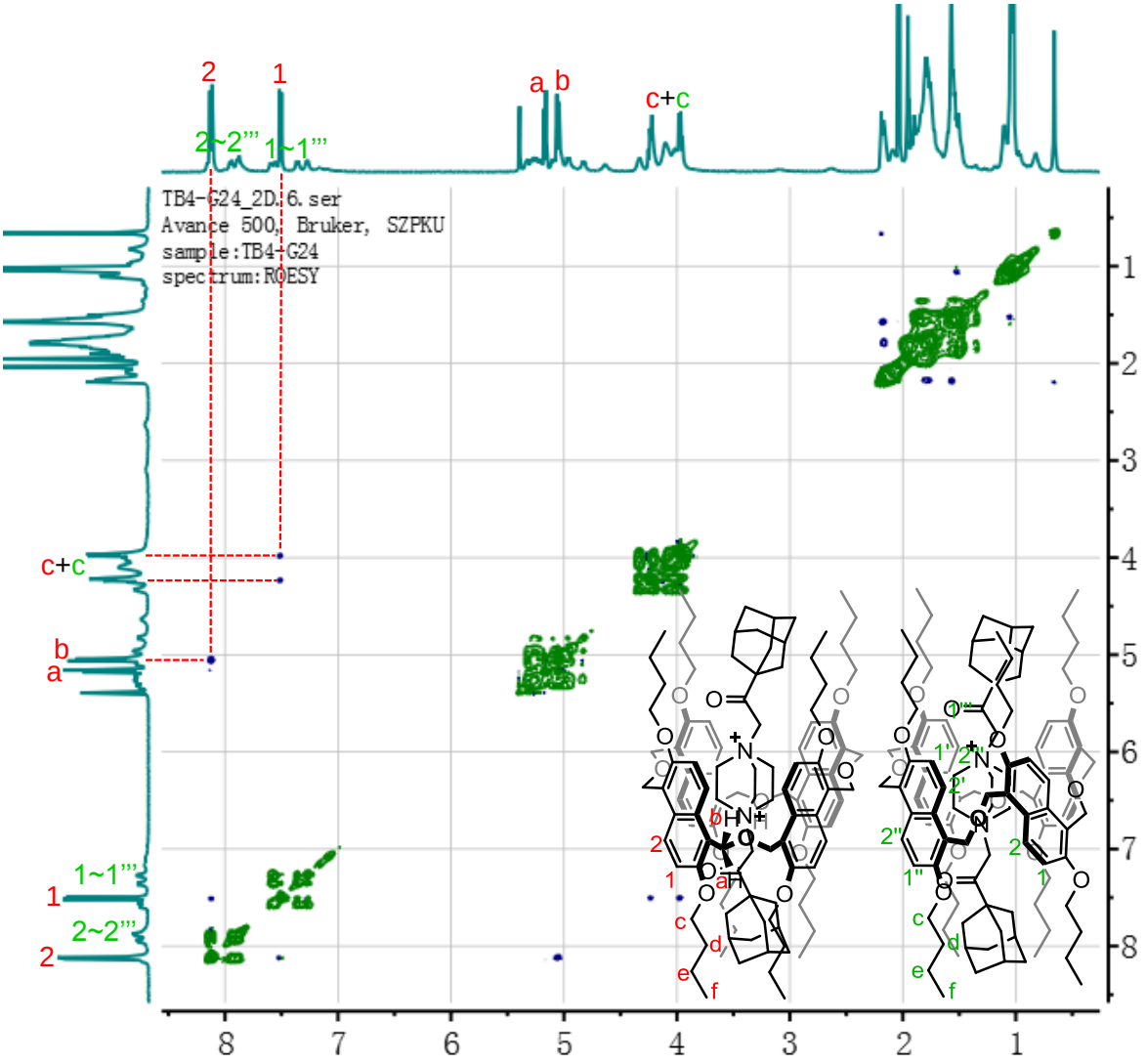


***Fig. S51.*** Full $^{1}$H, $^{1}$H-ROESY NMR spectrum (500 MHz, $CD_2Cl_2$:$CD_3CN$=1:1, 6.0 mM, 298 K) of **ADA**-2$PF_6$**@TA4**.

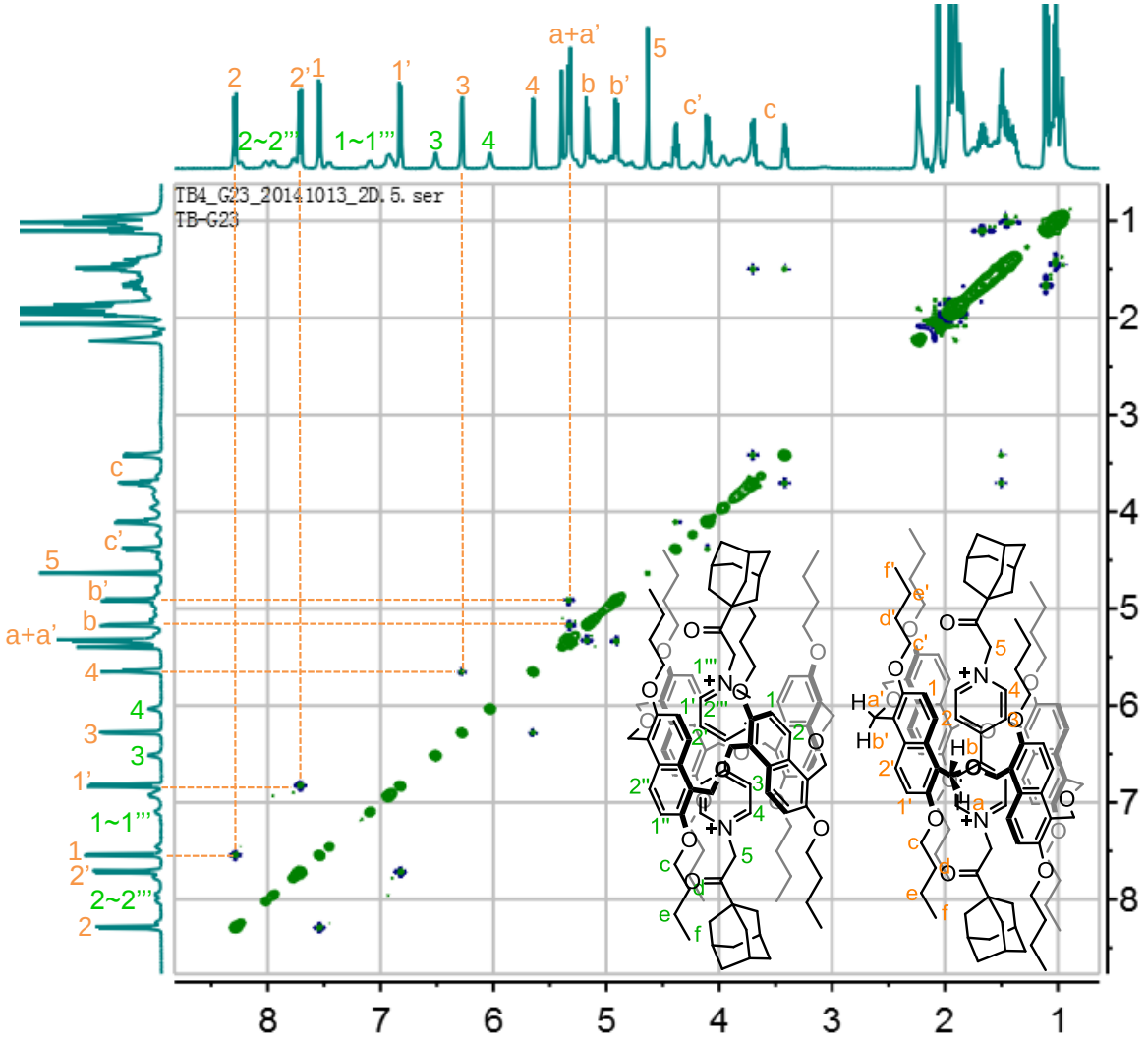


***Fig. S52.*** Full $^{1}$H, $^{1}$H-COSY NMR spectrum (500 MHz, $CD_2Cl_2$:$CD_3CN$=1:1, 6.0 mM, 298 K) of **AVA-**2$PF_6$**@TA4**.

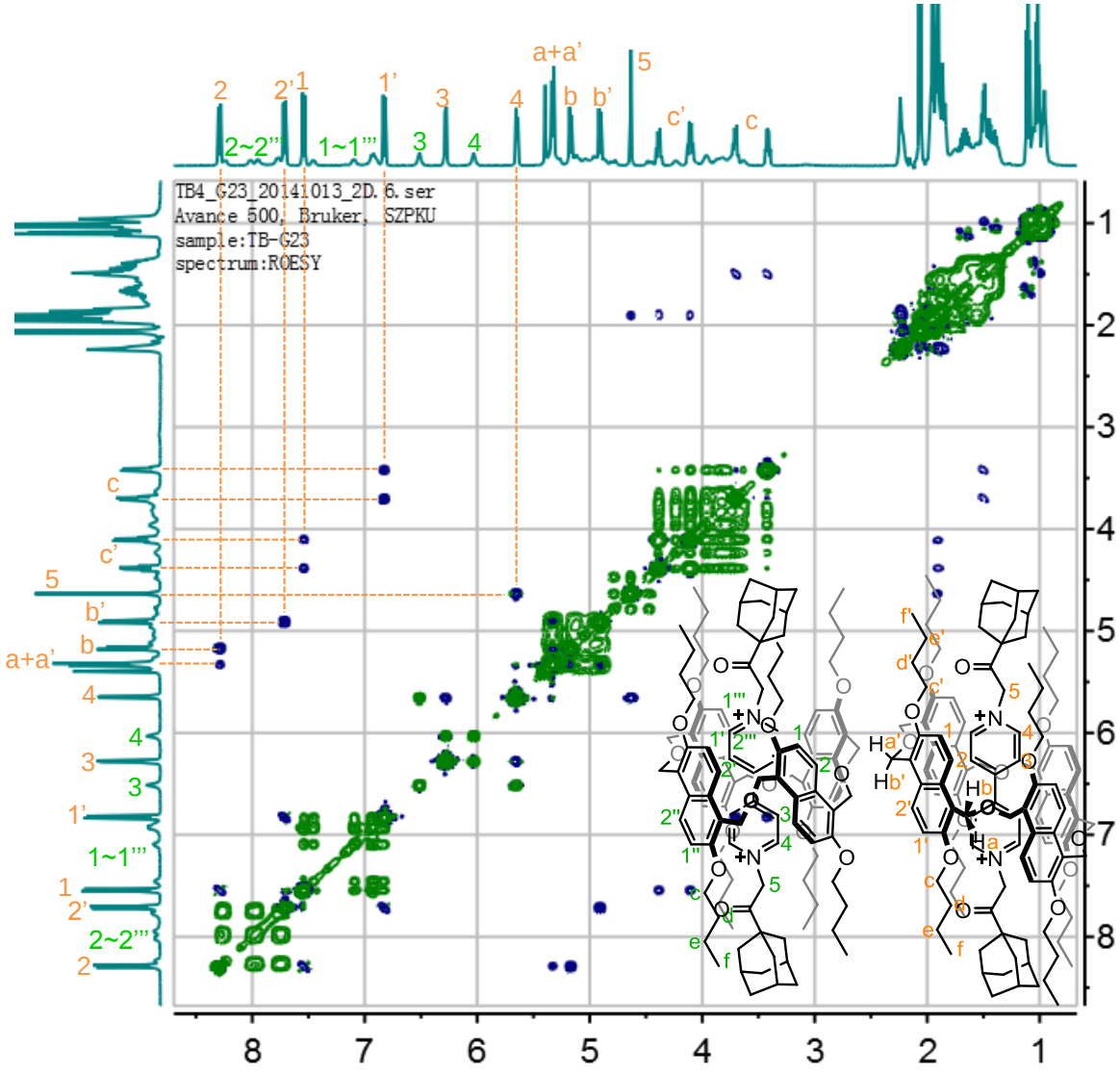


***Fig. S53.*** Full $^{1}$H, $^{1}$H-ROESY NMR spectrum (500 MHz, $CD_2Cl_2$:$CD_3CN$=1:1, 6.0 mM, 298 K) of **AVA-**2$PF_6$**@TA4**. The green peaks are the EXSY signals due to the quick exchange (at the subsecond timescale) between two host conformers at the present condition.

## 5. Single Crystal Structures

**X-ray Crystallographic Analysis of MeV$^{2+}$-2PF$_6$@TA4**. By slow vapor diffusion of diethyl ether into the solution of **MeV$^{2+}$-2PF$_6$@TA4** in the 1:1 mixture of MeCN and $CH_2Cl_2$, red prism-like crystals were obtained. Data were collected using a Sapphire CCD with a graphite monochromated CuKα radiation, $\lambda$ = 1.54184 Å at 173.00(10) K. Crystal data: $C_{92}H_{118}F_{12}N_2O_{12}P_2$, $M$ = 1733.86, trigonal, space group $R$-3; unit cell dimensions were determined to be $a$ = 43.2165(13) Å, $b$ = 43.2165(13) Å, $c$ = 12.4664(4) Å, $\alpha$ = 90°, $\beta$ = 90 °, $\gamma$ = 120 °, $V$ = 20163.7(11)Å$^3$, $Z$ = 6, $Dx$ = 1.261 g/cm$^3$, $F$ (000) = 7974, $\mu$ (Cu K$_\alpha$) = 1.163 mm$^{-1}$. 12674 reflections (7042 reflections were unique) were collected until $\theta_{max}$ = 62.69°, in which 5492 reflections were observed [$F^2 > 4\sigma(F^2)$]. The structure was solved by direct methods using the SHELXS-97 program, and refined by the full-matrix least-squares method (SHELXS-97 software package). In the structure refinements, hydrogen atoms bonded to carbons were placed on the geometrically ideal positions by the "ride on" method with isotropic temperature factors. The final refinement gave $R$ = 0.0712, $R_W$ = 0.0862, and $S$ = 1.056.

Crystal data of **MeV$^{2+}$-2PF$_6$@TA4** has been deposited with the Cambridge Crystallographic Data Centre (CCDC reference number: 1043636).

**Validation Reply Form:** responses to alerts in the crystal of **MeV$^{2+}$-2PF$_6$@TA4**

PLAT213_ALERT_2_A
**Problem:** Atom C17 has ADP max/min Ratio ..... 5.7 prolat
**Response**: C17 is on the side chain which is disordered, and thus the anisotropic displacement parameters are not reasonable.

PLAT213_ALERT_2_A
**Problem:** Atom C17A has ADP max/min Ratio ..... 5.2 prolat
**Response**: C17A (the second site of C17) is on the side chain which is disordered, and thus the anisotropic displacement parameters are not reasonable.

PLAT230_ALERT_2_B
**Problem:** Hirshfeld Test Diff for C15 -- C16 .. 12.6 su
**Response**: C15 and C16 are on the side chain which is disordered, and thus the anisotropic displacement parameters are not reasonable.

PLAT601_ALERT_2_B
**Problem:** Structure Contains Solvent Accessible VOIDS of . 149 Ang3
**Response**: the structure is a supermolecular assembly. The host molecule containing four rigid naphthalene moieties formed a large cavity.

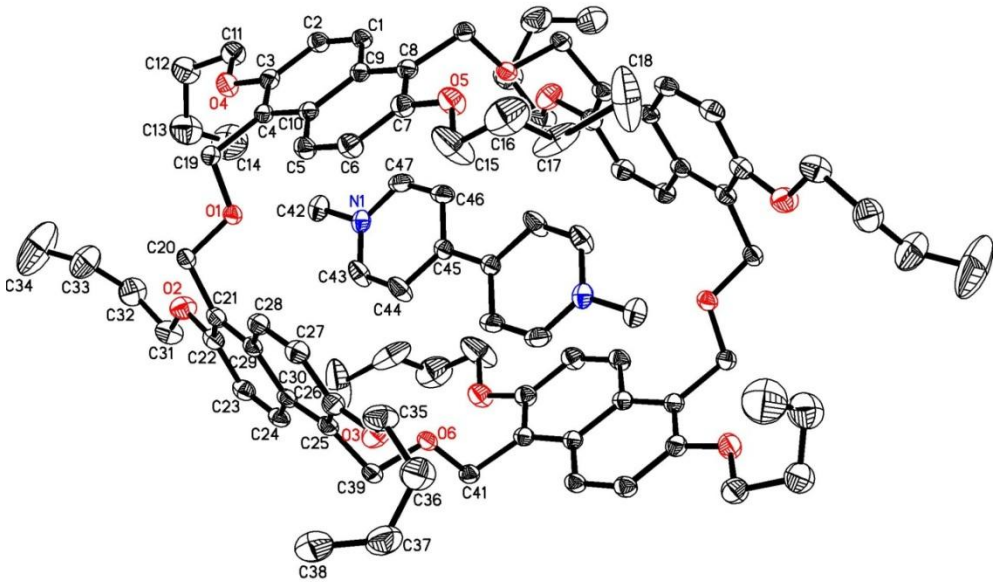


***Fig. S54.*** Single crystal structure of **MeV**$^{2+}$-2$PF_6$**@TA4**. The asymmetric unit was labeled. The C, N and O atoms are drawn as 30% thermal ellipsoids. Disordered $PF_6^-$ was omitted for clarity.

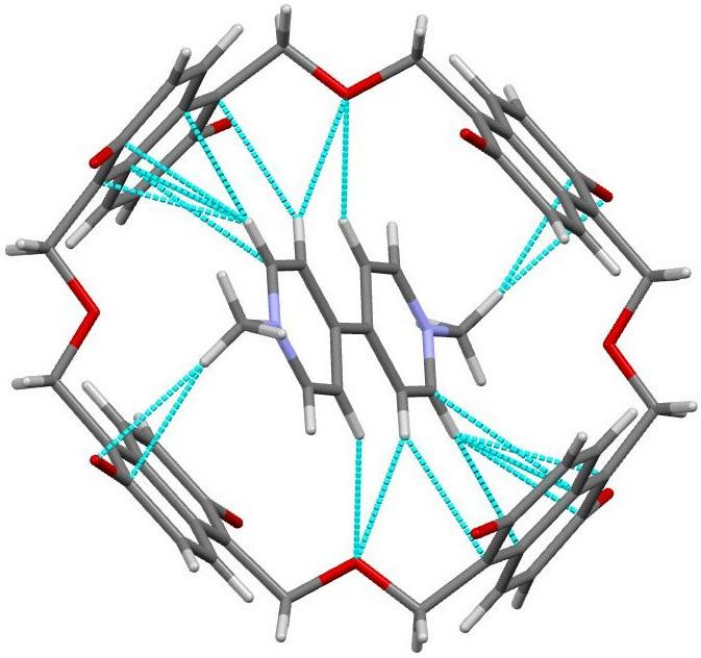

***Fig. S55.*** The solid structure of **MeV**$^{2+}$-2$PF_6$**@TA4** rendered to show the noncovalent interactions between the host and the guest. Multiple C-H···O, C-H···π, and cation···π interactions were observed. The oxygen atoms of the linker $CH_2$-O-$CH_2$ are involved in the C-H···O hydrogen bonds, suggesting a non-innocent spacer. Butyl groups and disordered $PF_6^-$ were omitted for clarity.

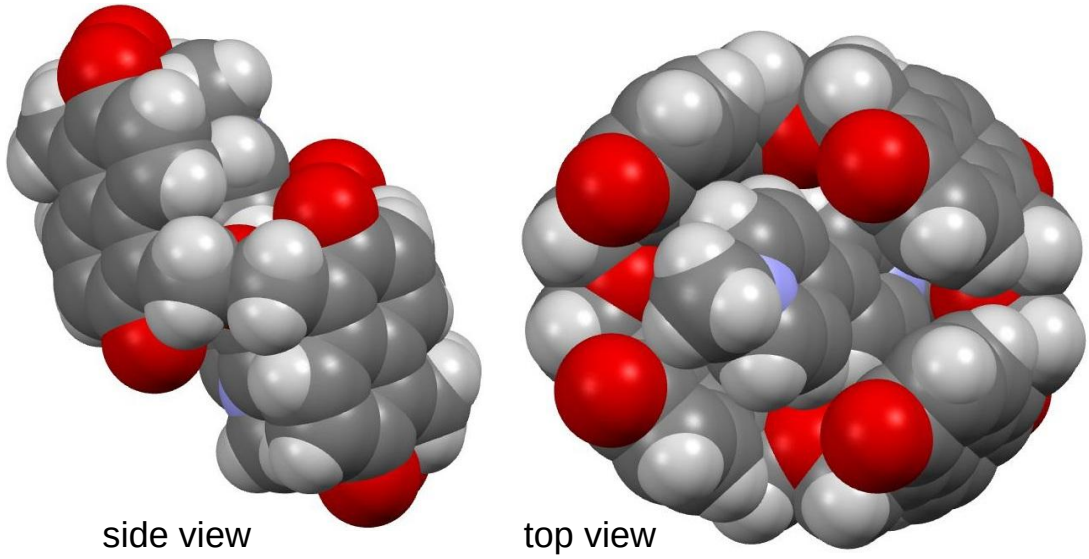


***Fig. S56.*** The space-filling structure of **MeV**$^{2+}$-2$PF_6$**@TA4** in the solid state. Butyl groups and disordered $PF_6^-$ were omitted for clarity.

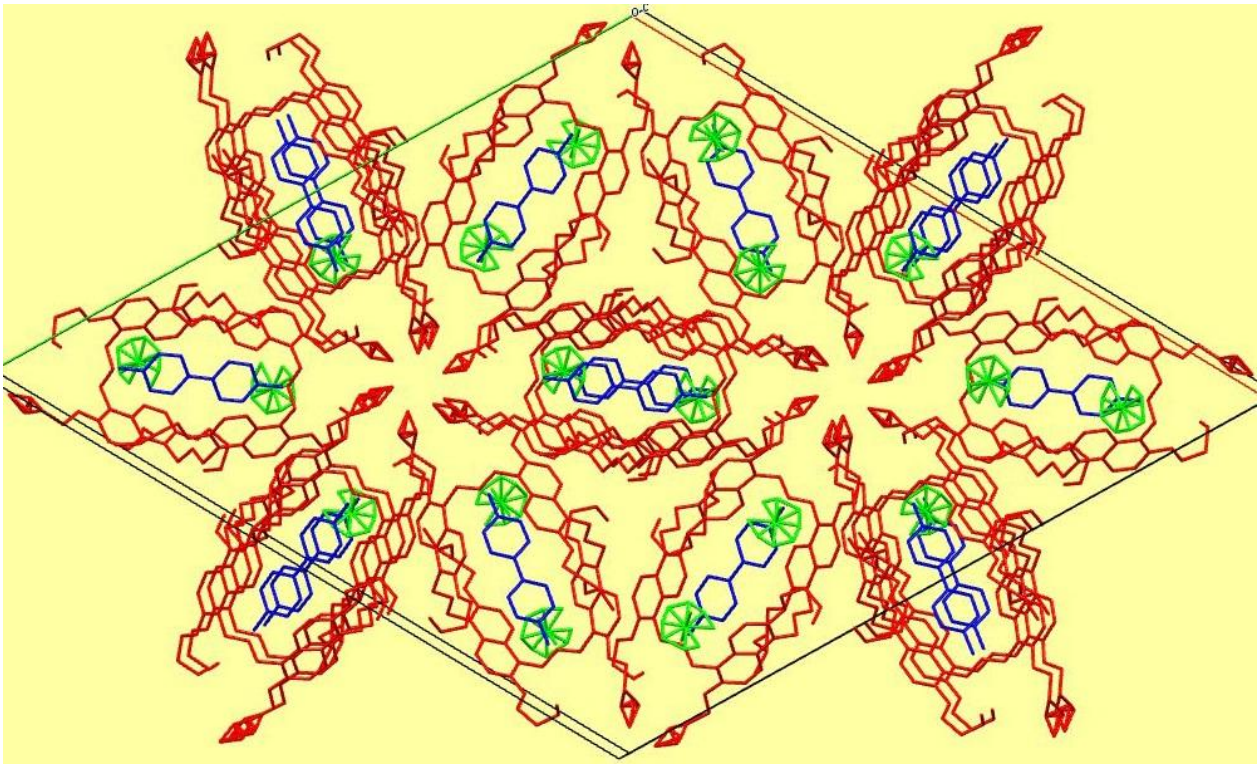

***Fig. S57.*** Crystal packing of **MeV**$^{2+}$-2$PF_6$**@TA4** in a unit cell. The hosts, the guests, and $PF_6^-$ were colored in red, blue, and green, respectively.

**X-ray Crystallographic Analysis of 1D1$^{2+}$-2PF$_6$@TA4**. By slow vapor diffusion of diethyl ether into the solution of **1D1**$^{2+}$-2PF$_6$**@TA4** in the 1:1 mixture of MeCN and $CH_2Cl_2$, colorless block-like crystals were obtained. Data were collected using a Sapphire CCD with a graphite monochromated CuKα radiation, $\lambda$ = 1.54184 Å at 173.00(10) K. Crystal data: $C_{94}H_{132}F_{12}N_4O_{12}P_2$, $M$ = 1800.00, monoclinic, space group $P2/c$; unit cell dimensions were determined to be $a$ = 15.9874(6) Å, $b$ = 18.0758(4) Å, $c$ = 18.1871(6) Å, $\alpha$ = 90°, $\beta$ = 107.850(4) °, $\gamma$ = 90°, $V$ = 5002.8(3)Å$^3$, $Z$ = 4, $Dx$ = 1.200 g/cm$^3$, $F$ (000) = 1916, $\mu$ (Cu K$_\alpha$) = 1.073 mm$^{-1}$. 23136 reflections (7965 reflections were unique) were collected until $\theta_{max}$ = 62.68°, in which 6021 reflections were observed [$F^2 > 4\sigma(F^2)$]. The structure was solved by direct methods using the SHELXS-97 program, and refined by the full-matrix least-squares method (SHELXS-97 software package). In the structure refinements, hydrogen atoms bonded to carbons were placed on the geometrically ideal positions by the "ride on" method with isotropic temperature factors. The final refinement gave $R$ = 0.0907, $R_W$ = 0.1088, and $S$ = 1.349.

Crystal data of **1D1**$^{2+}$-2PF$_6$**@TA4** has been deposited with the Cambridge Crystallographic Data Centre (CCDC reference number: 1043635).

**Validation Reply Form:** responses to alerts in the crystal of **1D1**$^{2+}$-2PF$_6$**@TA4**

PLAT360_ALERT_2_A
**Problem:** Short C(sp3)-C(sp3) Bond C13 - C14 ... 1.15 Ang.
**Response**: the side chain containing C13 and C14 is extremely disordered though low temperature 173K was used for the data collection

PLAT220_ALERT_2_B
**Problem:** Large Non-Solvent C Ueq(max)/Ueq(min) Range 8.7 Ratio
**Response:** the side chain containing C15 is extremely disordered, and thus C15 shows the largest Ueq.

PLAT222_ALERT_3_B
**Problem:** Large Non-Solvent H Uiso(max)/Uiso(min) ... 8.2 Ratio
**Response:** the side chain containing C15 is extremely disordered. Thus C15 shows the largest Ueq. and the bonded non-solvent H show the largest Uiso.

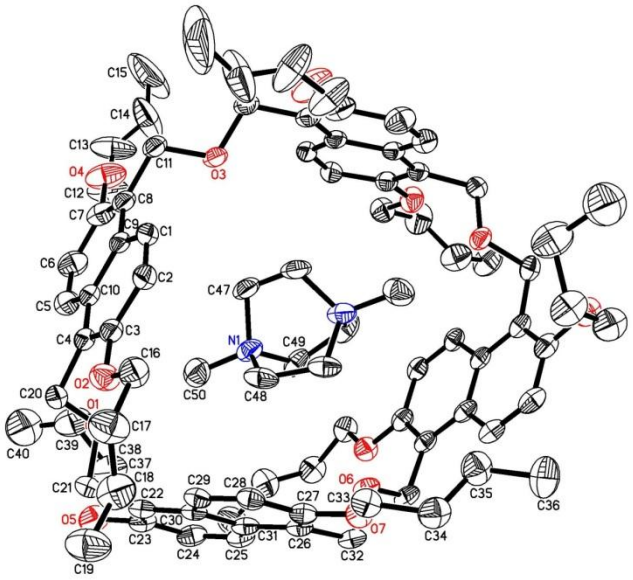


***Fig. S58.*** Single crystal structure of **1D1**$^{2+}$-2$PF_6$**@TA4**. The asymmetric unit was labeled. The C, N and O atoms are drawn as 30% thermal ellipsoids. Disordered solvents and $PF_6^-$ was omitted for clarity.

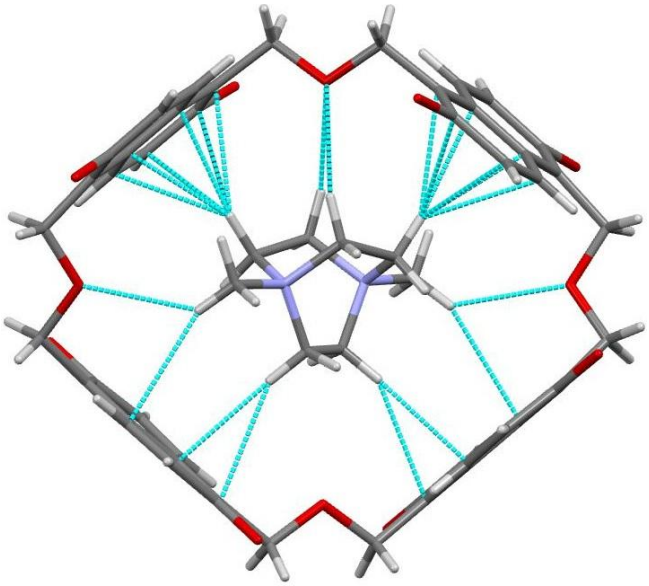

***Fig. S59.*** The solid structure of **1D1**$^{2+}$-2$PF_6$**@TA4** rendered to show the noncovalent interactions between the host and the guest. Multiple C-H···O, C-H···π, and cation···π interactions were observed. The oxygen atoms of the linker $CH_2$-O-$CH_2$ are involved in the C-H···O hydrogen bonds, suggesting a non-innocent spacer. Butyl groups and disordered solvents and $PF_6^-$ were omitted for clarity.

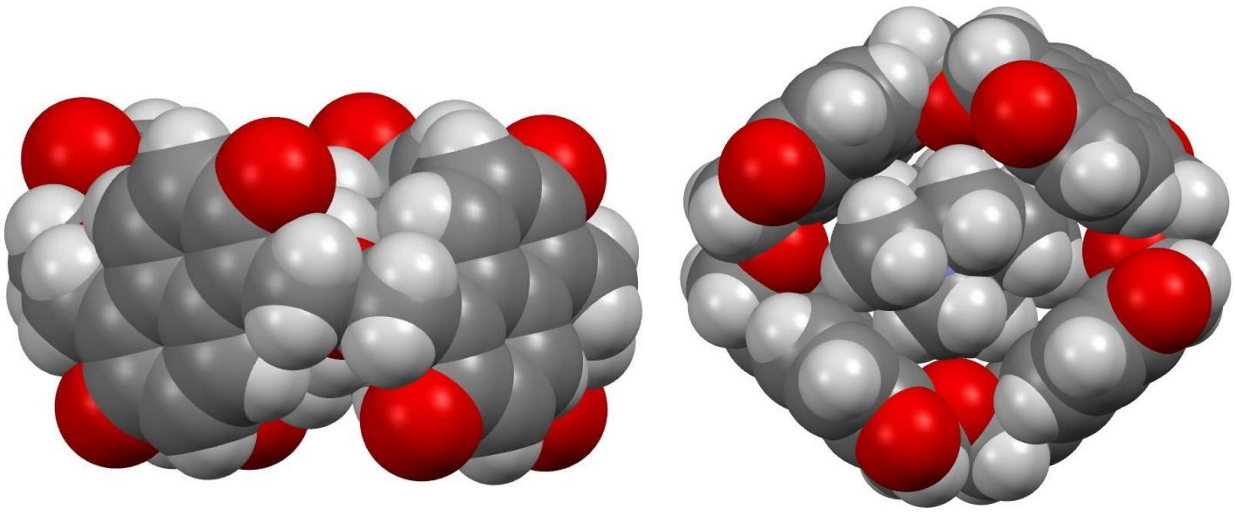


***Fig. S60.*** The space-filling structure of **1D1**$^{2+}$-2$PF_6$**@TA4** in the solid state. Butyl groups and disordered solvents and $PF_6^-$ were omitted for clarity.

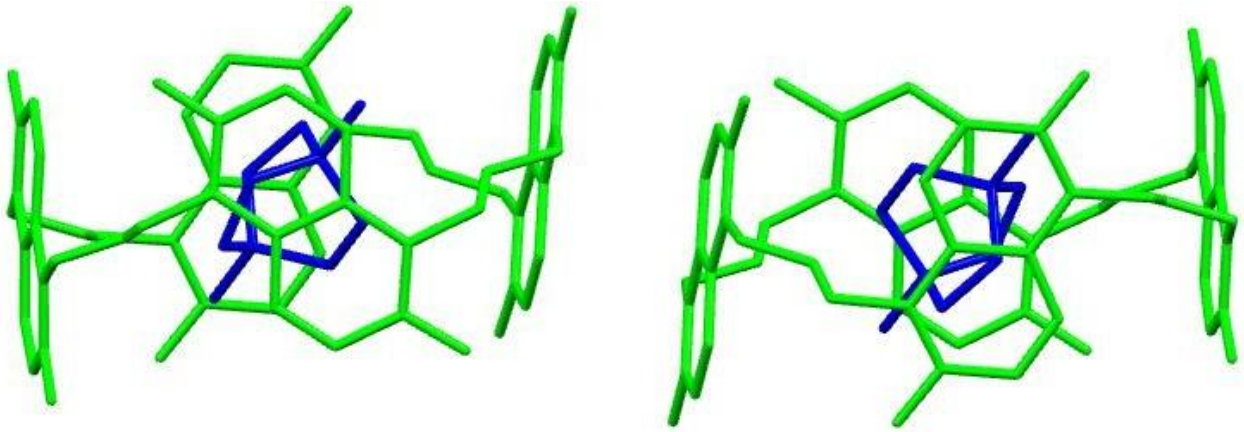


***Fig. S61.*** Two enantiomers of **1D1**$^{2+}$-2$PF_6$**@TA4** are paired in the solid state. Butyl groups and disordered solvents and $PF_6^-$ were omitted for clarity.

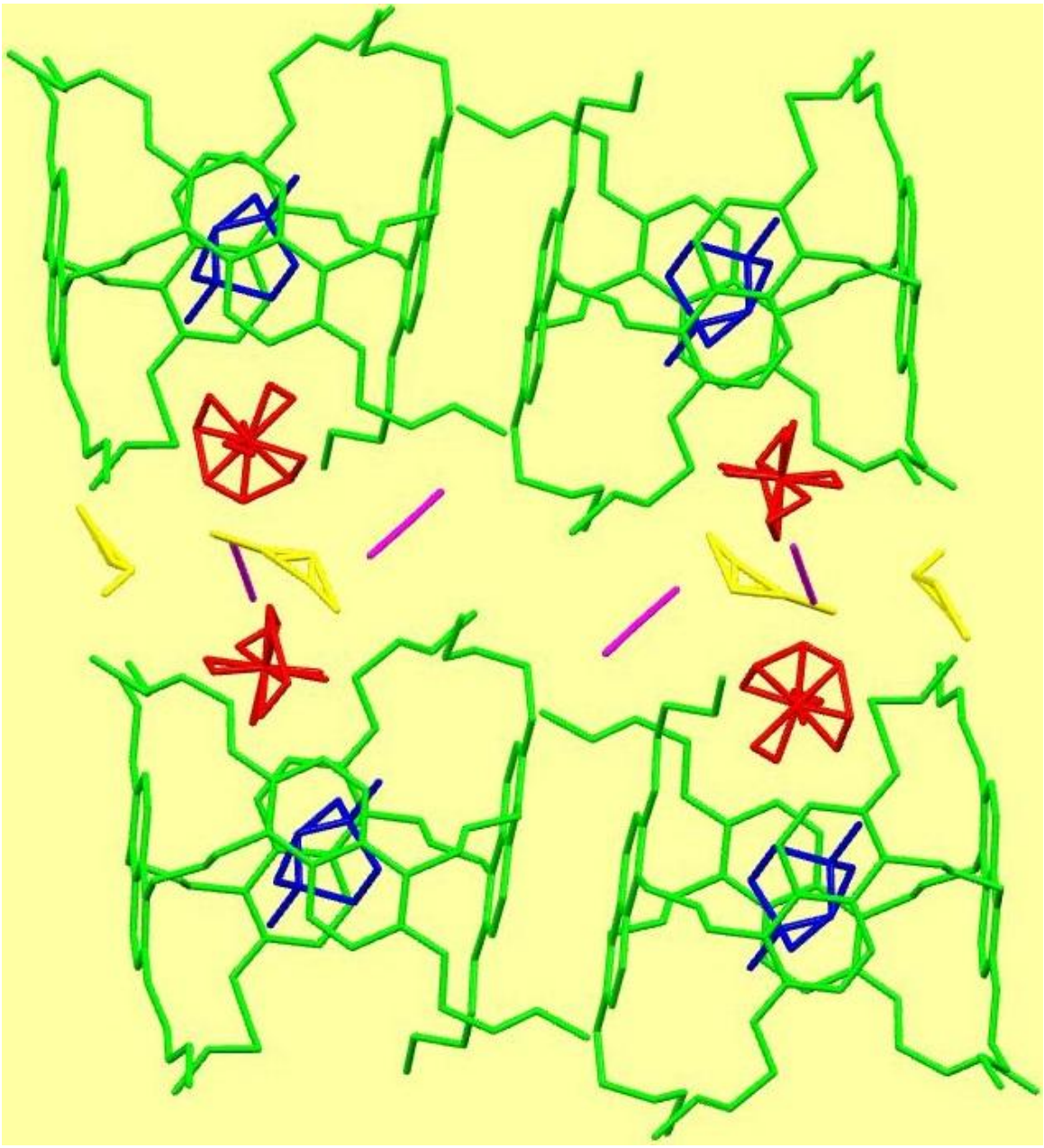

***Fig. S62.*** Crystal packing of **1D1**$^{2+}$-2$PF_6$**@TA4** in a unit cell. The hosts, the guests, and $PF_6^-$ were colored in green, blue, and red, respectively.

## 6. UV-Vis Spectroscopy

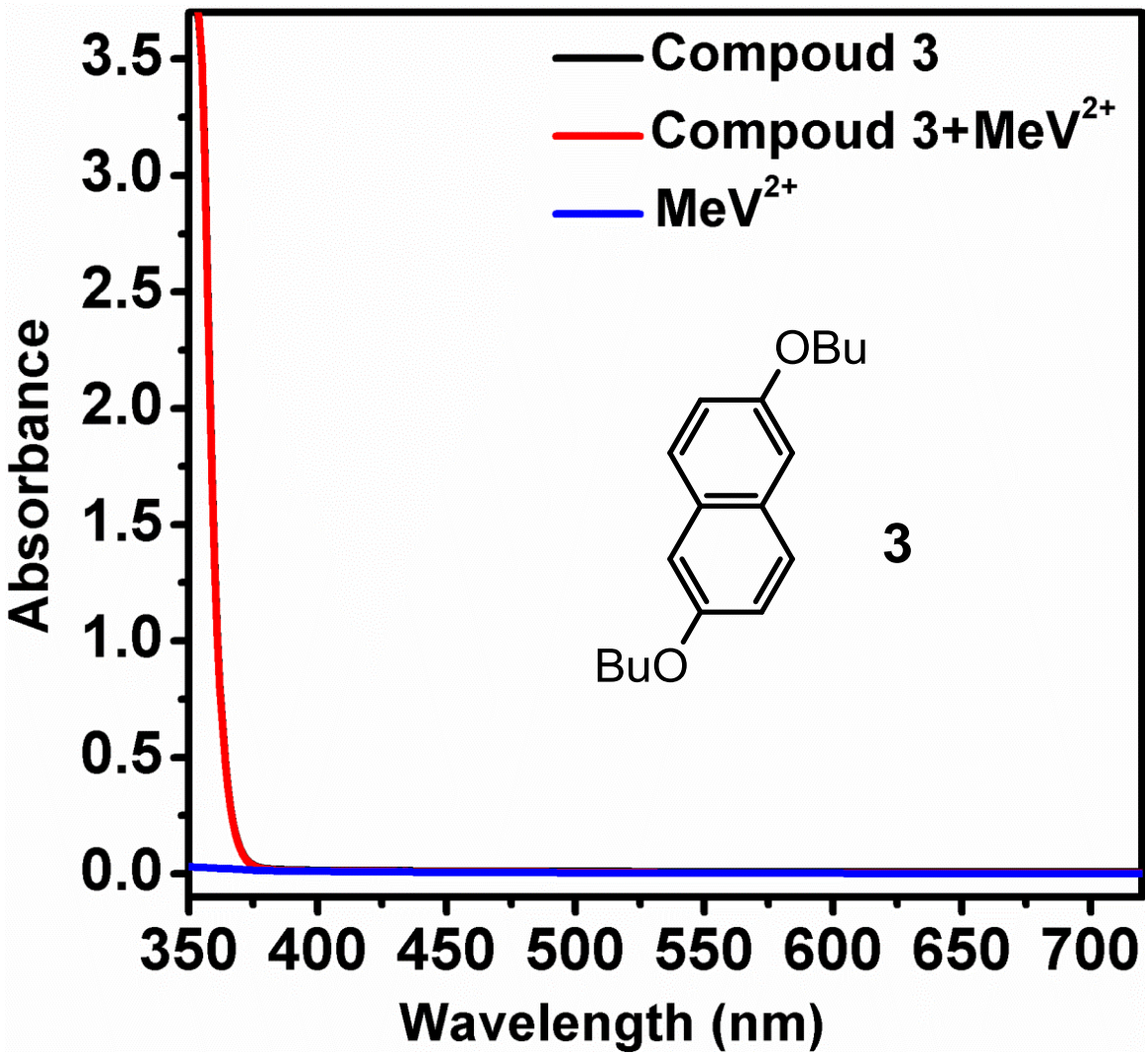


***Fig. S63.*** UV-vis absorption spectra of **3** (4.0 mM), **MeV**$^{2+}$-2$PF_6$ (1.0 mM), and their 4:1 mixture. This control experiment suggests that the macrocyclic structure of **TA4** played important roles in the formation of charge transfer complex in **MeV**$^{2+}$-2$PF_6$***@***TA4** and **AVA**$^{2+}$-2$PF_6$***@***TA4**.

## 7. Association Constants Determined by ITC

***Table S1.*** Thermodynamic association data as obtained from ITC titrations (1,2-dichloroethane/$CH_3CN$ = 1:1, 298 K).

| Guests | $K_a$($\times 10^5$) | n[a] | $\Delta$G(kJ·mol$^{-1}$) | $\Delta$H (kJ·mol$^{-1}$) | $\Delta$S (J·mol$^{-1}$·K$^{-1}$) |
|---|---|---|---|---|---|
| **D2D**$^{2+}$ | 2.34±0.63 | 1 | -30.7±0.9 | -15.4 | 51.1 |
| **D3D**$^{2+}$ | 1.56±0.32 | 1 | -29.6±0.8 | -8.7 | 70.4 |
| **D4D**$^{2+}$ | 1.09±0.19 | 1 | -28.8±0.8 | -13.1 | 52.4 |
| **D5D**$^{2+}$ | 0.75±0.16 | 1 | -27.8±0.9 | -8.43 | 65.0 |
| **1D1**$^{2+}$ | 0.18±0.03 | 1 | -24.3±0.7 | 3.10 | 91.7 |
| **2D2**$^{2+}$ | 1.44±0.26 | 1 | -29.4±0.8 | -7.30 | 74.3 |
| **3D3**$^{2+}$ | 4.57±0.52 | 1 | -32.3±0.6 | -13.0 | 64.8 |
| **4D4**$^{2+}$ | 4.30±0.77 | 1 | -32.2±0.8 | -11.9 | 67.9 |
| **MeV**$^{2+}$ | 1.31±0.19 | 1 | -29.2±0.7 | -14.0 | 51.0 |
| **AVA**$^{2+}$ | 1.82±0.30 | 1 | -30.0±0.7 | -15.3 | 49.5 |

[a] The binding stoichiometry for all of these guests is 1:1 as determined by ITC, which is also confirmed by ESI-MS experiments (see above).

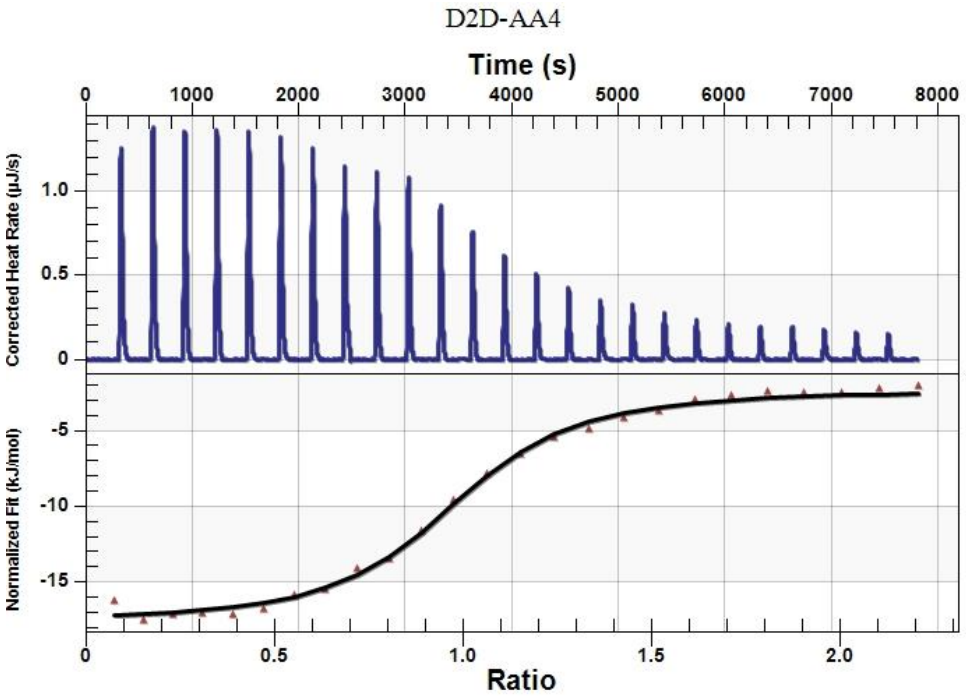


***Fig. S64.*** Titration plots (heat flow versus time and heat versus guest/host ratio) obtained from ITC experiments of **TA4** with **D2D-**$2PF_6$ in the 1:1 mixture of 1,2-dichloroethane and $CH_3CN$.

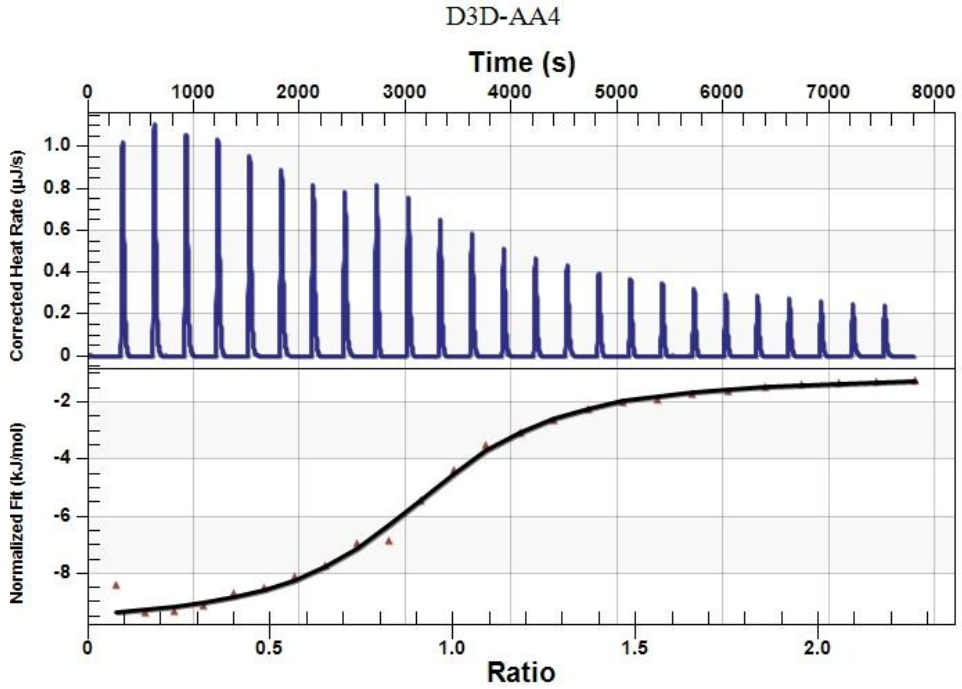


***Fig. S65.*** Titration plots (heat rate versus time and heat versus guest/host ratio) obtained from ITC experiments of **TA4** with **D3D-**$2PF_6$ in the 1:1 mixture of 1,2-dichloroethane and $CH_3CN$.

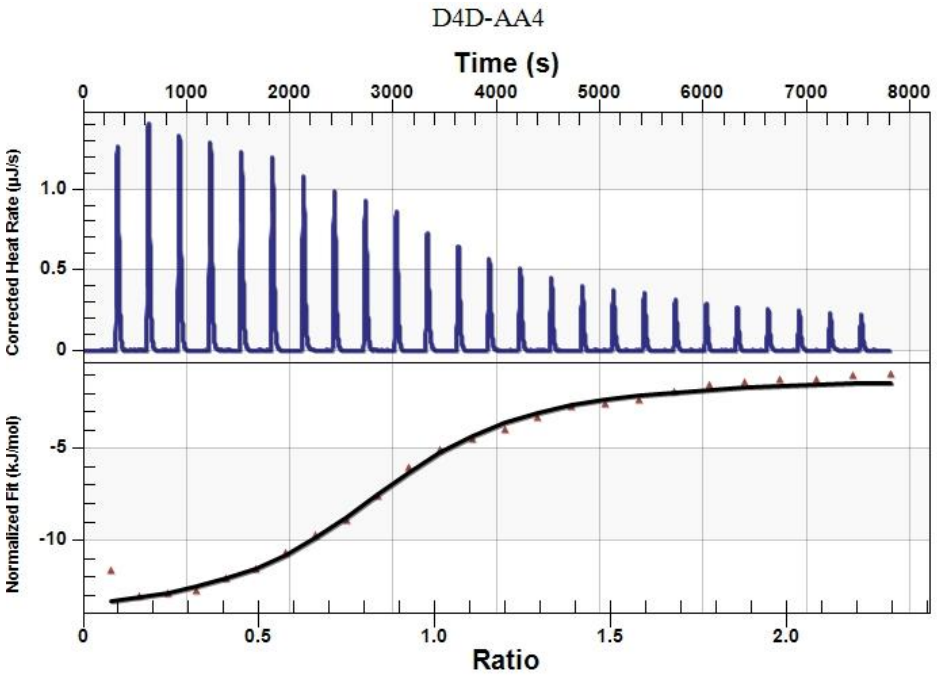


***Fig. S66.*** Titration plots (heat rate versus time and heat versus guest/host ratio) obtained from ITC experiments of **TA4** with **D4D**-2$PF_6$ in the 1:1 mixture of 1,2-dichloroethane and $CH_3CN$.

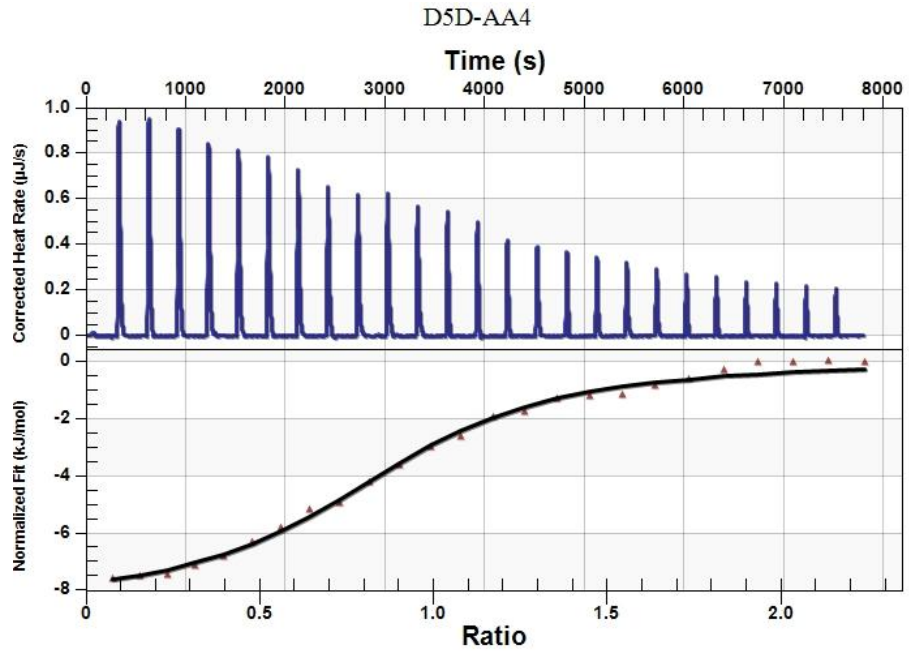


***Fig. S67.*** Titration plots (heat rate versus time and heat versus guest/host ratio) obtained from ITC experiments of **TA4** with **D5D**-2$PF_6$ in the 1:1 mixture of 1,2-dichloroethane and $CH_3CN$.

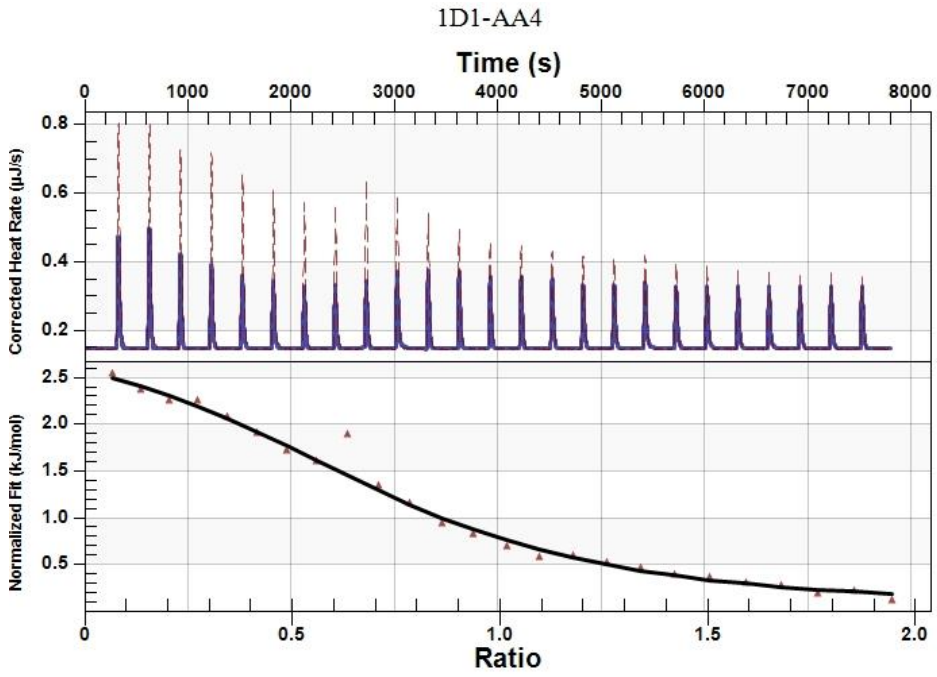


***Fig. S68.*** Titration plots (heat rate versus time and heat versus guest/host ratio) obtained from ITC experiments of **TA4** with **1D1-**2$PF_6$ in the 1:1 mixture of 1,2-dichloroethane and $CH_3CN$.

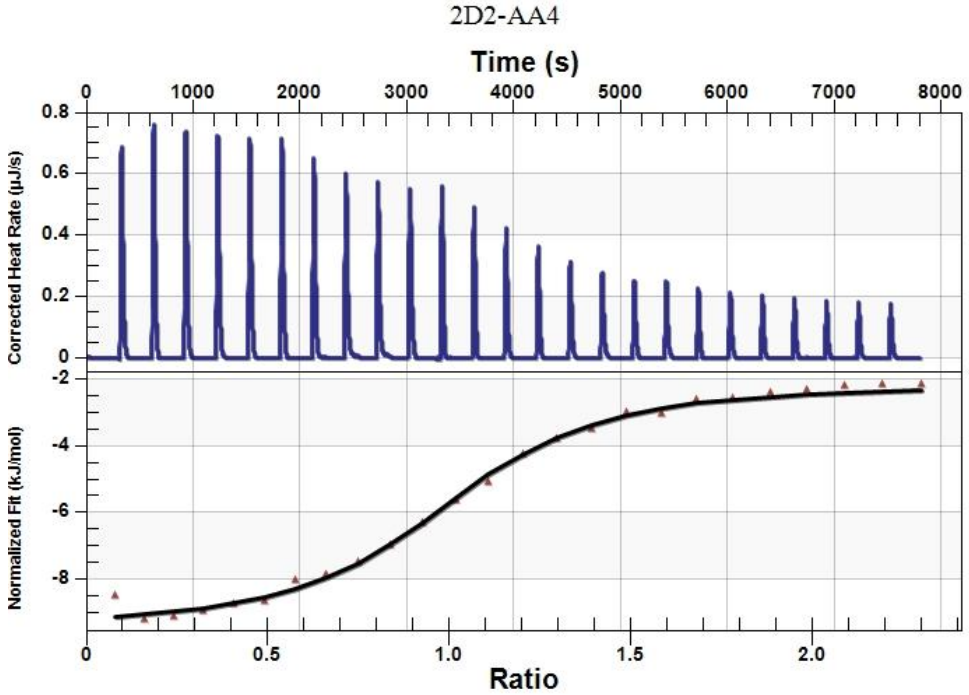


***Fig. S69.*** Titration plots (heat rate versus time and heat versus guest/host ratio) obtained from ITC experiments of **TA4** with **2D2-**2$PF_6$ in the 1:1 mixture of 1,2-dichloroethane and $CH_3CN$.

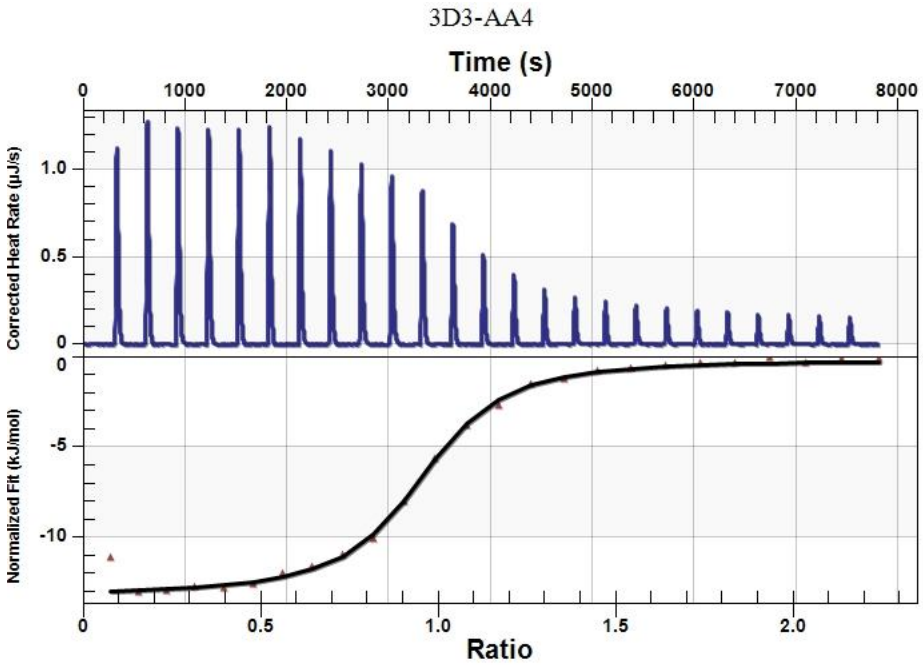


***Fig. S70.*** Titration plots (heat rate versus time and heat versus guest/host ratio) obtained from ITC experiments of **TA4** with **3D3-**$2PF_6$ in the 1:1 mixture of 1,2-dichloroethane and $CH_3CN$.

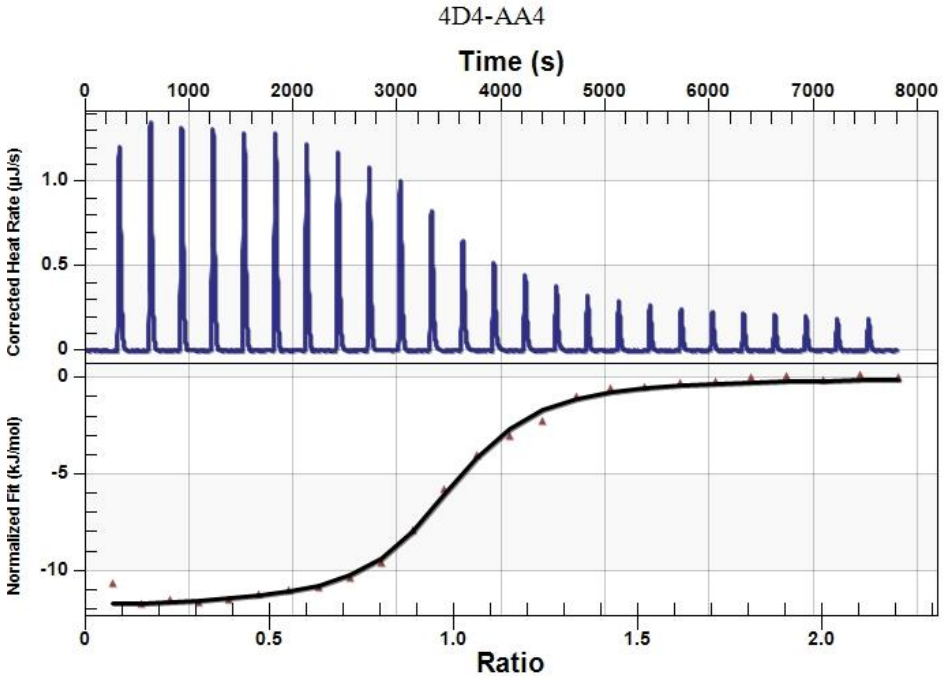


***Fig. S71.*** Titration plots (heat rate versus time and heat versus guest/host ratio) obtained from ITC experiments of **TA4** with **4D4-**$2PF_6$ in the 1:1 mixture of 1,2-dichloroethane and $CH_3CN$.

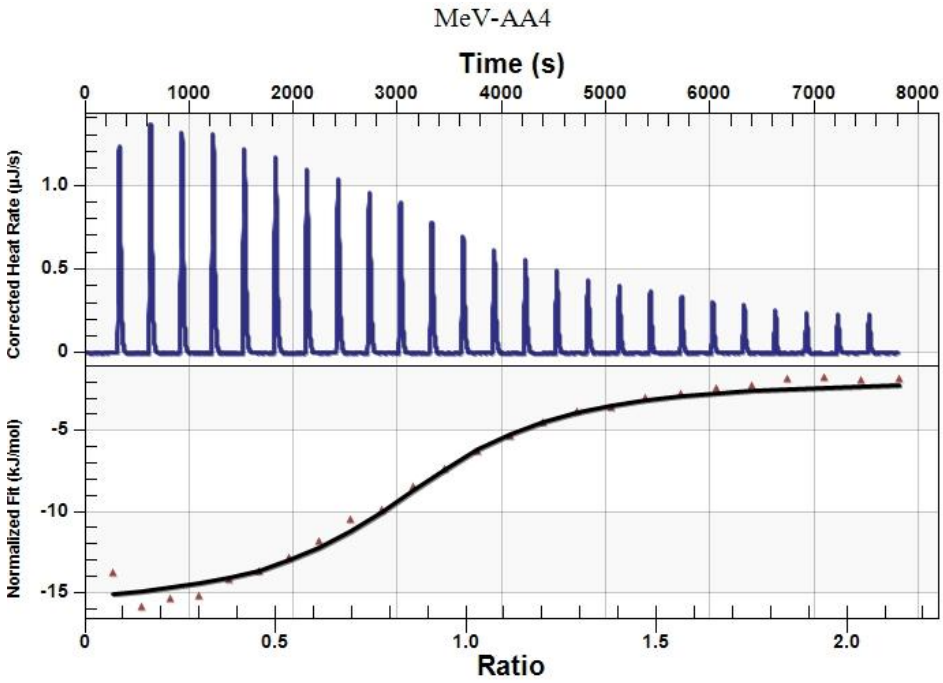


***Fig. S72.*** Titration plots (heat rate versus time and heat versus guest/host ratio) obtained from ITC experiments of **TA4** with **MeV**-$2PF_6$ in the 1:1 mixture of 1,2-dichloroethane and $CH_3CN$.

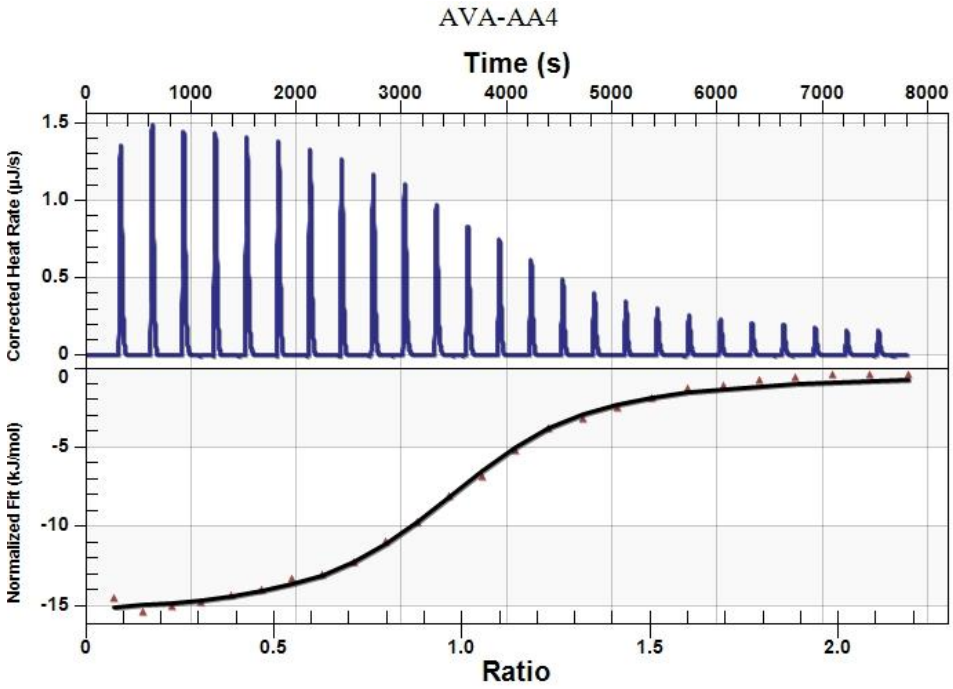


***Fig. S73.*** Titration plots (heat rate versus time and heat versus guest/host ratio) obtained from ITC experiments of **TA4** with **AVA**-$2PF_6$ in the 1:1 mixture of 1,2-dichloroethane and $CH_3CN$.